EXPERIMENTAL STUDY ON TRIANGULAR APERTURE GEOGRID-REINFORCED BASES OVER WEAK SUBGRADE UNDER CYCLIC LOADING

By

Yu Qian

Submitted to the graduate degree program in Civil Engineering and the Graduate Faculty of the University of Kansas School of Engineering in partial fulfillment of the degree of Master of Science.

Dr. Jie Han, Chairperson

Committee members

Dr. Anil Misra

Dr. Robert L. Parsons

Date defended:

The Thesis Committee for Yu Qian certifies that this is the approved version of the following thesis:

EXPERIMENTAL STUDY ON TRIANGULAR APERTURE GEOGRID-REINFORCED BASES OVER WEAK SUBGRADE UNDER CYCLIC LOADING

Committee:

Dr. Jie Han, Chairperson

Dr. Anil Misra

Dr. Robert L. Parsons

Date approved:

Acknowledgement

I would like express my sincerely appreciation to my advisor Dr. Jie Han for providing me the great opportunity to work in such an interesting project. Every progress of this work would not have been possible without his guidance, support and encouragement. I also wish to thank Dr. Robert L. Parsons and Dr. Anil Misra for their advice and support.

This research project was financially supported by Tensar International Corporation. This support is greatly appreciated.

I got great cooperation from Mr. Sanat K. Pokharel, Ph.D. candidate and Mr. Milad Jowkar, undergraduate student in the Department of Civil, Environmental, and Architectural Engineering (CEAE) at the University of Kansas (KU) during the entire process of this study. This project would not have come to this stage without the great support from our laboratory supervisor Mr. Howard J. Weaver. I express my special thanks to all of them.

I would like also thank all of my teammates in the KU Geotechnical Society who always helped and supported me whenever I needed.

Finally, I would like to express my emotional gratitude to my parents, my wife, and my sister for their understanding, support, and encouragement.

Table of Contents

Abstract

The objective of this study is to investigate the behavior of triangular aperture geogrid-reinforced bases over weak subgrade under cyclic loading through laboratory testing. Behavior of unpaved structures, such as permanent displacement, percentage of resilient displacement, stress distribution, and modulus variation were investigated. Nineteen large-scale laboratory cyclic plate loading tests were conducted on unpaved sections with three different base course thicknesses. Three types of triangular aperture geogrids were selected to reinforce the bases respectively. The results indicated that the triangular aperture geogrids effectively reduced permanent displacement and maximum vertical stress, distributed the load wider and more uniformly, increased the modulus of the base, and reduced the degradation rate of the base course. Generally, the performance of the specific geogrids tested in this study, all of which are from the same family of geogrids, improved as the level of robustness, unit weight, rib thickness, and mechanical properties increased.

List of Figures

List of Tables

Chapter 1 INTRODUCTION

1.1 Background

Geosynthetics have been successfully used for subgrade improvement and base reinforcement for unpaved and paved roads in the past several decades. Due to their successful applications, geosynthetics are available worldwide and their market is steadily growing. The synthetic nature of the products makes them suitable for uses in the ground where the soil condition is poor. Geosynthetics are available in a wide range of forms and manufactured using different materials and processes. They have been used for a wide range of applications in civil engineering including roads, airfields, railroads, embankments, earth retaining structures, reservoirs, canals, dams, and bank and coastal protection. Geosynthetics can be divided into nine main types: (1) geotextile, (2) geogrid, (3) geonet, (4) geomembrane, (5) geosynthetic clay liner, (6) geopipe, (7) geofoam, (8) geocell, and (9) geocomposite. Geosynthetics are used to perform five major functions: (1) separation, (2) reinforcement, (3) drainage, (4) filtration, and (5) containment.

1.2 Problem Statement

Geosynthetics have been successfully used for subgrade improvement and base reinforcement for unpaved and paved roads in the past several decades. Research and field data show that a properly designed and placed geosynthetic does improve

the performance of roads. Das et al. (1998) pointed out that the most effective location of the geosynthetic for subgrade improvement is at the interface between the selected granular material and the subgrade. At this location the geosynthetic provides full or partial separation, lateral restraint of the overlying granular material, and a tensioned membrane effect when deformed extensively. Geotextiles and geogrids are two main types of geosynthetics used in unpaved roads. However, there is a significant difference between geotextiles and geogrids. Nonwoven geotextiles are mainly used for separation, filtration, and drainage; woven geotextiles are used for separation and reinforcement; and geogrids are typically used for confinement and reinforcement. The confinement due to the geogrid interlocking with aggregate minimizes lateral movement of aggregate particles and increases the modulus of the base course, which leads to a wider vertical stress distribution over the subgrade and consequently a reduction of vertical subgrade deformation (Love 1984; Haas et al 1988). The effectiveness of interlocking between the geogrid apertures and the aggregates in the base course depends on the relationship between the aperture size of the geogrid and the particle size of the aggregate (Giroud and Han 2004a, b). The reduction in the shear stress at the geogrid-subgrade interface can reduce the deformation of the subgrade as well (Perkins 1999).

In the past, geogrids were classified as uniaxial and biaxial, as shown in Figures 1.1 and 1.2. As Dong et al. (2010) demonstrated, biaxial geogrids cannot provide uniform tensile strengths when subjected to tension in different directions. The

uniaxial geogrids have tensile strength only in one direction. A new geogrid product with triangular apertures, as shown in Figure 1.3, was developed to overcome this limitation and to further advance the technology of mechanical reinforcement of soils. Since the triangular aperture geogrid has a more stable grid structure, it provides near-uniform properties in all directions as compared with uniaxial and biaxial geogrids. Giroud (2009, Geogrid Jubilee Symposium in London) noted that the triangular structure for a geogrid presents many probable benefits over biaxial structures including improved interlock, improved stress transfer from soil to geogrid, and improved distribution of stresses within the geogrid structure. Giroud also proposed that the mechanisms of interaction between geogrids and soils are (1) extremely complex and, (2) that highly effective geogrids, when used to reinforce appropriately selected fill soils, likely create a new, "composite" stabilized layer of soil and geogrid that can significantly enhance load carrying and load distribution capabilities and improve ductility and resistance to fatigue than the original unreinforced or unimproved layer. Due to the extreme complexities of the mechanisms of interaction between various geogrid types and soil types, and the likelihood of future new geogrid configurations, Giroud stated that our focus for research, development, and practical design should shift towards developing better understandings of the composite materials created by the combination of geogrids and soils, and move away from studying the potential benefits of one product feature compared to another product feature. Thus, to develop an effective understanding of how different geogrids will perform in variations of soils, experiments must be

performed wherein the combined materials, or the composite itself, are tested.

The biaxial geogrid structure has been extensively researched since its introduction in the 1980s. However, due to their relatively recent commercial availability the performance capabilities of the family of triangular aperture geogrids for reinforced bases have not been well tested and evaluated outside of the extensive research and development program undertaken by the manufacturer. As a result, the experiments performed herein serve to establish a strong initial understanding of the performance capabilities of this new family of geogrids, and provide the necessary and appropriate data for use in calibration with existing design methods, and/or development of new design approaches.

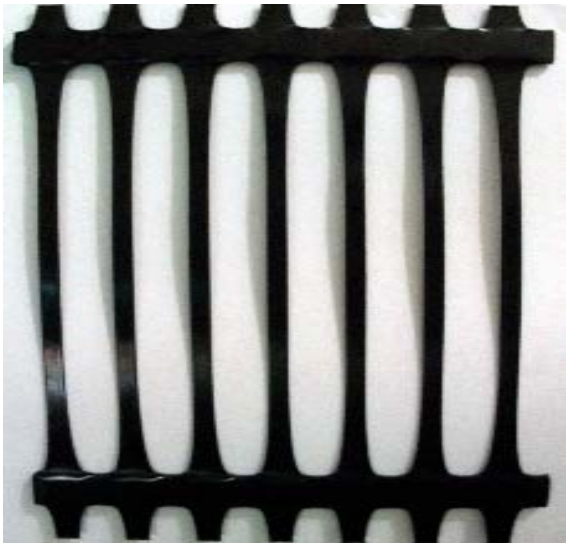

Figure 1.1 Uniaxial geogrid (Tensar Uniaxial Geogrid)

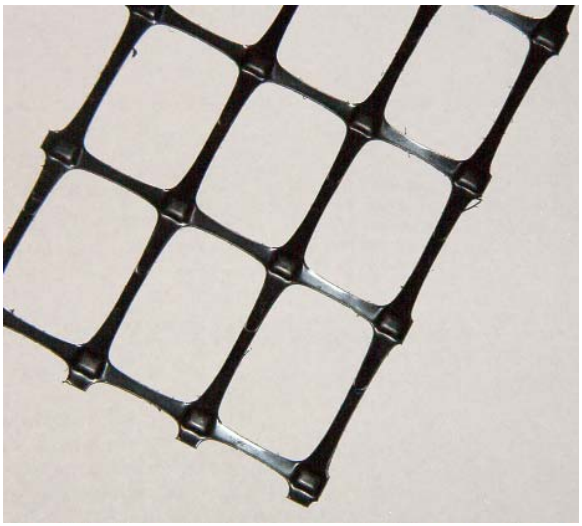

Figure 1.2 Biaxial geogrid (Tensar Biaxial Geogrid)

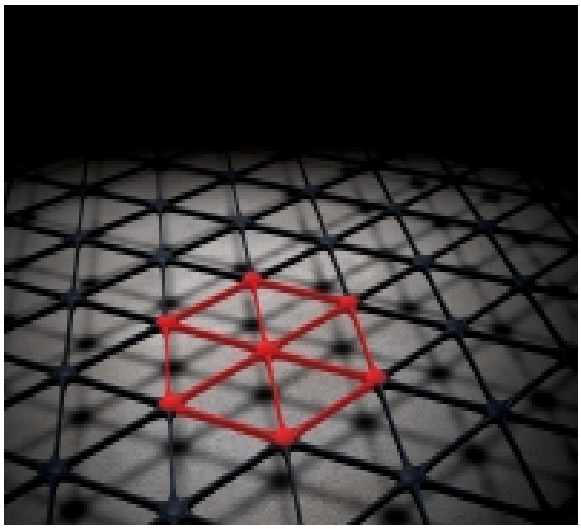

Figure 1.3 Tensar Triangular Aperture Geogrid

1.3 Objective

The objective of this study was to investigate the performance of triangular aperture geogrid-reinforced bases over weak subgrade under cyclic loading. A series of

laboratory tests were conducted to investigate the influence of triangular aperture geogrids on the reduction in the permanent deformations and the vertical stresses at the interface between the base and the subgrade as compared with unreinforced bases.

Laboratory tests were prepared in different test conditions in order to evaluate the performance of triangular aperture geogrids with different base course thickness, base course stiffness, and subgrade stiffness. Also, repeated tests were conducted to verify the repeatability of the test method and condition.

1.4 Organization

This thesis contains five chapters. Chapter 1 provides introduction and overview of this study.

Chapter 2 provides the literature review of the functions and mechanisms associated with geosynthetics, especially geogrids and previous experimental studies, and summarizes the current design methods for subgrade improvement of unpaved roads.

Chapter 3 presents the experimental study on geogrid-reinforced bases over weak subgrade under cyclic loading including the properties of base, subgrade, and geogrid, test facilities and setup, test procedures, data acquisition system, test plan, and test results.

Chapter 4 presents the interpretation and analysis of the test data. This chapter

examines the effects of base course thickness, base course stiffness, subgrade stiffness, and type of geogrid on the performance of geogrid-reinforced bases over weak subgrade under cyclic loading including permanent displacement, percentage of resilient displacement, maximum vertical stress, stress distribution, and modulus of the reinforced base course.

Chapter 5 presents the conclusions from this study and the recommendations for future study.

Chapter 2 LITERATURE REVIEW

2.1 Introduction

This chapter provides a brief literature review of geogrid types, functions, previous experimental studies, and design methods for unpaved roads.

2.2 Geogrid

Geogrid has longitudinal and transverse ribs, which form apertures as showed in Figures 1.1 and 1.2. Figure 1.3 shows triangular aperture geogrid with ribs in more directions. The apertures allow soil particles to interact with ribs. The interaction between the aggregates and the ribs is referred to as interlocking. In the past, geogrid had two types: uniaxial and biaxial geogrids. Uniaxial geogrid has a tensile strength in one direction while biaxial geogrid has tensile strengths in two directions. Uniaxial geogrids are mainly used for slopes, retaining walls, and embankments. However, biaxial geogrids are commonly used for roadways including unpaved roads, paved roads, and railroads.

As Dong et al. (2010) demonstrated, biaxial geogrids cannot provide uniform tensile strengths when subjected to tension in different directions. A new product with triangular apertures was developed by the manufacturer to overcome this limitation. Since the triangular aperture geogrid has a more stable grid structure, it is expected to provide uniform tensile strengths in all directions as compared with uniaxial and

biaxial geogrids. However, due to their relatively recent introduction, the effects of the triangular aperture geogrids on the performance of reinforced bases have not been well tested and evaluated.

2.3 Functions of Geogrid

Giroud and Noiray (1981) pointed out that geosynthetics, especially geotextiles, can be placed between an aggregate base and a subgrade soil to perform the following functions: (1) separation; (2) filtration; (3) drainage; and (4) reinforcement. Geogrids can provide partial separation, confinement, and reinforcement.

Geogrids can provide confinement and reinforcement to base and subgrade due to their tensile strength and stiffness. The confinement is developed through the interlocking between geogrid apertures and granular particles as shown in Figure 2.1. The degree of interlocking depends on the relationship between geogrid aperture size and aggregate particle size and the effectiveness of interlocking depends on the in-plane stiffness of the geogrid and the stability of the geogrid ribs and junctions (Webster, 1993).

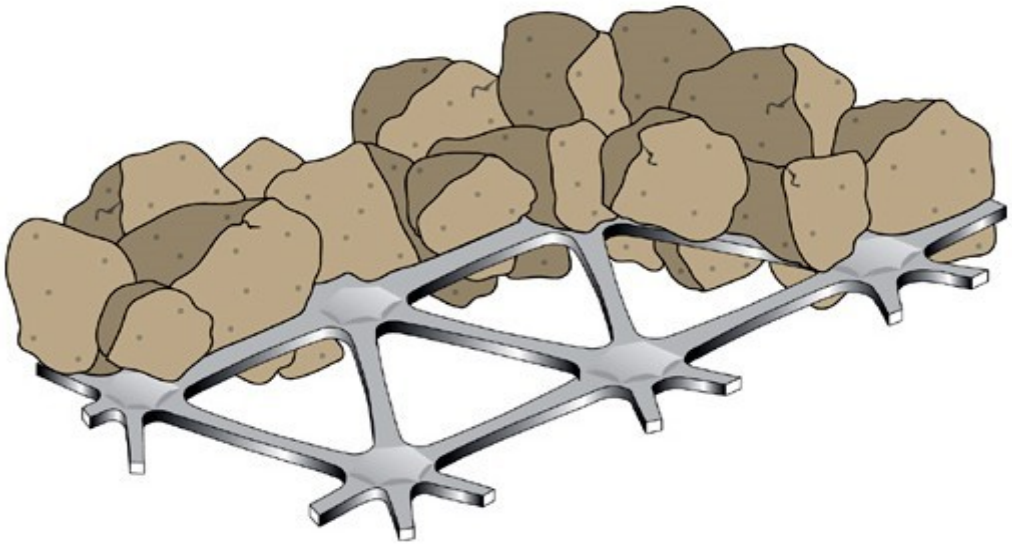

Figure 2.1 Interlock between geogrid and aggregate (Tensar triangular aperture geogrid)

Maxwell et al. (2005) summarized the contributions of geosynthetic reinforcement. Under traffic loading, the granular base would be pushed down and out laterally if there is no geogrid, which would induce shear stresses at the interface between the base and the subgrade. Due to the interlocking between the geogrid and aggregate particles, these shear stresses are absorbed by the stiffer geosynthetic, thus reducing lateral strain in the granular layer. Given a proper ratio of geogrid aperture size to aggregate grain size, geogrids provide lateral confinement to the aggregate base course through shear resistance and friction between the geogrid and its surrounding aggregate. The confinement due to the geogrid increases the modulus of the aggregate, which leads to an improved vertical stress distribution over the subgrade and consequent reduction of vertical subgrade deformation (Love 1984; Haas et al

1988). As shown in Figure 2.2, the shear stress absorbed by the stiff geosynthetic layer results in less shear stress transferred to the subgrade. As a result of the contributions by the geosynthetic layer discussed above, the subgrade is subjected to less vertical and shear stresses, which would increase the bearing capacity and reduce the deformation of the subgrade.

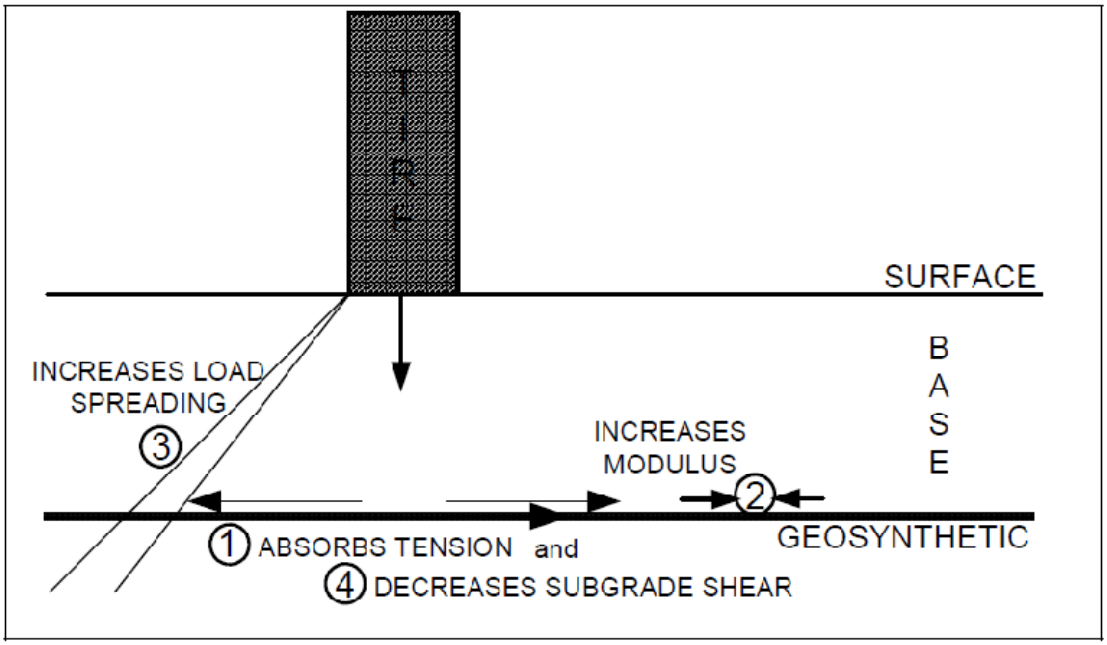

Figure 2.2 Contributions of geosynthetic reinforcement (Maxwell et al. 2005)

Since a geosynthetic layer is a thin and flexible material, it stretches to form a curved concave shape as a membrane under a perpendicular load. This geosynthetic layer is often called a tensioned membrane. As shown in Figure 2.3, under the wheel, the geosynthetic layer develops tension and reduces the pressure applied on the subgrade by the wheel. Beyond the wheel, however, the geosynthetic layer counteracts the heaving of the subgrade under the wheel loading. This counteraction increases the

pressure applied on the subgrade beyond the wheel so that it stabilizes the subgrade and reduces its heave. This effect by the geosynthetic layer is referred to as the tensioned membrane effect (Giroud and Noiray, 1981). Giroud and Han (2004a) pointed out that the tensioned membrane effect becomes important only if the traffic is channelized and the rut depth is large (for example, greater than 100 mm).

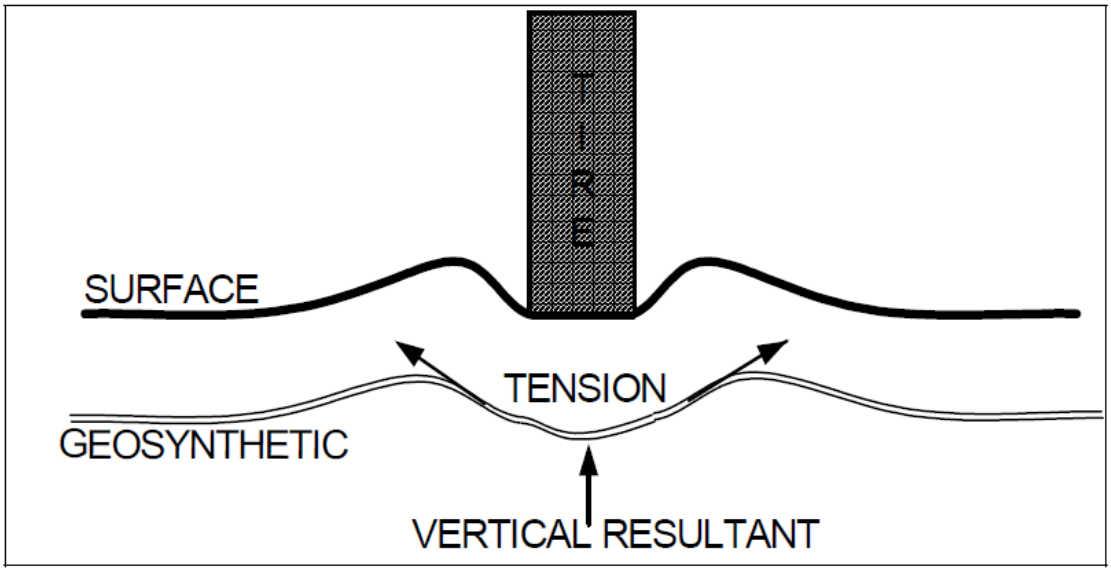

Figure 2.3 Tensioned membrane effect (Maxwell et al. 2005)

For geogrids, not only the rib strength but also the junction strength is important because the soil particles striking through and within the apertures bear loads against the transverse ribs. These loads are transmitted to the longitudinal ribs via the junctions.

2.4 Previous Experimental Studies

Duncan-Williams and Attoh-Okine (2008) conducted an experimental study to evaluate the effect of geogrid on the strengths of granular bases. In their study, standard CBR tests were selected. Unreinforced and reinforced samples were prepared in the CBR molds with the geogrid layer placed at the mid-depth of the sample. The test results showed that the inclusion of the geogrid increased the CBR value of the sample.

Both laboratory tests and field full-scale experiments have shown that the inclusion of a geogrid at the interface between a base curse and a subgrade can improve the performance of the roadway system (Barksdale et al 1984, Al-Qadi 1994, Perkins 1999, Hufenus et al. 2006, and Al-Qadi et al. 2007). A properly placed geosynthetic does improve the performance of an unpaved road. Das et al. (1998) pointed out that the most effective location of the geosynthetic is at the interface of the granular material and the subgrade surface. In this location the geosynthetic provides separation, lateral restraint of the upper granular course, and a tensioned membrane effect when strained extensively.

Plate loading tests were conducted in a large test box at North Carolina State University to evaluate the performance of biaxial geogrid-reinforced bases (Leng, 2002). The dimension of the test box was 1.5 m x 1.5 m x 1.35 m high. A total of

14 cyclic plate loading tests were conducted on granular bases over subgrade. The test results showed that biaxial geogrids improved the performance of the unpaved sections under cyclic loading.

2.5 Design Methods

Several design methodologies have emerged since the late 1970s that address geosynthetic reinforcement for unpaved roads. These methods include: (1) Barenburg et al. (1975), (2) Giroud and Noiray (1981), and (3) Giroud and Han (2004). A brief review of these methods is presented below.

2.5.1 The Barenburg et al. Method

Barenburg et al. (1975) proposed a method that utilizes different bearing capacity factors for unpaved roads with or without a geotextile. "Lateral restraint theory" is the core of this method. This method assumed soft, cohesive subgrade overlain by a crushed-rock aggregate base subjected to less than 100 load repetitions. The vertical stress at the interface between the base and the subgrade was calculated using the Boussinesq solution based on a circular contact area. Small-scale laboratory tests by Barenburg et al. (1975) showed that bearing capacity factors (N_c) of 6 and 3.3 were appropriate for a geotextile-reinforced base and an unreinforced base, respectively. Currently, the United States Army Corp utilizes the same approach for construction of low-volume unpaved roads with minor design improvements made by Steward et al. (1977) and Henry (1999). This design procedure can be summarized as follows:

1. Determine an equivalent cohesion (C) for the subgrade soil, often based on undrained shear strength.
2. Determine a maximum wheel load.
3. Choose the appropriate bearing capacity factor (N_c), where $N_c = 6$ (with geotextile) and $N_c = 3.3$ (without geotextile).
4. Calculate the allowable bearing pressure on the subgrade (p_a), where $p_a = C (N_c)$ for the reinforced or unreinforced base.
5. Determine the crushed-rock aggregate thickness for each base utilizing the corresponding design chart, based on the expected maximum wheel load and the allowable bearing pressure.
6. Choose a geotextile based on installation and environmental considerations, and then determine its cost.
7. Evaluate both reinforced and unreinforced bases to determine the economical solution.

Earlier research by Rodin (1965) indicated that at the onset of localized bearing failure, $N_c = 6.2$ for a rigid footing and $N_c = 3.1$ for a flexible footing. The addition of the geotextile on the subgrade causes the subgrade to fail in the way similar to the rigid footing on the subgrade, which is a general bearing failure rather than a local bearing failure. Steward et al. (1977) extended the Barenburg et al. (1975) method to address a slightly greater number of load repetitions by further reduction of the recommended bearing capacity factors. The Barenburg et al. (1975) design method

did not take into consideration of geotextile properties, such as its strength and modulus.

2.5.2 The Giroud and Noiray Method

Giroud and Noiray (1981) considered the effect of the tensile modulus of the geotextile on the required base thickness using the tensioned membrane theory. In their study, Giroud and Noiray (1981) assumed a soft, saturated clay subgrade that is undrained and a granular base that has a California Bearing Ratio (CBR) of at least 80. In addition, Giroud and Noiray (1981) assumed a rectangular contact area and a fixed stress distribution angle. A stress distribution method was used to estimate the vertical stress at the interface of the base and the subgrade. Henry (1999) compared the Giroud and Noiray method with the Barenburg et al. method and demonstrated their differences.

2.5.3 The Giroud and Han Method

Giroud and Han (2004) developed a unified equation for determining the required base course thickness for unreinforced, geotextile-reinforced, and geogrid-reinforced bases over an undrained, cohesive subgrade. This method considered the type of the geosynthetic, the aperture stability modulus of the geogrid, the modulus of the base course, and the modulus of the subgrade in addition to the traffic volume, the wheel load, the tire pressure, the undrained shear strength of subgrade, and the rut depth as considered in other design methods. Different bearing capacity factors were

suggested for unreinforced, geotextile-reinforced, and geogrid-reinforced bases.

Different from the Giroud and Noiray Method, the Giroud and Han Method assumed a circular tire contact area and considered the effect of the base course stiffness, which is empirically correlated to the California Bearing Ratio of the base. This is an important feature of the Giroud and Han method. This consideration is consistent with the conclusion by Barber et al. (1978) that the base course *CBR* value plays an important role in the number of axle passes an unpaved road could carry. Another significant difference between the Giroud and Noiray method and the Giroud and Han method is the consideration of the stress distribution angle. In the Giroud and Noiray method, the stress distribution angle is fixed while in the Giroud and Han method, the stress distribution angle changes with the number of passes, the thickness of the base, the radius of the contact area, and the geosynthetic reinforcement, which make this design method more realistic.

Giroud and Han (2004a, b) selected the aperture stability modulus (ASM) of a geogrid as the performance property when they developed the method for geogrid-reinforced unpaved roads. ASM is an index representing the in-plane stiffness of the geogrid by measuring the torsional load required to twist the geogrid node to a particular in-plane angular distortion. This procedure is to quantify the combined effect of the tensile modulus and the junction strength. Webster (1993) and Kinney (1995) correlated the performance of geogrid-reinforced bases to ASM. However, there is no consensus standardized test method for ASM (J) at this time.

Iowa State University conducted a series of experiments (White et al. 2007) to evaluate geogrid-reinforced bases using the Giroud and Han method and the equation developed by the U.S. Army Corps of Engineers in 1989 for low-volume roads (Bolander et al.). Figure 2.4 shows the rut development versus the subgrade CBR value under different loading cycles. Figure 2.5 shows the rut development versus the subgrade CBR value at different base thicknesses. Figure 2.6 shows the rut development versus the subgrade CBR value under different axle loads.

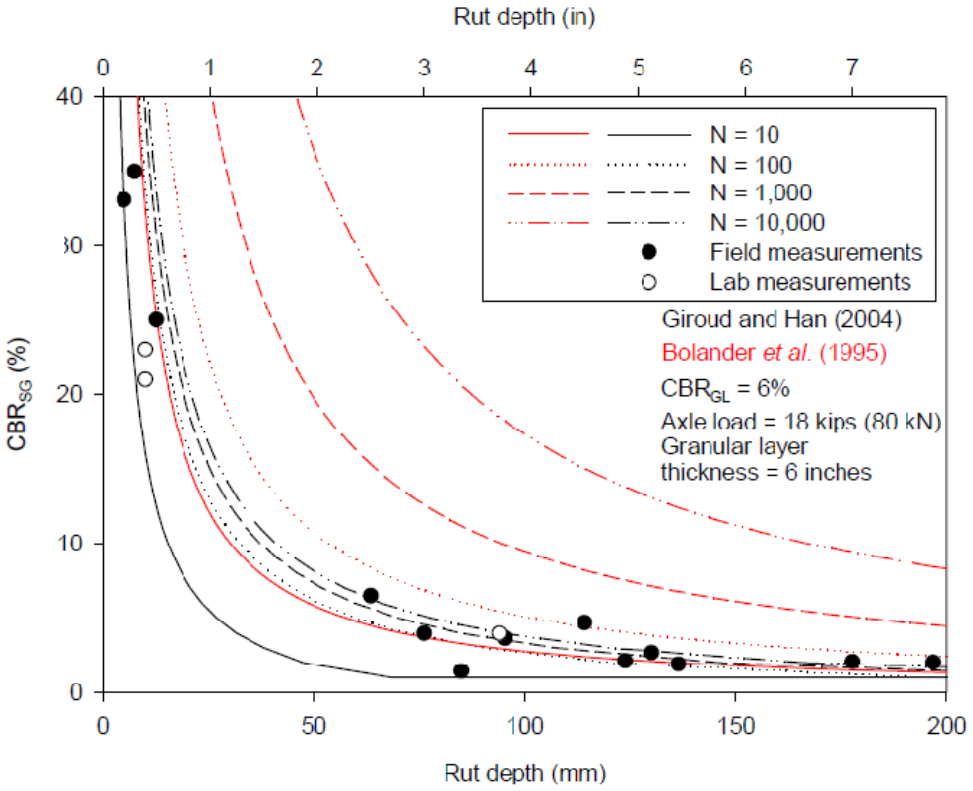

Figure 2.4 Rut depth versus subgrade CBR at different load cycles (White et al. 2007)

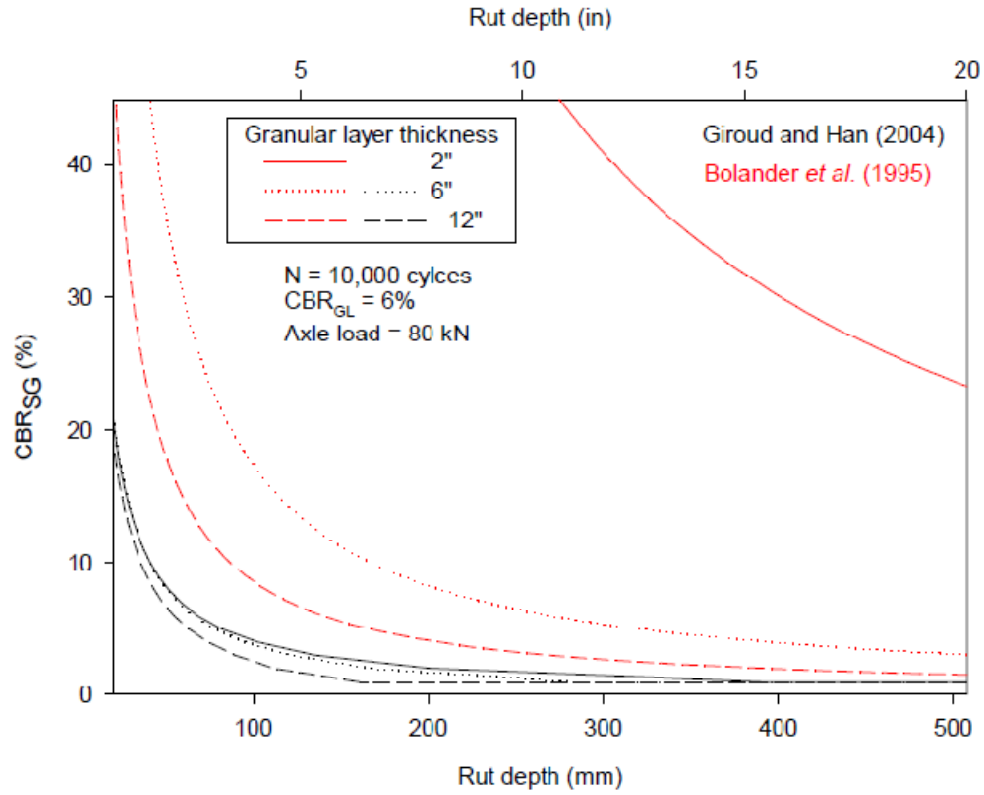

Figure 2.5 Rut depth versus subgrade CBR at different base thicknesses (White et al. 2007)

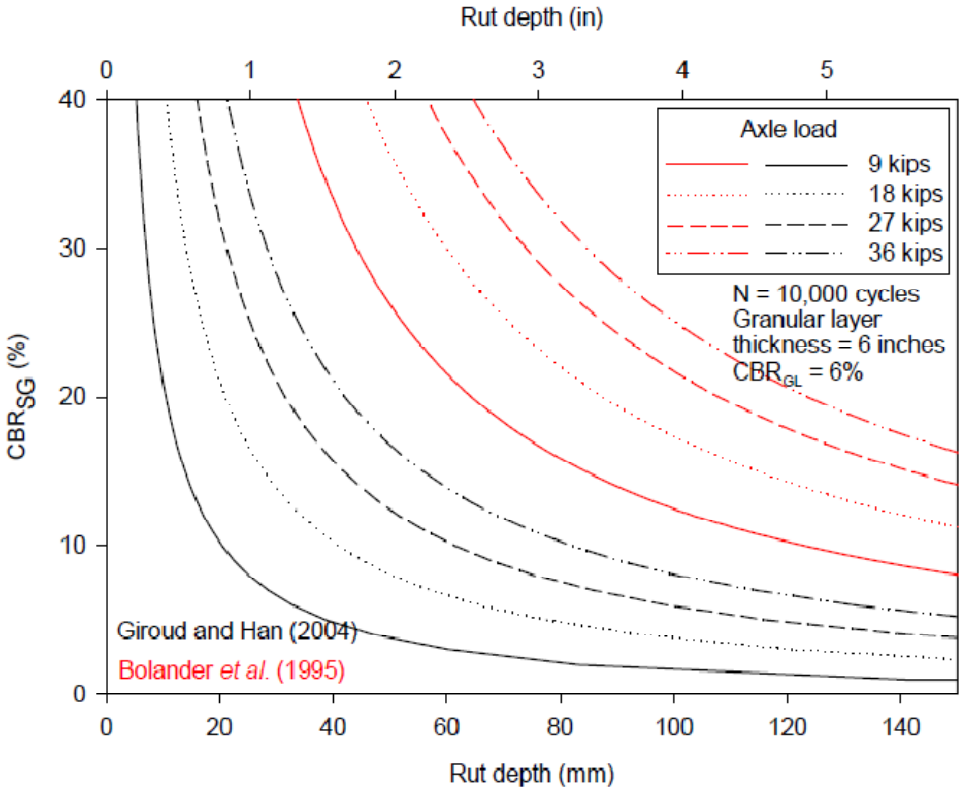

Figure 2.6 Rut depth versus subgrade CBR at different axle loads (White et al. 2007)

The following paragraph summarizes the findings from the above figures:

1. The measured rut depths are in reasonable agreement with those estimated using the Giroud and Han method. This comparison indicates that the Giroud and Han method is applicable for designing granular shoulders. The method proposed by the U.S. Army Corps of Engineers, however, appears to overestimate the rut depths.
2. The Giroud and Han method indicates that an increase of the thickness of the granular layer results in a slight reduction in the rut depth value. This method considers the CBR of the subgrade as the controlling factor for the rut depth. The reduction in the rut depth value is more substantial, however, if the U.S. Army Corps of Engineers' design method is used.
3. Both methods indicate that rut depth increases considerably with the axle load. The axle load is therefore an important factor for the rut depth development.

2.6 Summary

Geogrid, a major type of geosynthetics, has been commonly used for soil reinforcement. Laboratory and field test data have demonstrated the improved performance of geogrid-reinforced roads. In the past, biaxial geogrids have been commonly used for unpaved roads. Triangular aperture geogrid is a geogrid recently introduced in the market, which is expected to have more uniform tensile strength and stiffness in all directions. Research is needed to evaluate the performance of this new type of geogrid.

Studies have confirmed that geogrids can make the following contributions when they are placed at the interface of the base and the subgrade: (1) confinement of aggregate particles, (2) increase of the base modulus, (3) reduction of the shear stress at the interface, (4) increase of the stress distribution, and (5) tensioned membrane effect.

Laboratory cyclic plate loading tests in a large box have been successfully used by researchers to evaluate the performance of geogrid-reinforced unpaved road sections.

Different design methods have been developed in the past to estimate the required base thickness for unreinforced, geotextile-reinforced, and geogrid-reinforced unpaved road sections. These methods should be verified against the triangular aperture geogrid.

Chapter 3 EXPERIMENTAL STUDY

3.1 Test Materials

3.1.1 Geogrid

Three triangular aperture geogrids (a regular duty grade, T1; a medium duty grade T2; and a heavy duty grade, T3), made of polypropylene, were used in this experimental study. Some properties of these geogrids are presented in Table 3.1. For the three triangular aperture geogrids, all physical properties increase from T1, T2, to T3.

The three geogrids included in this study are all of the same "family" of geogrids, i.e., a family of geogrids being defined as having the same manufacturing type (same manufacturer with identical polymer, process method and equipment), and only differing in one variable of product design. T1, T2 and T3 differ only in that different thicknesses of starting sheet are used in manufacturing the three geogrids and all other chemical and physical parameters that influence end-product characteristics are the same. For this particular family of products and manufacturing process (extruded sheet which is then punched and then stretched), the resulting end products differ essentially in terms of levels of robustness, unit weight, rib thicknesses, and mechanical properties. By performing tests on representative product variants from within a given geogrid family and establishing correlations to performance based on indicative or characteristic properties of the specific geogrid family tested, reliable predictions of performance can be made for untested geogrids

provided they are members of the same family of geogrids. The data from this particular study, provided it is combined with other results of performance testing conducted by other researchers using the same family of geogrid, can provide a basis for the development of a design method for geogrid-reinforced bases for the family of triangular aperture geogrids.

3.1.2 Base material

AB3 aggregate, commonly used in Kansas, was used as the material for the base course. This material has the following physical properties: specific gravity (Gs) =2.69, liquid limit (LL) =20, plastic limit (PL) =13, mean particle size (d_{50}) =7.0 mm, coefficient of curvature (C_c) =2.25, and coefficient of uniformity (C_u) =133. The grain size distribution of AB3 is presented in Figure 3.1. Compaction tests were performed to obtain the compaction curve as shown in Figure 3.2. The maximum dry density is 2.08 g/cm^3, which corresponds to the optimum moisture content of 10.2%. A series of laboratory unsoaked CBR tests (ASTM D 1188) for the subgrade were performed at different water contents. The CBR vs. moisture content curve is presented in Figure 3.3. To examine the effect of the base course stiffness, the base courses were compacted to two California Bearing Ratios (CBR) at approximately 5% and 20%. The CBR values were mainly estimated by the dynamic cone penetration (DCP) tests after the preparation of the base course in the large test box.

3.1.3 Subgrade material

The weak subgrade was an artificial soil composed of a mixture of 75 percent Kansas River sand and 25 percent kaolin by weight. The grain size distribution of Kansas River sand is presented in Figure 3.1. Compaction tests were performed to obtain the compaction curve as shown in Figure 3.4. The maximum dry density is 2.01 g/cm^3, which corresponds to the optimum moisture content of 10.8%. A series of laboratory unsoaked CBR tests (ASTM D 1188) for the subgrade were performed at different water contents. The CBR vs. moisture content curve is presented in Figure 3.4. The subgrade soil was compacted at a water content of 11.4% for the box tests to achieve its CBR at approximately 2%, which was verified by vane shear and DCP tests. In some tests, however, the subgrade was compacted to achieve its CBR at approximately 3% to investigate the influence of the subgrade strength on the performance.

Table 3.1 Index Properties of triangular aperture geogrids

Index Properties	Longitudinal			Diagonal			Transverse			General		
	T1	**T2**	**T3**	**T1**	**T2**	**T3**	**T1**	**T2**	**T3**	**T1**	**T2**	**T3**
Rib pitch (mm)	40	40	40	40	40	40						
Mid-rib depth (mm)				1.7	1.8	2.3	1.5	1.5	1.8			
Mid-rib width (mm)				1.1	1.1	1.2	1.3	1.3	1.3			
Rib shape										rectangular	rectangular	rectangular
Aperture shape										triangular	triangular	triangular

T1 – Regular Duty, T2 – Medium Duty, T3 – Heavy Duty

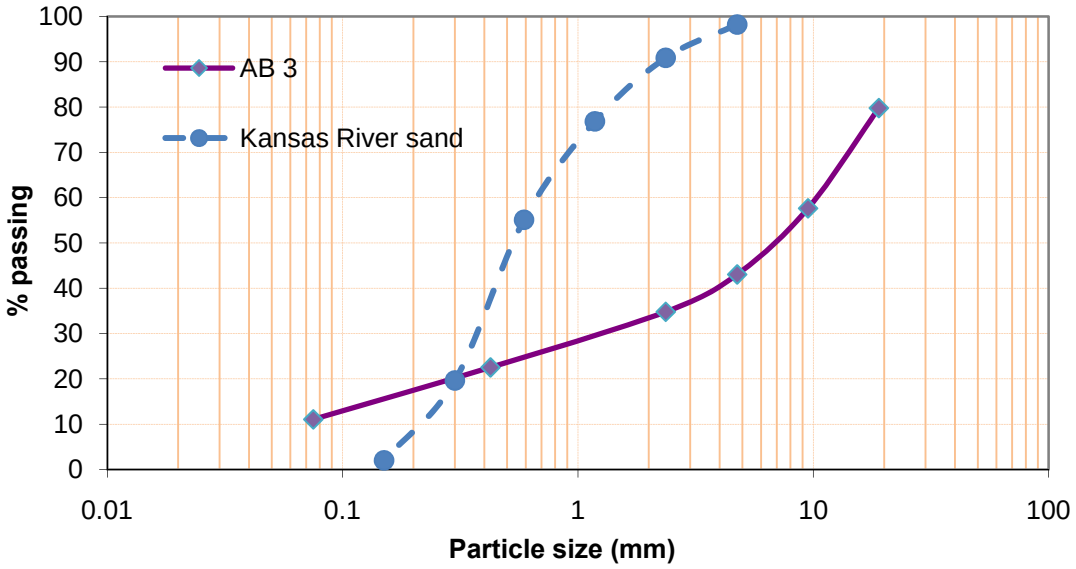

Figure 3.1 Grain size distribution curves of Kansas River sand (Han et al. 2008) and AB3 aggregate

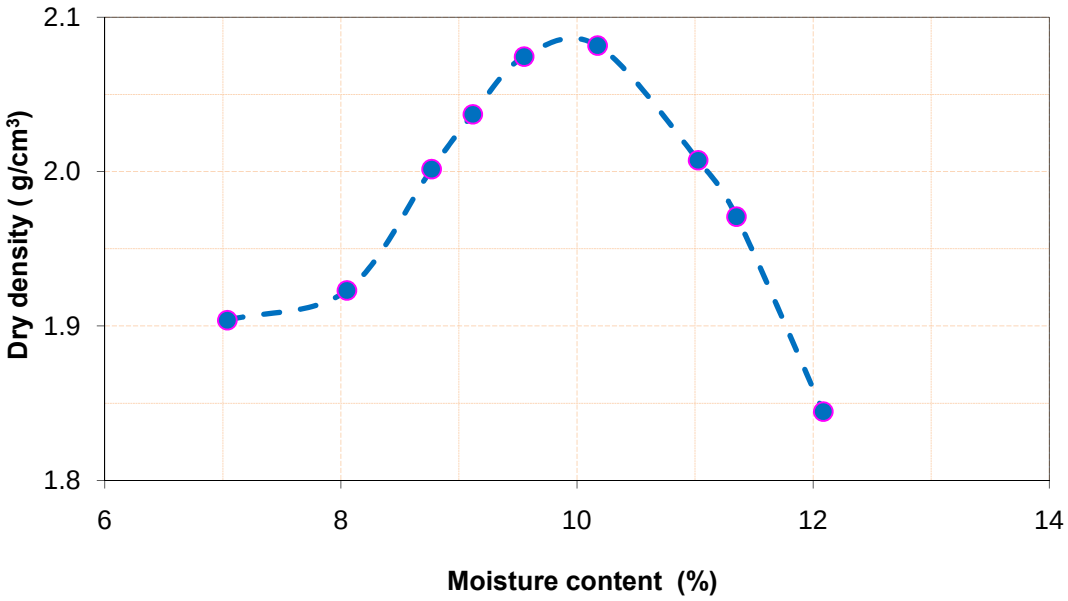

Figure 3.2 Compaction curve of the AB3

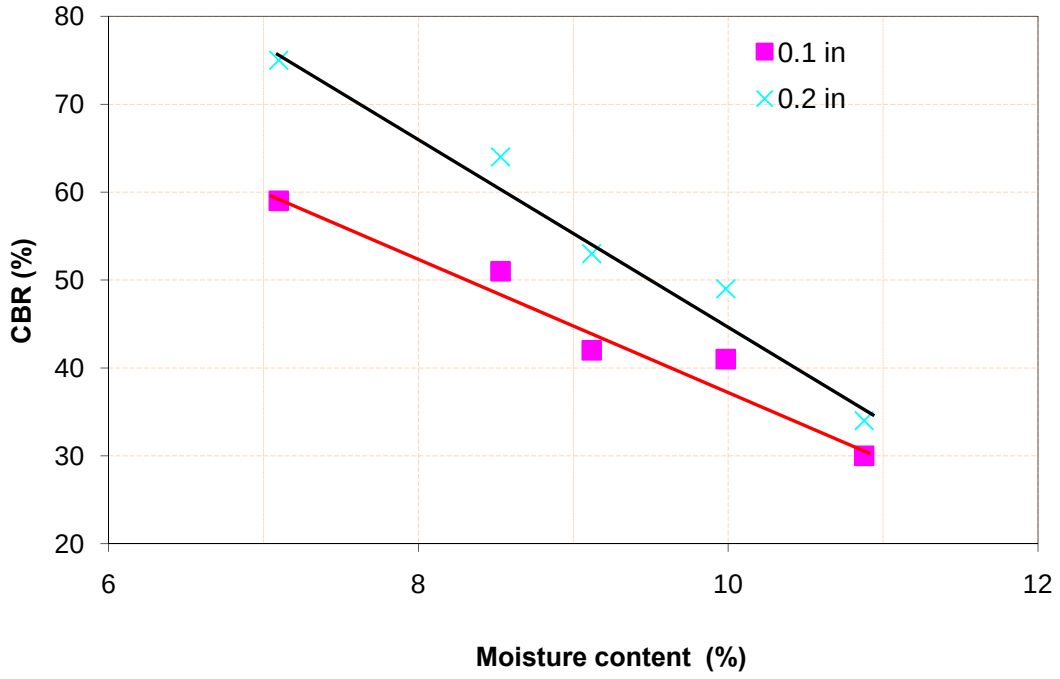

Figure 3.3 CBR vs. moisture content of the base course

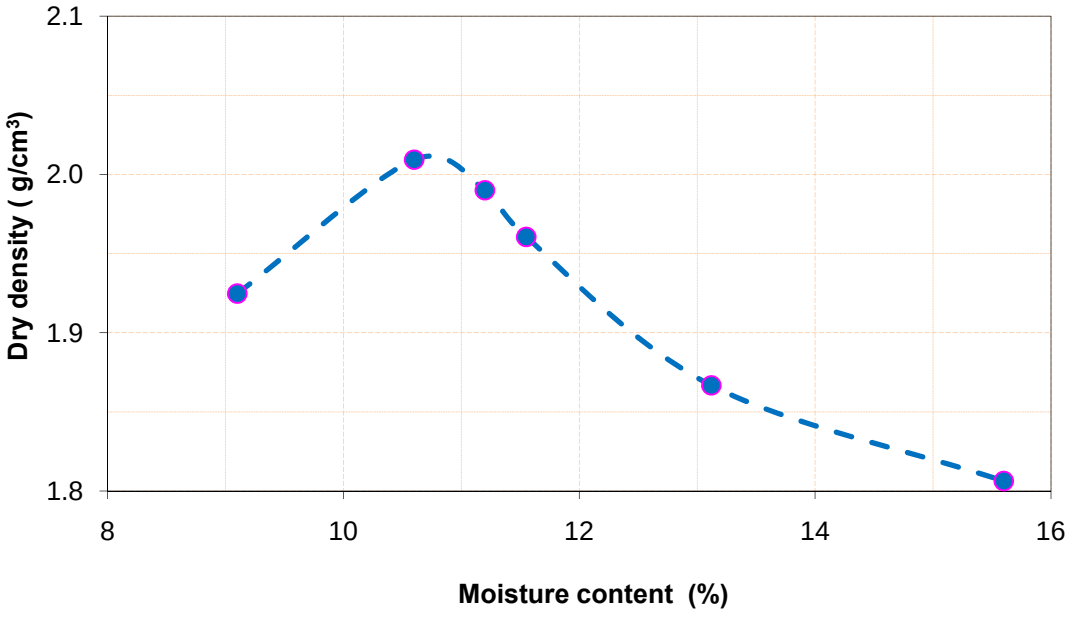

Figure 3.4 Compaction curve of the subgrade

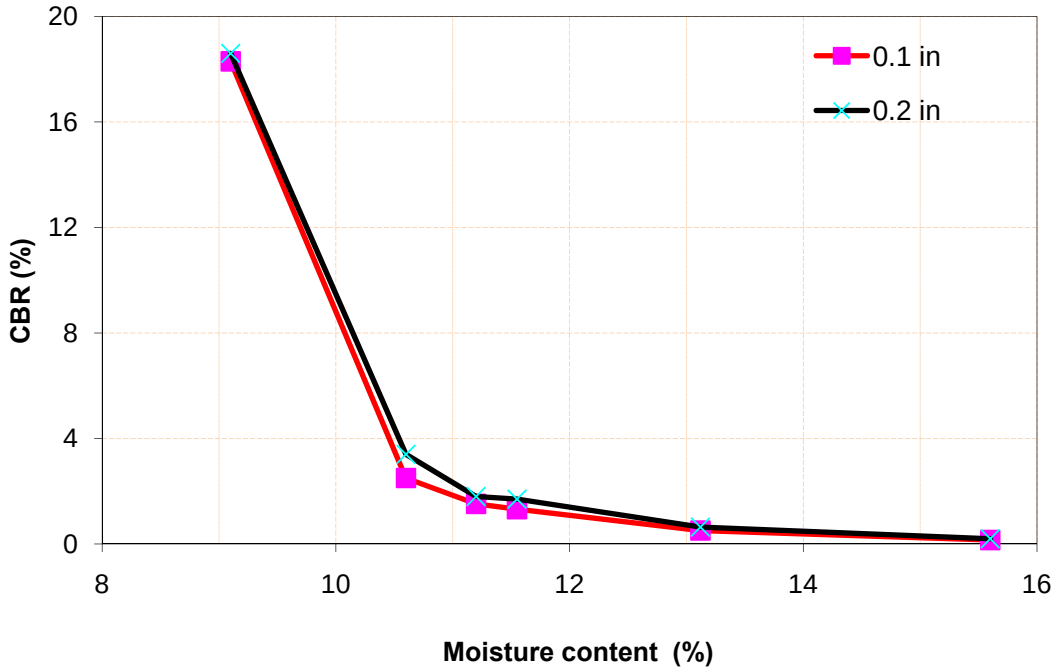

Figure 3.5 CBR vs. moisture content of the subgrade

3.2 Test Equipment

Cyclic plate loading tests were conducted in a large test box system designed and fabricated for the geotechnical laboratory at the Department of Civil, Environmental, and Architectural Engineering at the University of Kansas. This system includes a loading actuator, a data acquisition system, and a steel box (2 m x 2.2 m x 2 m high).

The loading system was an MTS hydraulic loading system. The steel loading plate had a diameter of 30 cm. For both unreinforced and reinforced tests, cyclic loading tests were conducted. The cyclic loading waves were generated with a peak force of 40 kN and a trough force of 0.5 kN as shown in Figure 3.6. The frequency of this wave was 0.77 Hz. The peak load was selected to simulate a single wheel load of 40

kN (equal to an axle load of 80 kN and a contact pressure of 566 kPa).

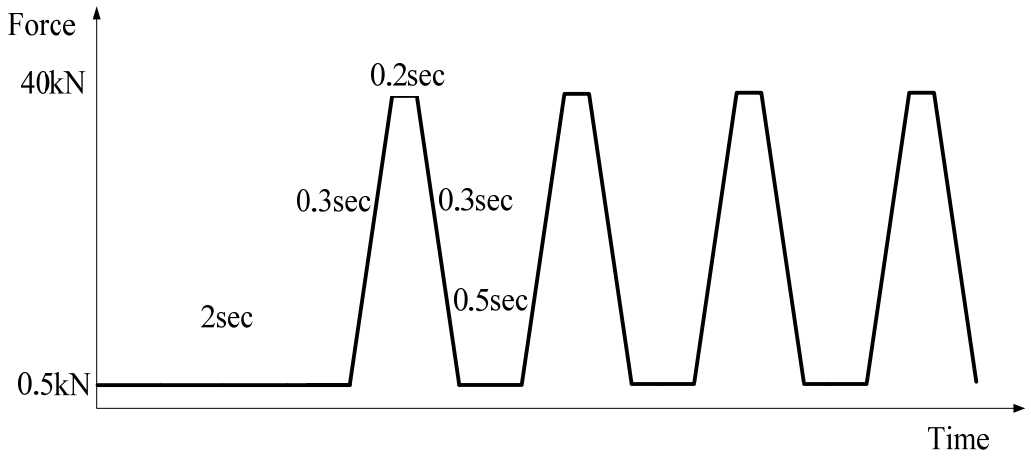

Figure 3.6 Cyclic loading wave

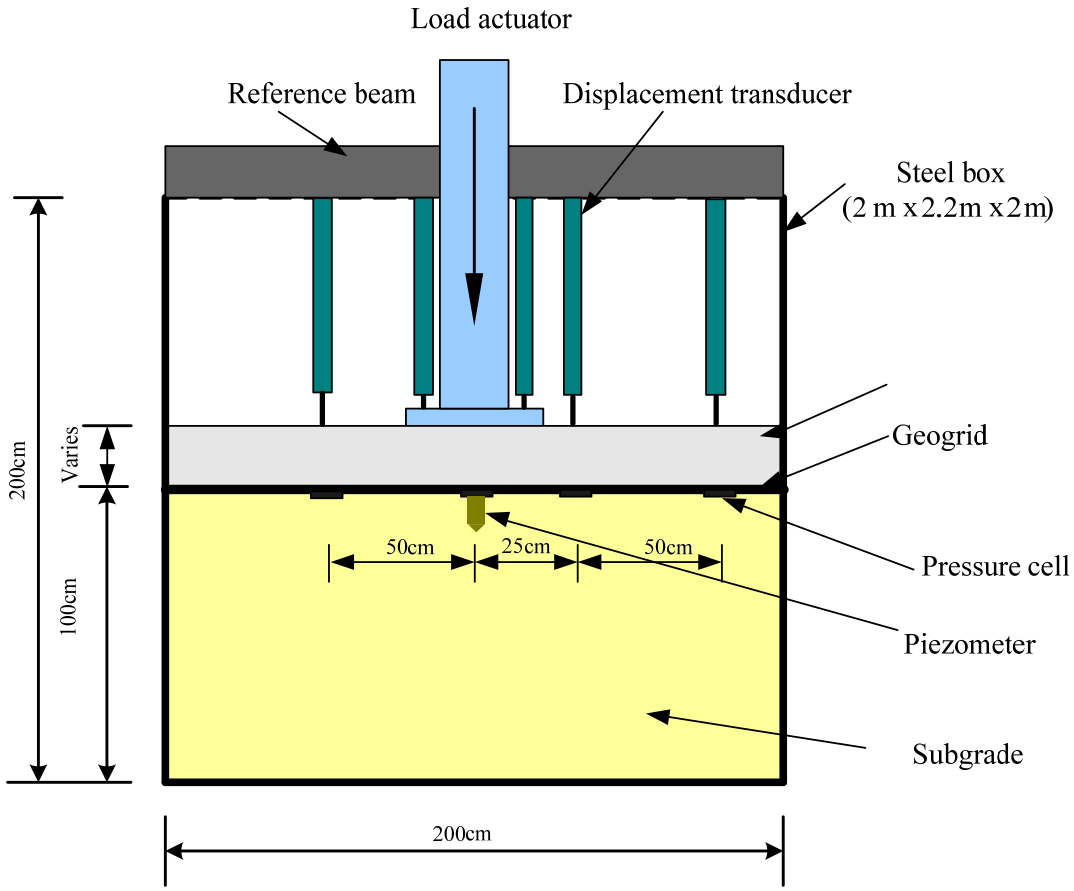

Figure 3.7 Configuration of plate load test

The instrumentation and data acquisition system included four earth pressure cells,

five displacement transducers, and two piezometers. Details of the test box system and the reinforced section are illustrated in Figure 3.7 as an example.

The subgrade was placed and compacted in four layers (150 mm thick for each layer) at the moisture content of 11.4% for the top 600 mm subgrade. The base course was compacted to a thickness of approximately 150 mm, 230 mm, or 300 mm at the moisture content of 8.9%. The geogrid was placed at the interface between the subgrade and the base course in each reinforced test section.

Figure 3.8 shows the actual test box and cyclic loading system in the laboratory.

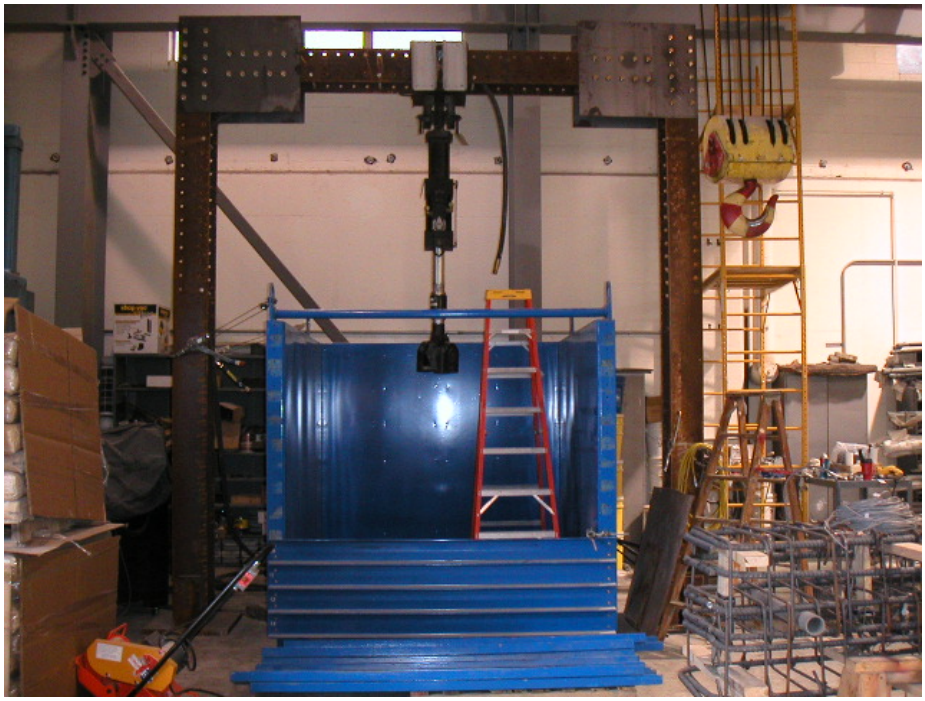

Figure 3.8 The test box and cyclic loading system

Figure 3.9 shows the compaction of the soil using the vibratory compactor. The level of compaction was controlled by the volume of the soil and the number of passes.

Figure 3.9 Compaction of soil using the vibratory compacter

Figure 3.10 shows the hand-operated vane shear test device used to control the CBR value of the subgrade soil after each lift of compaction. The range of the vane shear strength of the subgrade was controlled between 36 kPa and 43 kPa, usinging the correlation obtained in this study as follows:

$$CBR=C_U/20.5 \quad (3.1)$$

where C_U = undrained shear strength of the subgrade (kPa)

Figure 3.10 A vane shear test

Dynamic Cone Penetration (DCP) tests were conducted after the preparation of the subgrade and the base course to verify the strength and stiffness of the subgrade and the base course. Another four DCP tests were performed after each test. The locations of these tests were distributed within the test box. Only the DCP data after each test are reported in this thesis and will be presented later. The relationship between the DCP test result and the CBR value is presented below:

$$CBR=292/(PI \times 25.4)^{1.12} \quad (3.2)$$

where PI = Penetration Index (in/blow). There are also other formulas to calculate

the CBR value from the Penetration Index, however, Eq. (3.2) worked well in this study.

Figure 3.11 A dynamic cone penetration (DCP) test

Figure 3.12 shows an earth pressure cell used in this study. The diameter and thickness of this pressure cell are 50 mm and 11.3 mm, respectively. However, the diameter of the sensing area is 46 mm. Four earth pressure cells were used for each test section. They are strain gauge-type pressure cells, which are suitable for measuring dynamic earth pressures under cyclic loading.

Figure 3.13 shows a piezometer used to measure pore pressure for a few earlier tests

during the cyclic loading. Two piezometers were used in each section of those tests. They are strain gauge type-sensors. Since there was no noticeable relationship between the measured pore pressure and the cyclic loading, they were not used in later tests.

Figure 3.12 An earth pressure cell

Figure 3.13 A piezometer

Figure 3.14 shows the setup of the displacement gauges in each test. They are also strain gauge-type sensors and had two maximum measurement ranges: 10 cm and 5 cm. The displacement gauges with 10 cm measurement range were placed at the top of the loading plate and at the location 25 cm away from the center. The displacement gauges with 5 cm measurement length were placed at the locations 50 cm and 75 cm away from the center.

Figure 3.14 Setup of the displacement gauges

Figure 3.15 shows the GeoGauge used in this study for a few earlier tests. GeoGauge was used to measure the stiffness of the base course. Due to the difficulty in seating this device, the test results were not consistent. Therefore, it was not used for the later tests.

Figure 3.15 GeoGauge

3.3 Test Plan

Table 3.2 presents the test plan implemented in this study. Totally 19 cyclic plate loading tests were performed, which included 5 unreinforced test sections and 14 geogrid-reinforced test sections. There were three base course thicknesses. Three repeated tests were done to verify the repeatability of the test method.

Most tests were conducted on the base course at 20% CBR over the subgrade at 2% CBR unless noted otherwise.

Table 3.3 Test plan

Geogrid	Base course thickness		
	15 cm	23 cm	30 cm
Unreinforced	3[#@]	1	1
T1	1	3[*#]	1
T2	2[@]	1	2[*]
T3	2[@]	1	1

* one repeated test

one test with subgrade CBR=3%

@ one test with base course CBR=5%

3.4 Test Data

Significant amounts of test data were generated from 19 cyclic plate loading tests. The test results are presented for each test section including the DCP test profiles which were obtained prior to cyclic plate loading test, the permanent displacement at the center vs. the number of cycle, the maximum vertical stress vs. the number of cycle, and the surface profiles before and after testing. This section only provides the reduced test data and the analyses of these data will be provided in Chapter 4.

3.4.1 15 cm thick unreinforced base

Figure 3.16 shows the DCP test profiles for the 15 cm thick unreinforced base over weak subgrade. DCP tests were conducted at four randomly selected locations. The average penetration index was calculated at the same depth from the four profiles, which were used to obtain the CBR value for each test. The conversion from the DCP penetration index to the CBR value will be presented in Chapter 4. The average profile is shown in a dash line in Figure 3.16. The same approach was used to analyze the DCP data for all the other tests.

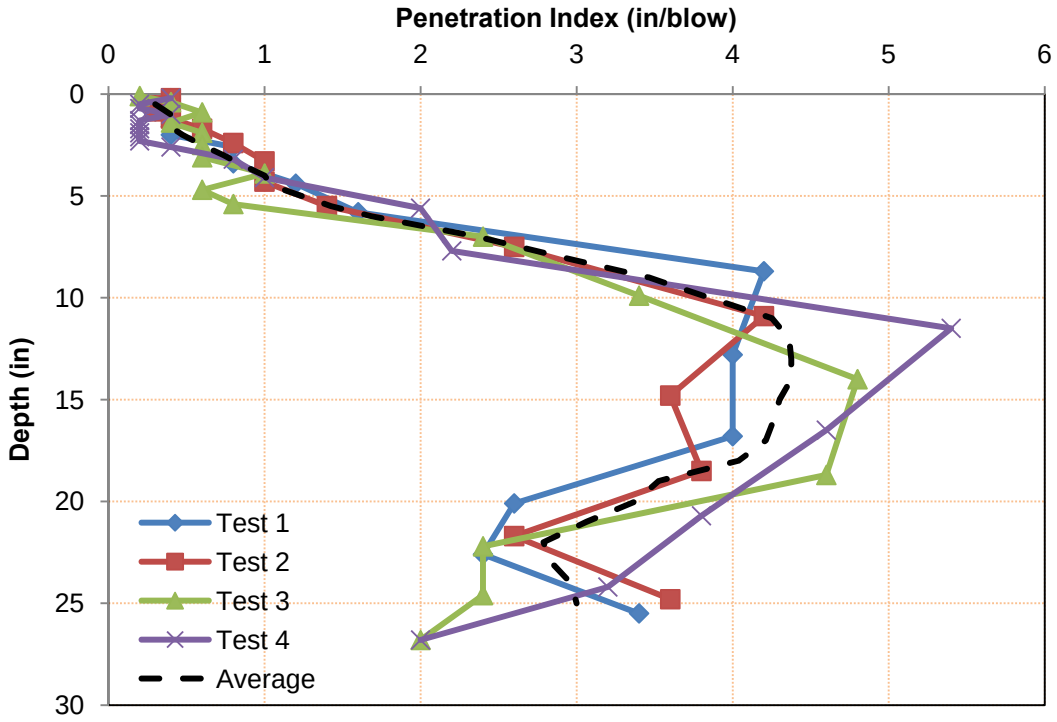

Figure 3.16 DCP test data for 15 cm thick unreinforced base

Figure 3.17 shows the permanent displacement of the loading plate versus the number of cycle for this test section. The permanent displacement was obtained from the lowest point of displacement in each cycle. The displacement during each cycle is shown in Figure 3.18.

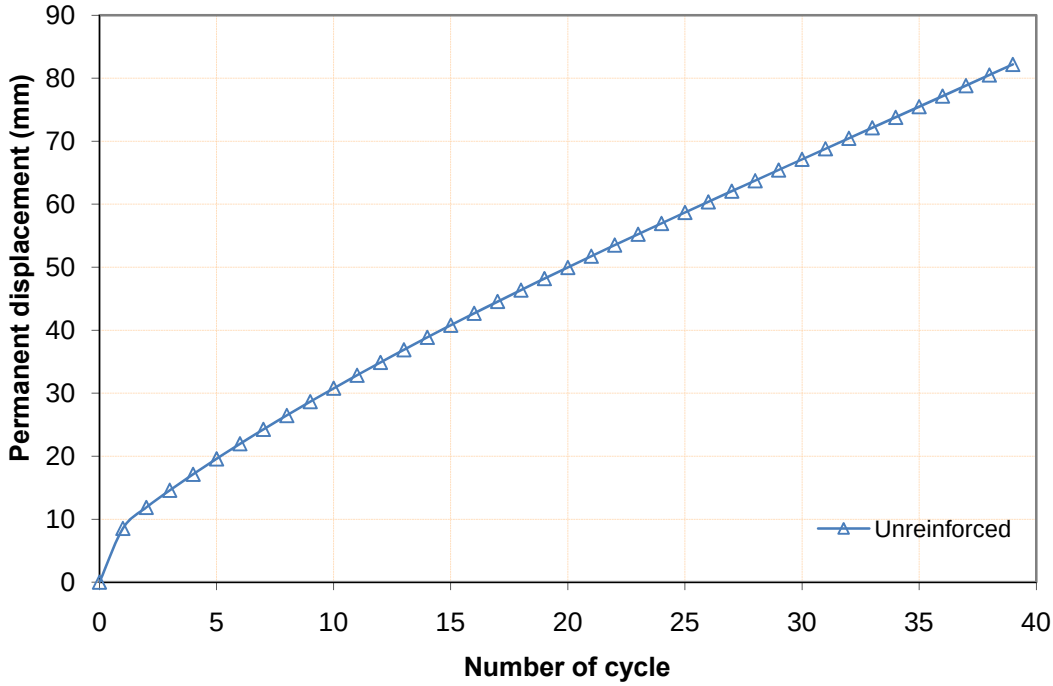

Figure 3.17 Permanent displacement of the loading plate vs. the number of cycle for 15 cm thick unreinforced base

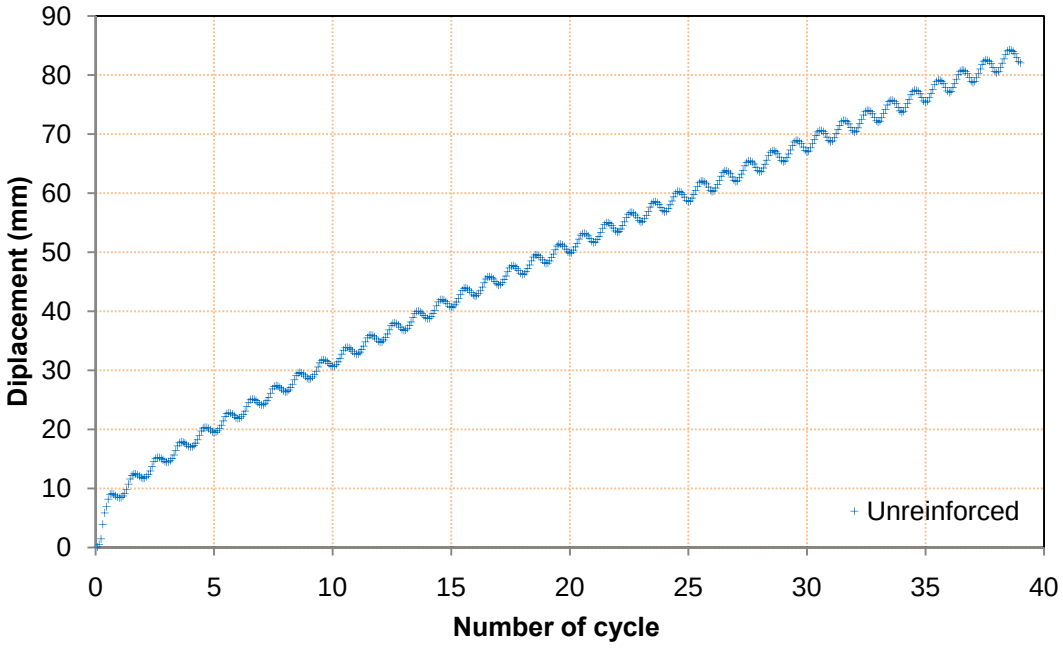

Figure 3.18 Displacement of the loading plate vs. the number of cycle for 15 cm thick unreinforced base

Figure 3.19 shows the maximum vertical stress at the center and the interface between the base course and the subgrade versus the number of cycle for the 15 cm unreinforced base course. The maximum vertical stress was obtained from the highest stress level of the measured curve from the earth pressure cell for each cycle.

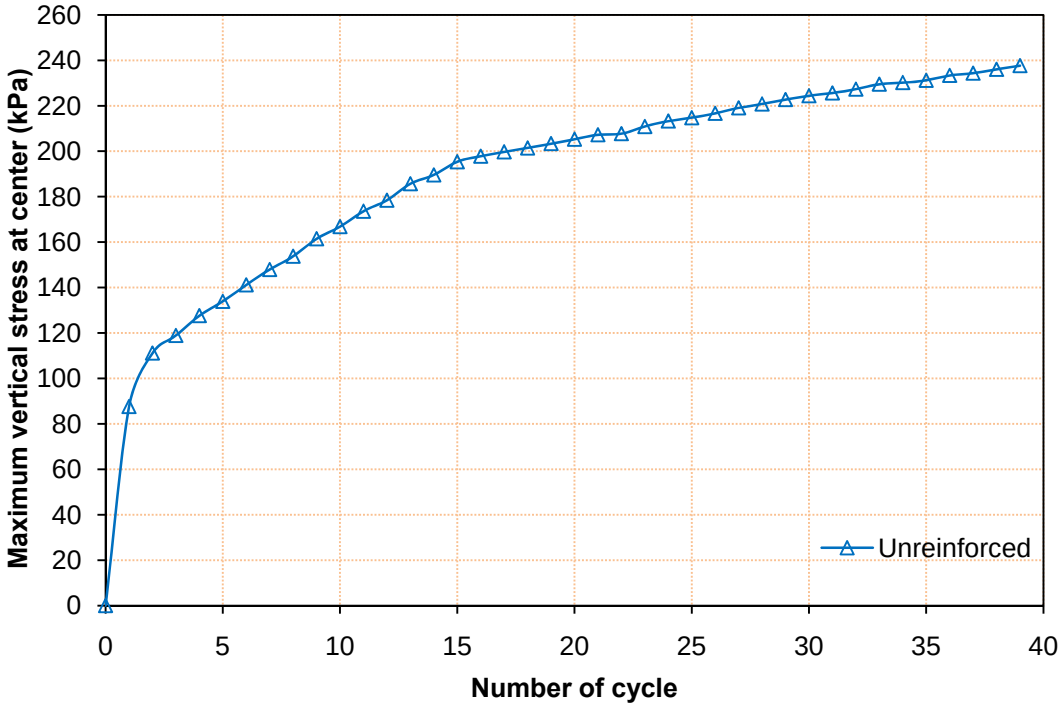

Figure 3.19 Maximum vertical stresses at the center and the interface between the base course and the subgrade for 15 cm thick unreinforced base

Figure 3.20 shows the surface profiles of the base course before and after the test and the subgrade after the test. The profiles for each test were measured manually.

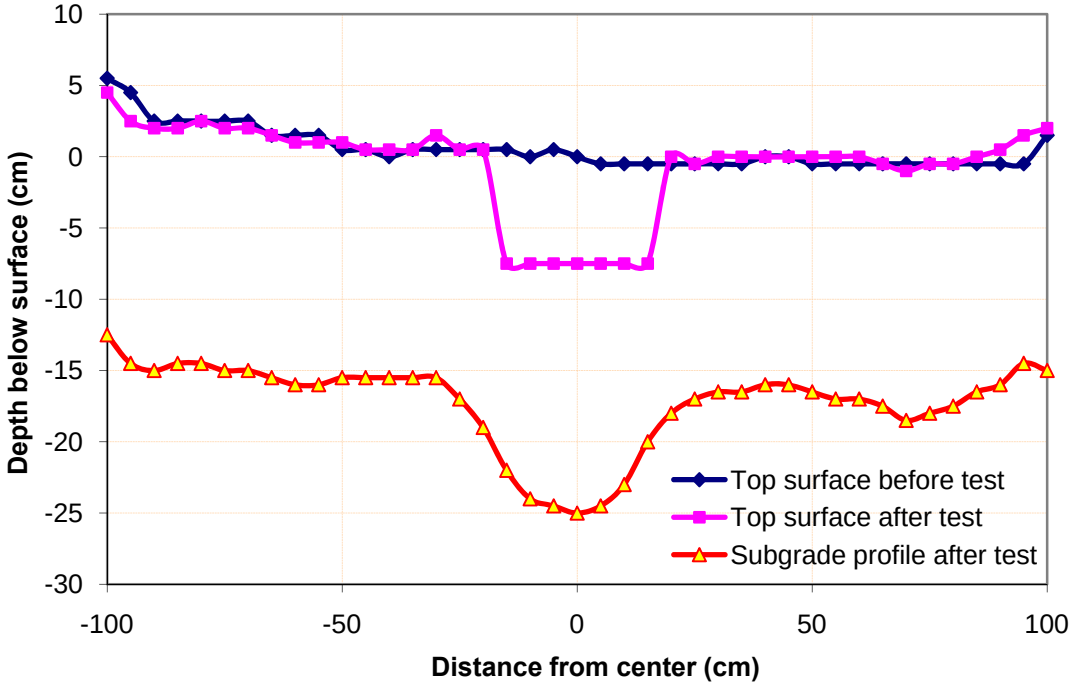

Figure 3.20 Surface profiles for 15 cm thick unreinforced base

3.4.2 15 cm thick base reinforced with T1 geogrid

Figures 3.21, 3.22, 3.23, and 3.24 show the results of DCP penetration index profiles, the permanent displacement of the loading plate versus the number of cycle, the maximum vertical stress at the center and the interface between the base and the subgrade, and the surface profiles of the 15 cm thick T1 geogrid-reinforced base over the weak subgrade.

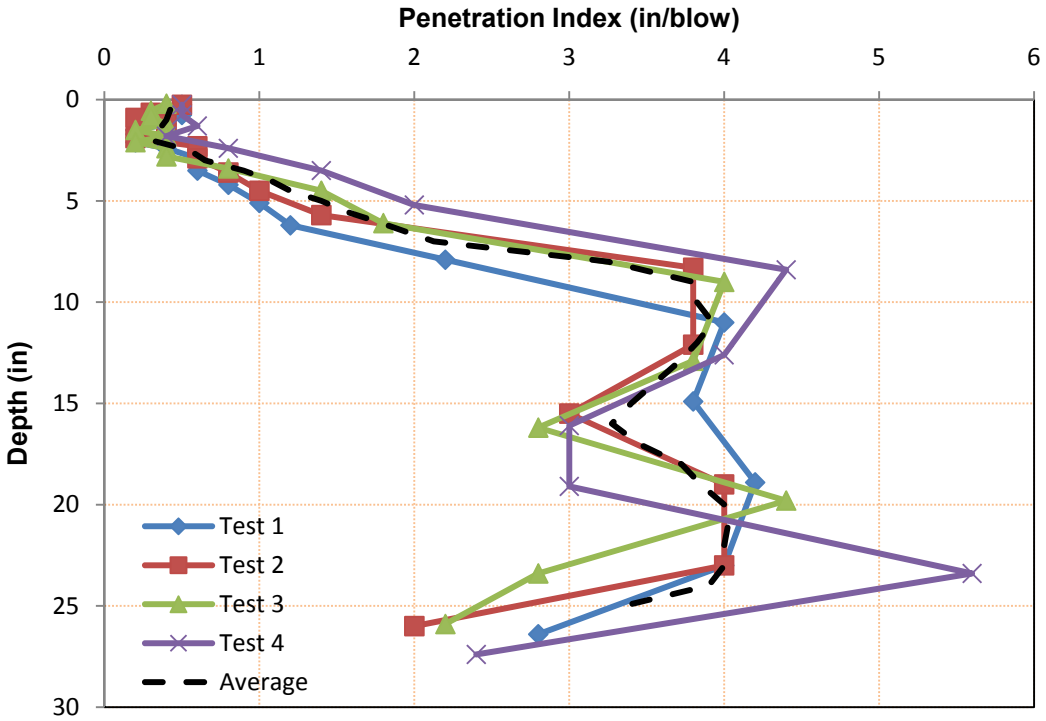

Figure 3.21 DCP test data for the 15 cm thick T1 geogrid-reinforced base

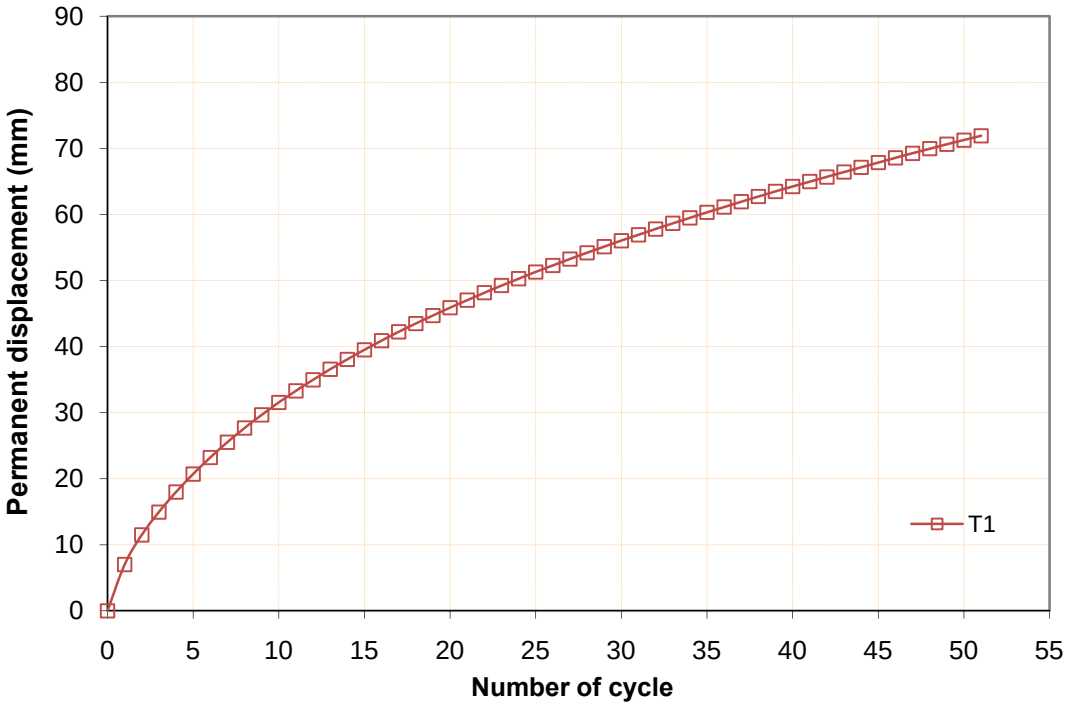

Figure 3.22 Permanent displacement of the loading plate versus the number of cycle for the 15 cm thick T1 geogrid-reinforced base

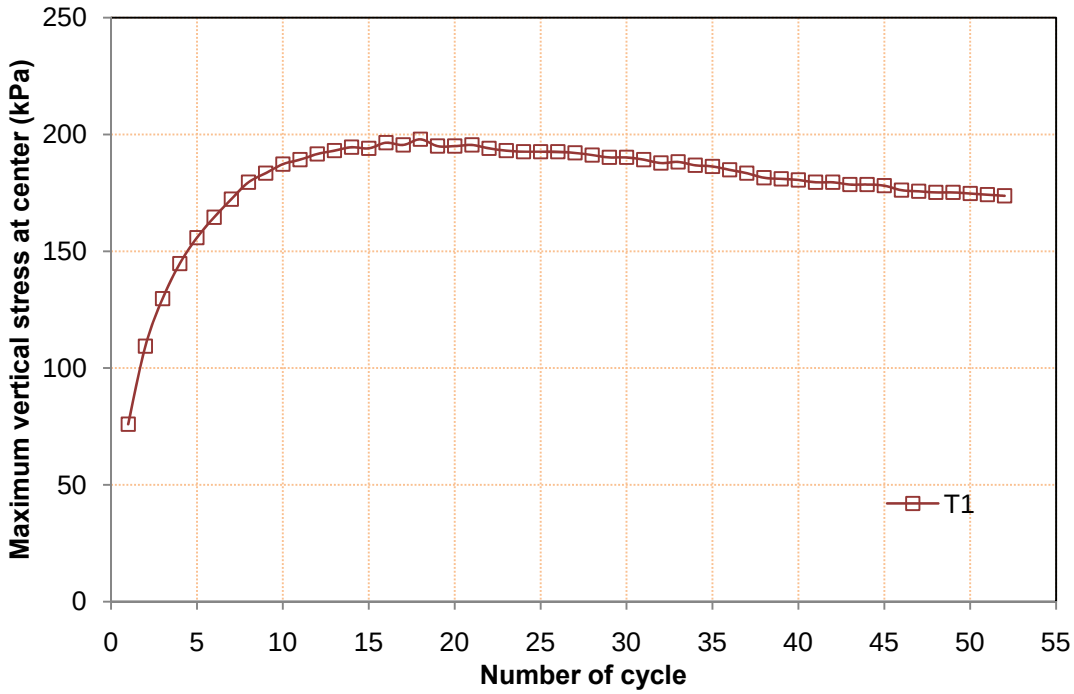

Figure 3.23 Maximum vertical stresses at the center and the interface between the base and the subgrade for 15 cm thick T1 geogrid-reinforced base

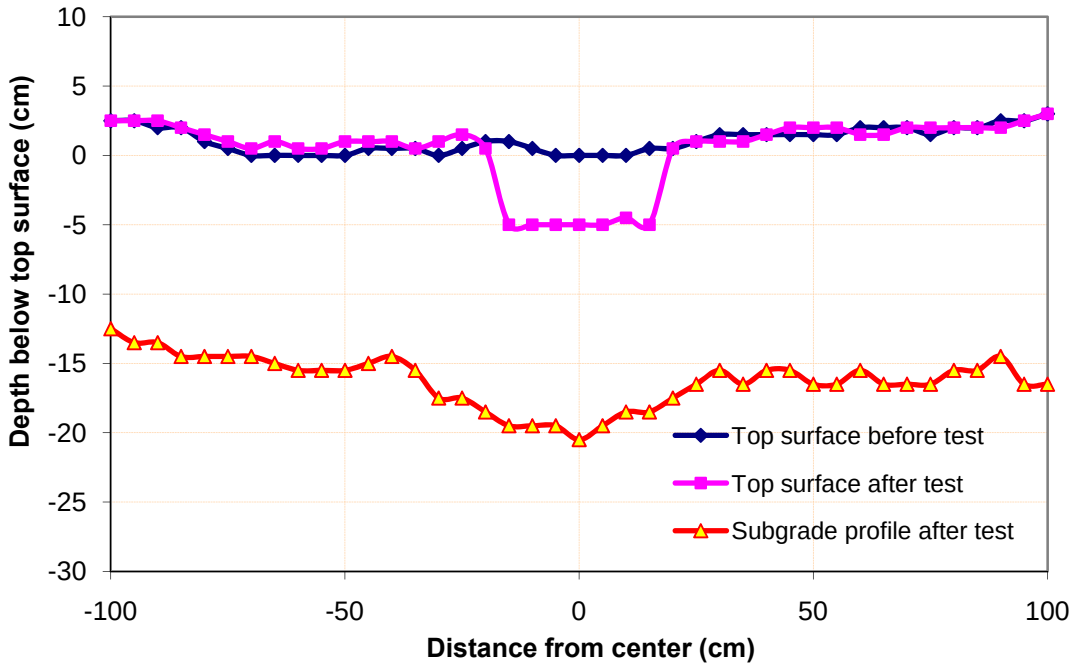

Figure 3.24 Surface profiles of the 15 cm thick T1 geogrid-reinforced base before and after loading

3.4.3 15 cm thick base reinforced with T2 geogrid

Figures 3.25, 3.26, 3.27, and 3.28 show the results of DCP penetration index profiles, the permanent displacement of the loading plate versus the number of cycle, the maximum vertical stress at the center and the interface between the base and the subgrade, and the surface profiles of the 15 cm thick T2 geogrid-reinforced base over the weak subgrade.

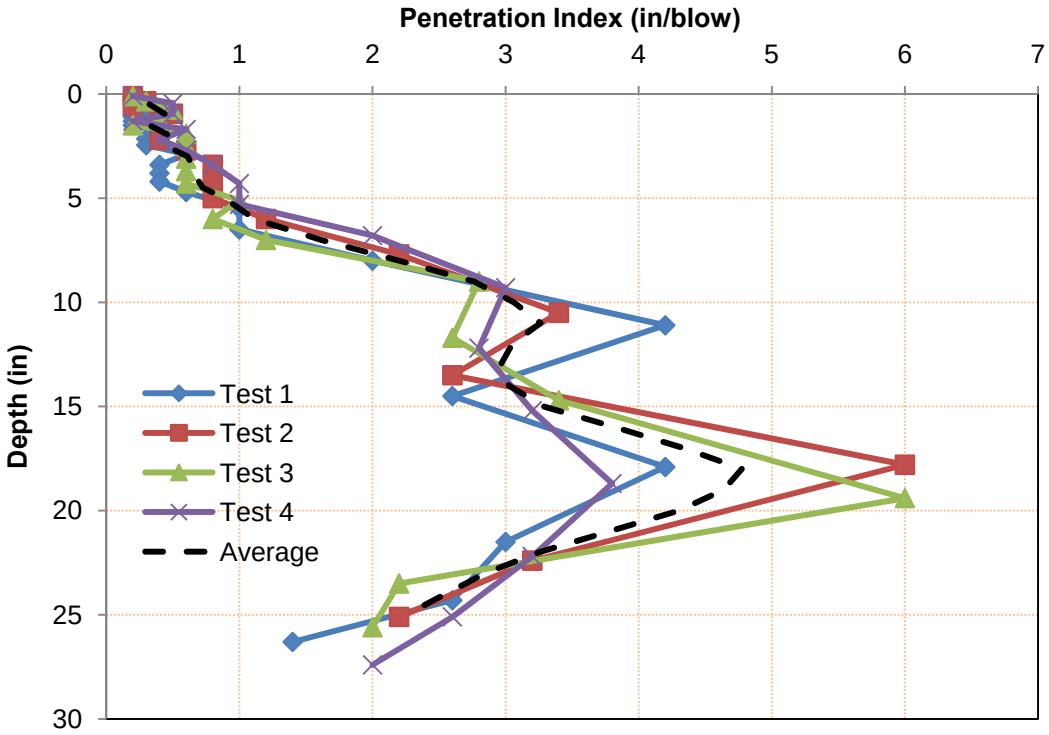

Figure 3.25 DCP test data for 15 cm thick T2 geogrid-reinforced base

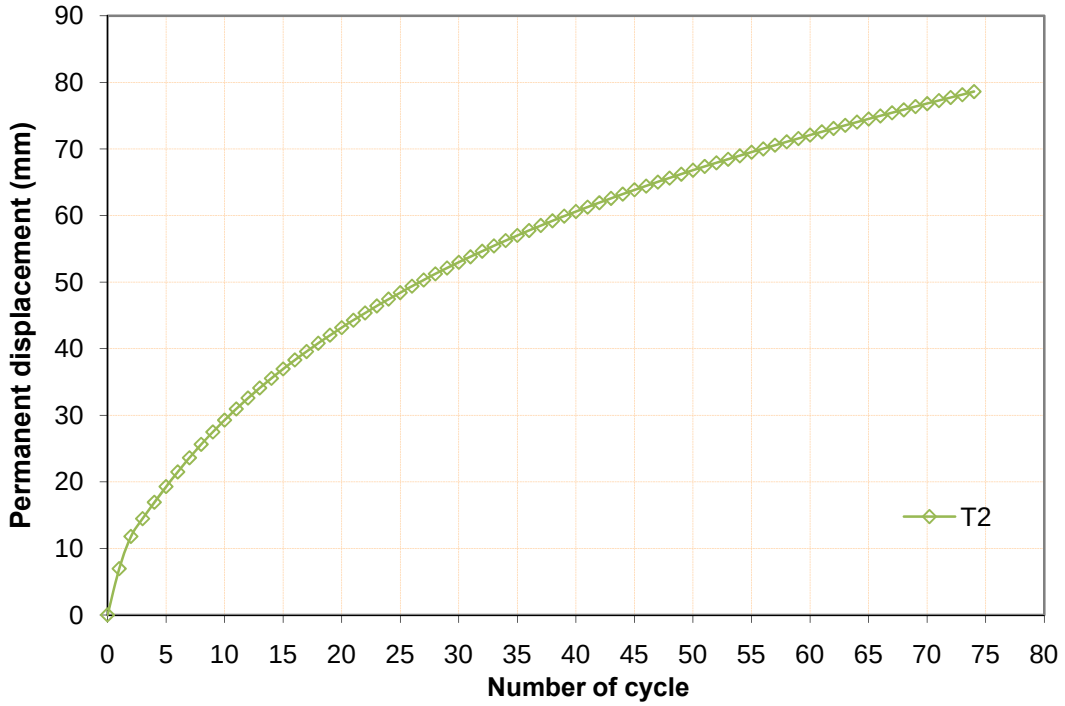

Figure 3.26 Permanent displacement of the loading plate versus the number of cycle for 15 cm thick T2 geogrid-reinforced base

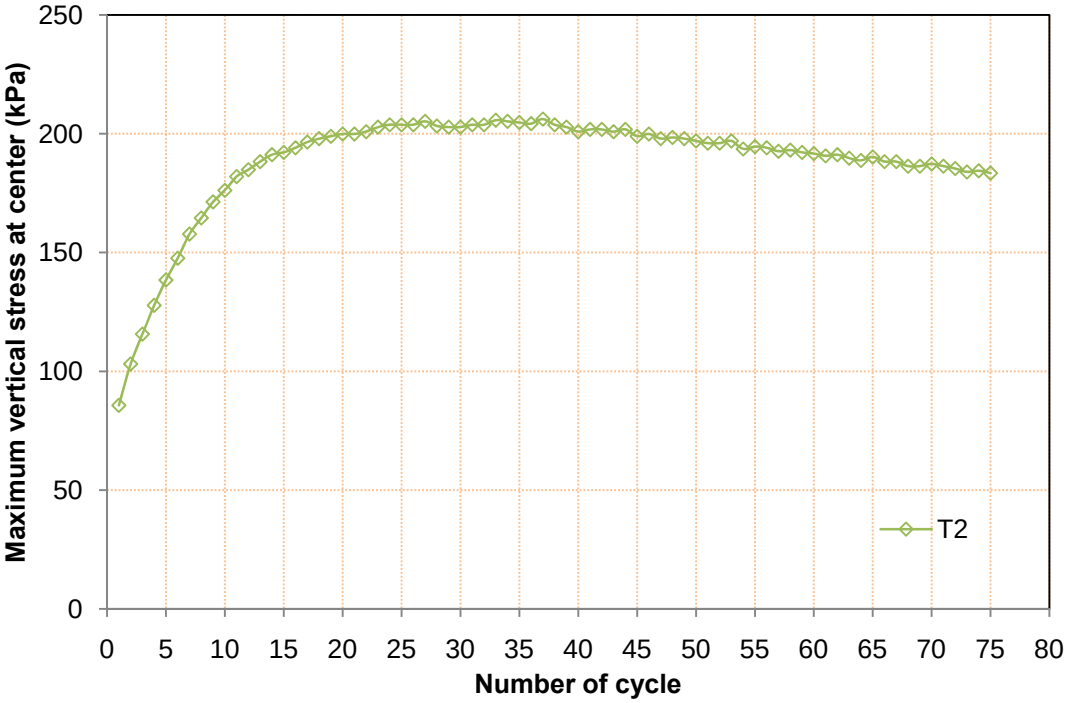

Figure 3.27 Maximum vertical stresses at the center and the interface between the base and the subgrade for 15 cm thick T2 geogrid-reinforced base

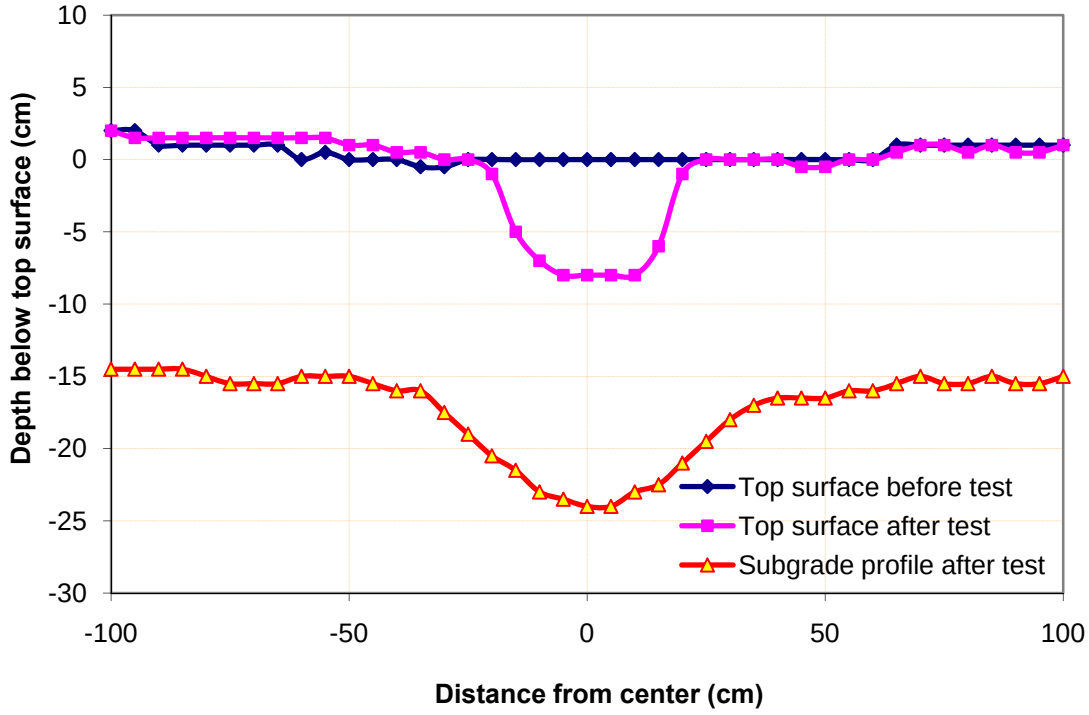

Figure 3.28 Surface profiles of 15 cm thick T2 geogrid-reinforced base

3.4.4 15 cm thick base reinforced with T3 geogrid

Figures 3.29, 3.30, 3.31, and 3.32 show the results of DCP penetration index profiles, the permanent displacement of the loading plate versus the number of cycle, the maximum vertical stress at the center and the interface between the base and the subgrade, and the surface profiles of the 15 cm thick T3 geogrid-reinforced base over the weak subgrade.

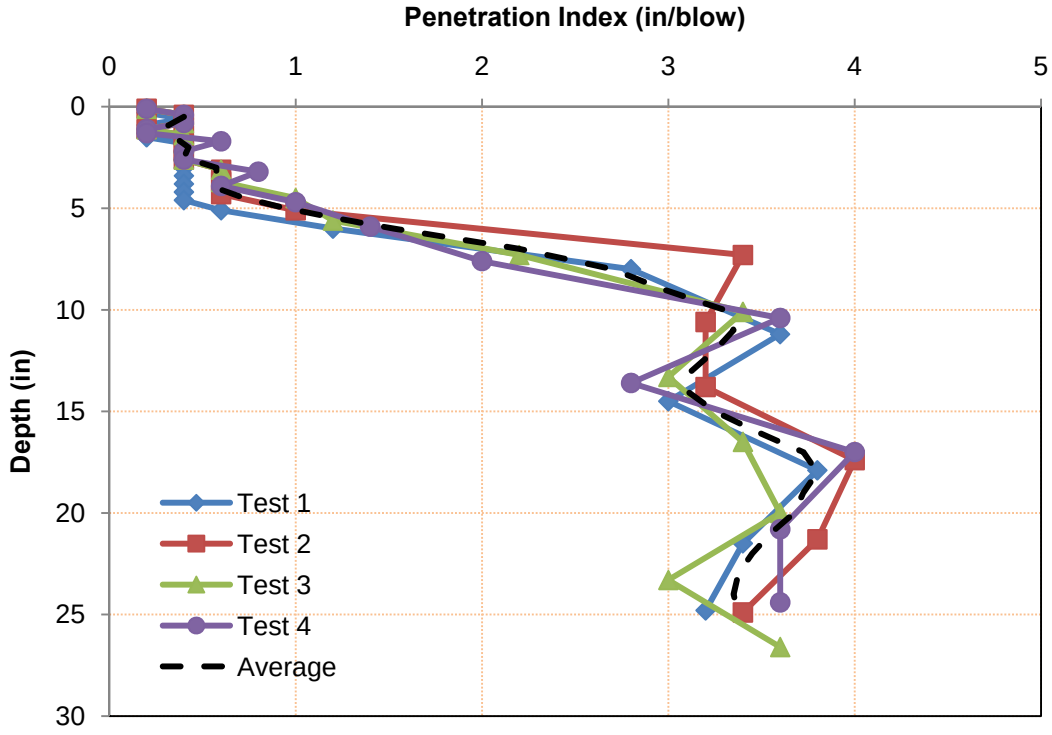

Figure 3.29 DCP test data for 15 cm thick T3 geogrid-reinforced base

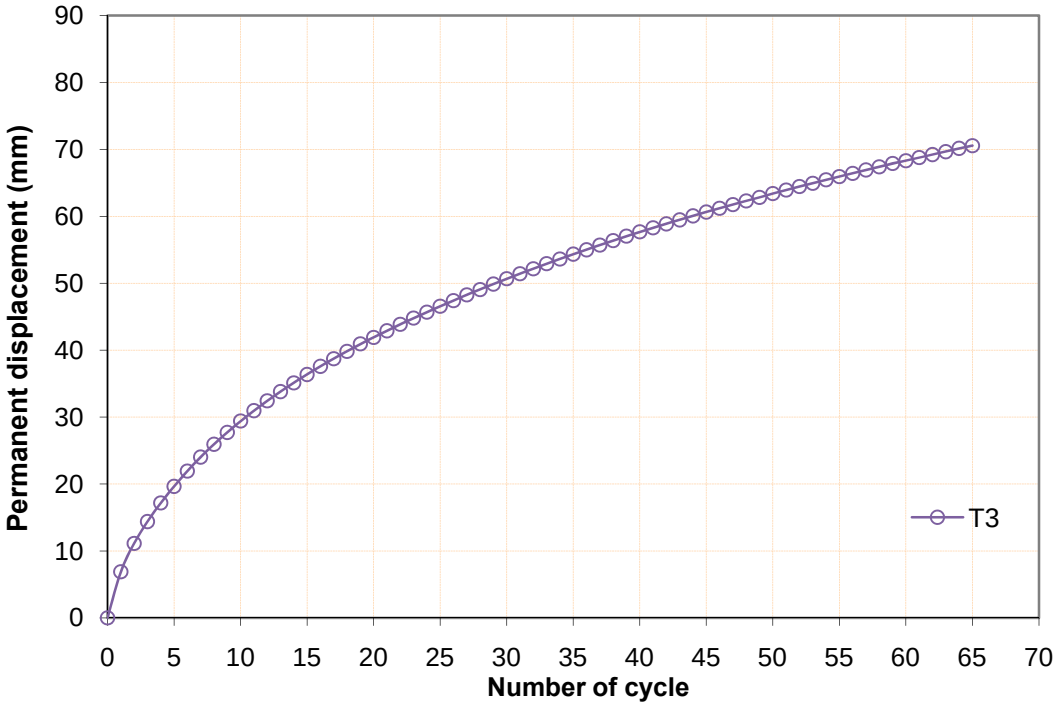

Figure 3.30 Permanent displacement of the loading plate versus the number of cycle for 15 cm thick T3 geogrid-reinforced base

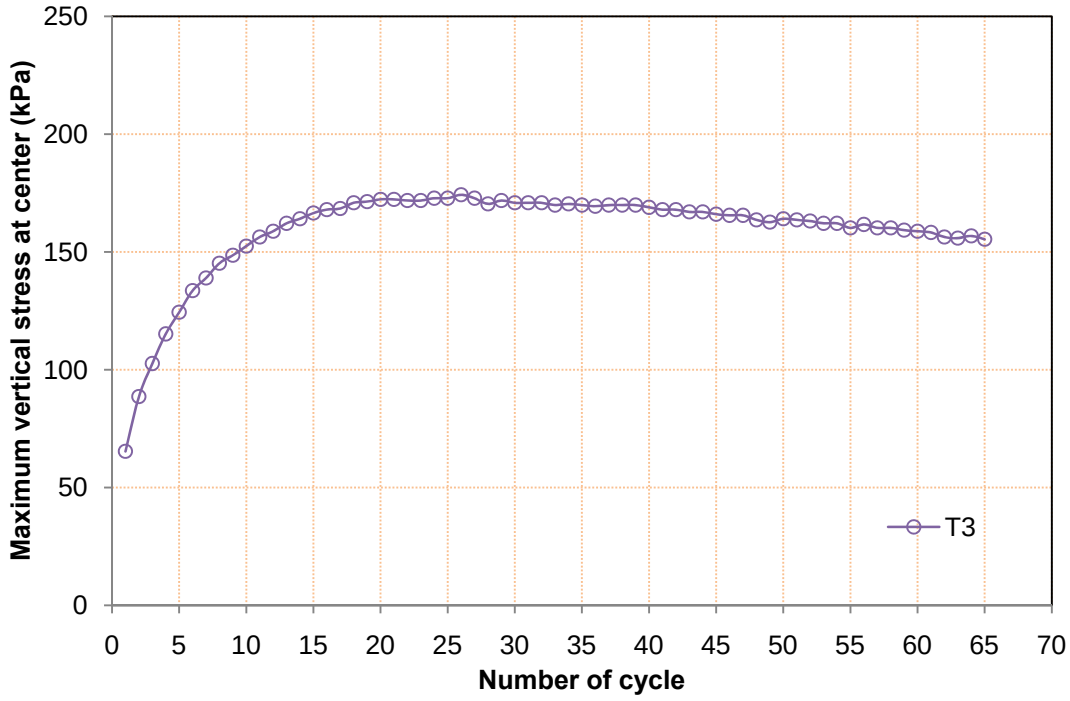

Figure 3.31 Maximum vertical stresses at the center and the interface between the base and the subgrade for 15 cm thick T3 geogrid-reinforced base

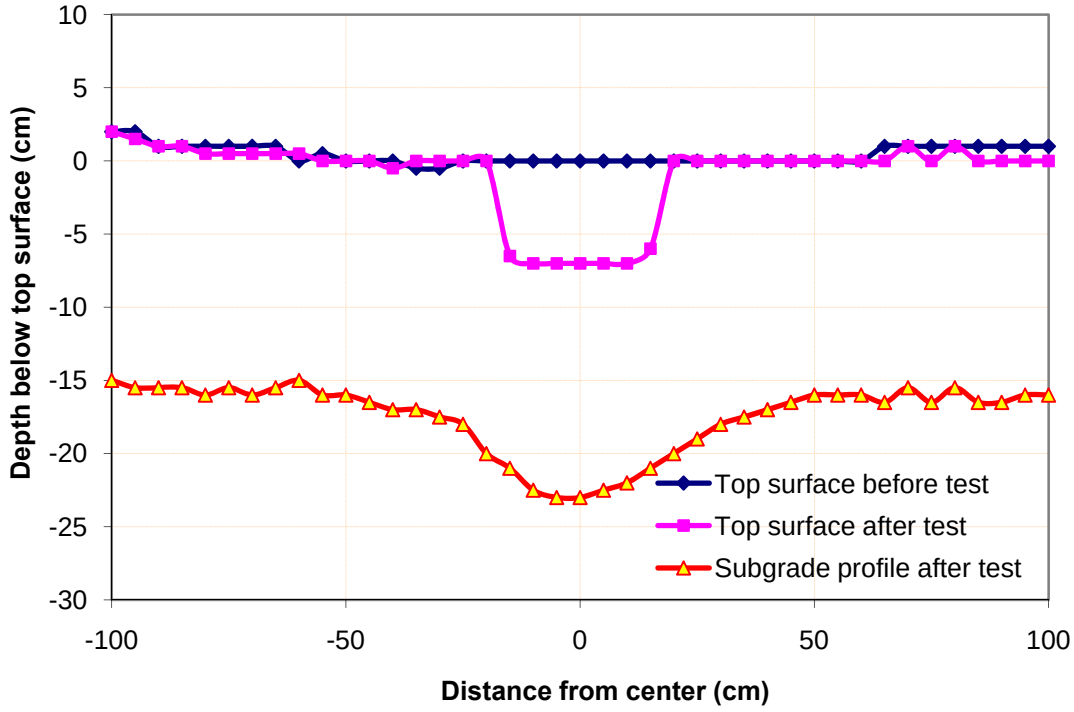

Figure 3.32 Surface profiles for 15 cm thick T3 geogrid-reinforced base

3.4.5 23 cm thick unreinforced base

Figures 3.33, 3.34, 3.35, and 3.36 show the results of DCP penetration index profiles, the permanent displacement of the loading plate versus the number of cycle, the maximum vertical stress at the center and the interface between the base and the subgrade, and the surface profiles of the 23 cm thick unreinforced base over the weak subgrade.

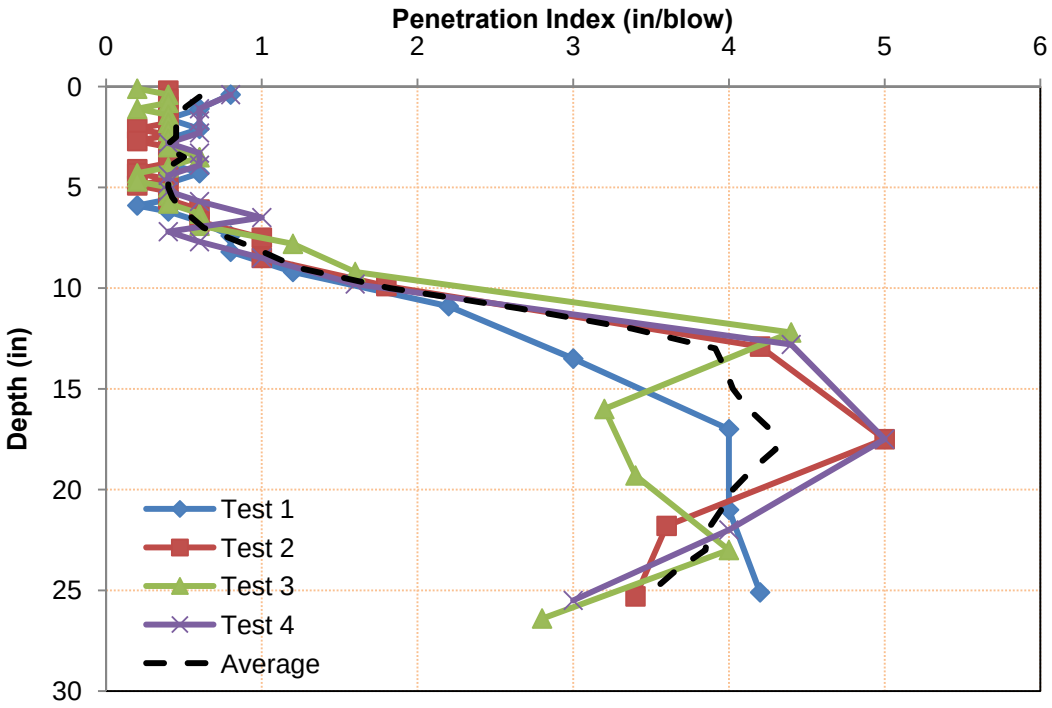

Figure 3.33 DCP test data for 23 cm thick unreinforced base

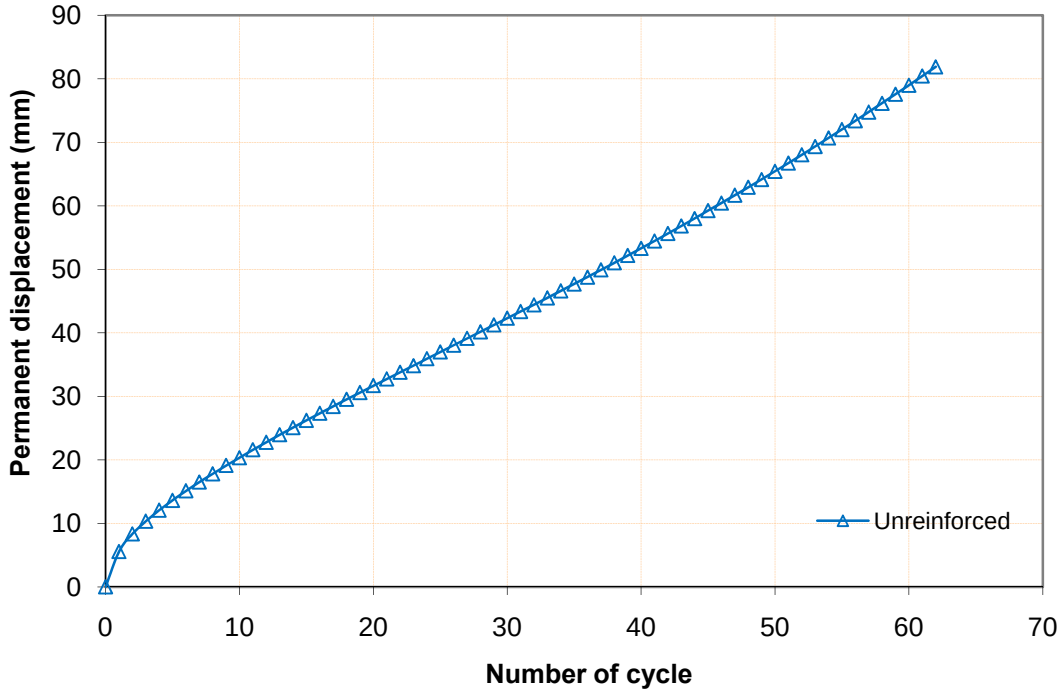

Figure 3.34 Permanent displacement of the loading plate vs. the number of cycle for 23 cm thick unreinforced base

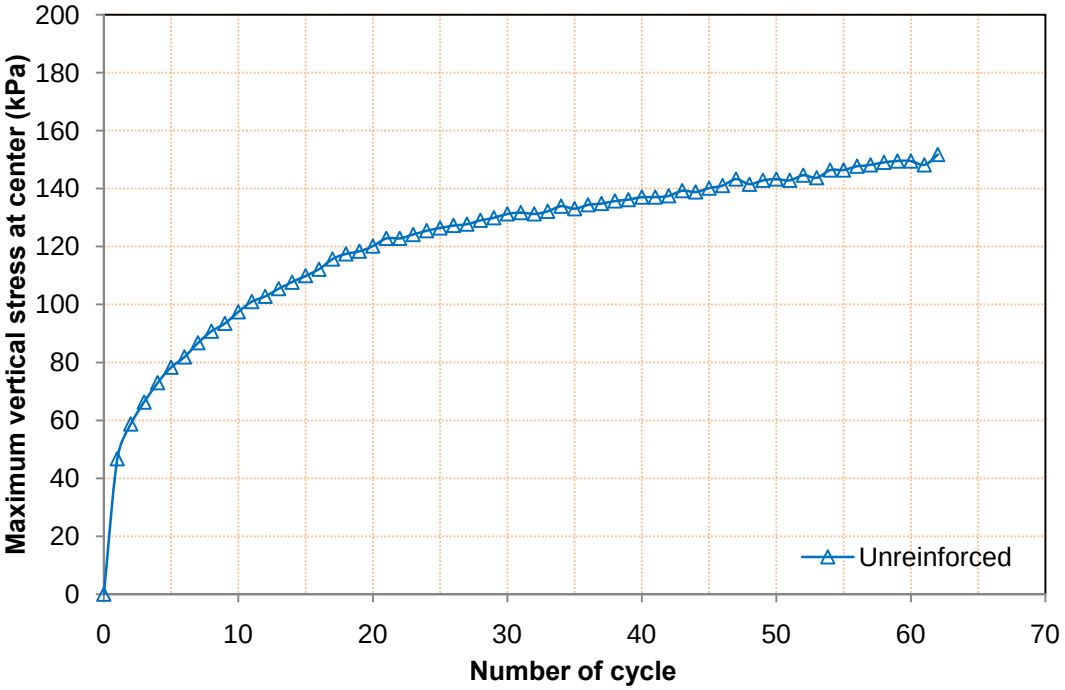

Figure 3.35 Maximum vertical stresses at the center and the interface between the base course and the subgrade for 23 cm thick unreinforced base

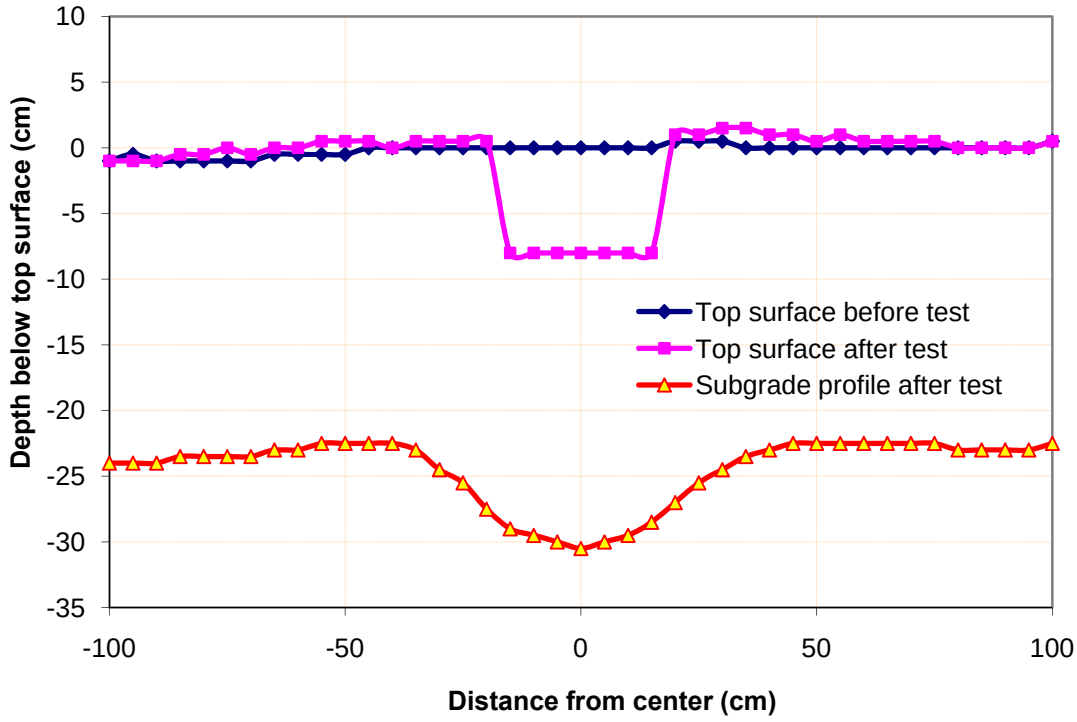

Figure 3.36 Surface profiles for 23 cm thick unreinforced base

3.4.6 23 cm thick unreinforced base (higher CBR subgrade)

Figures 3.37, 3.38, 3.39, and 3.40 show the results of DCP penetration index profiles, the permanent displacement of the loading plate versus the number of cycle, the maximum vertical stress at the center and the interface between the base and the subgrade, and the surface profiles of the 23 cm thick unreinforced base over the subgrade at 3% CBR.

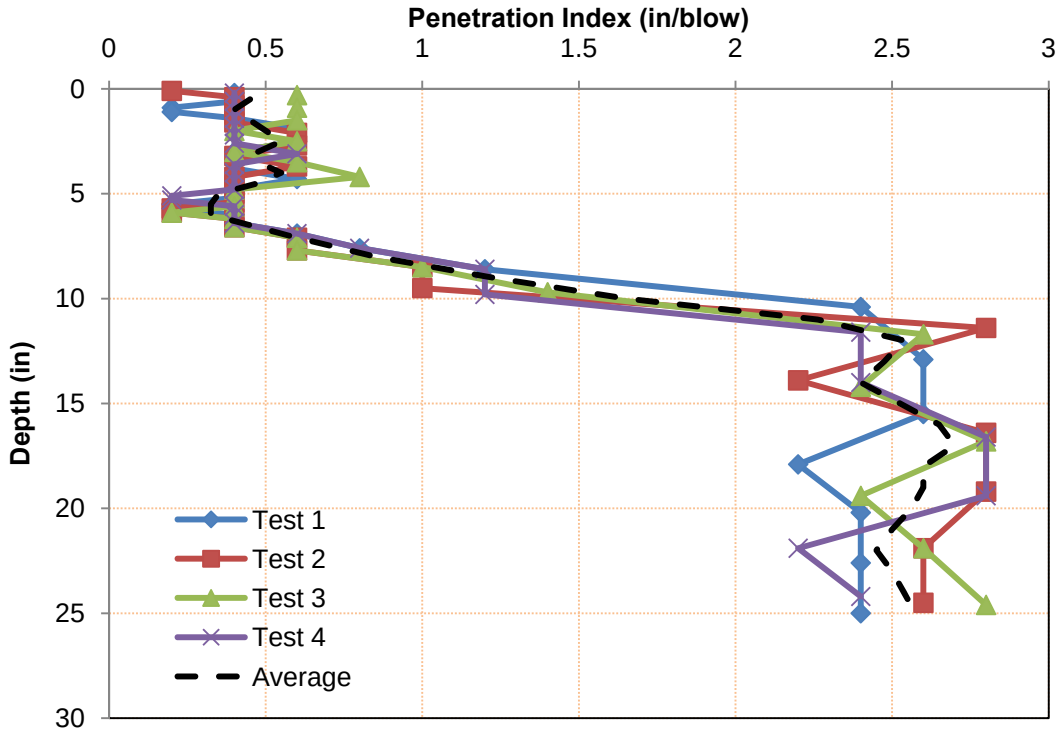

Figure 3.37DCP test data for 23 cm thick unreinforced base course (higher CBR subgrade)

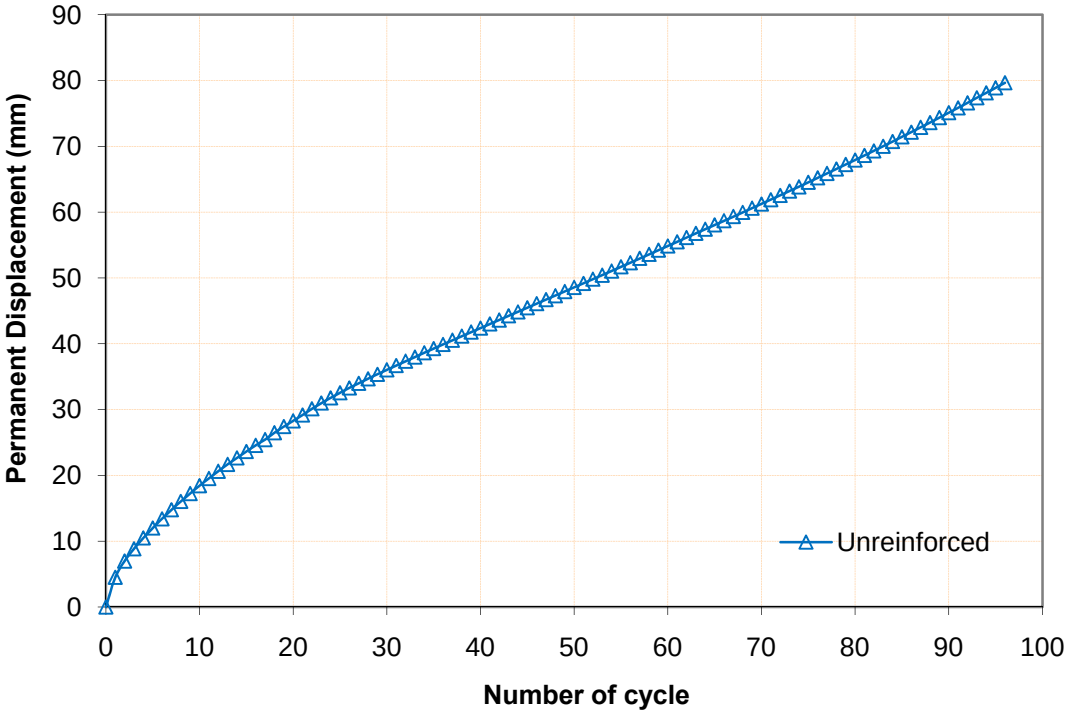

Figure 3.38 Permanent displacement of the loading plate vs. the number of cycle for 23 cm thick unreinforced base (higher CBR subgrade)

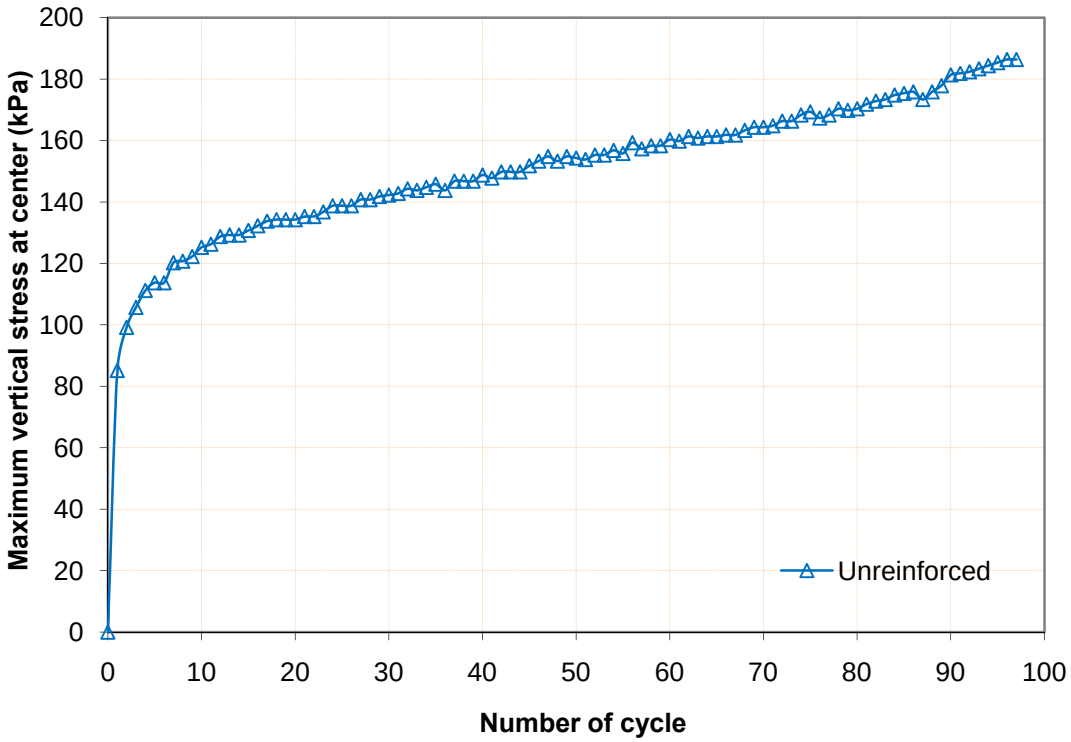

Figure 3.39 Maximum vertical stresses at the center and the interface between the base and the subgrade for 23 cm thick unreinforced base (higher CBR subgrade)

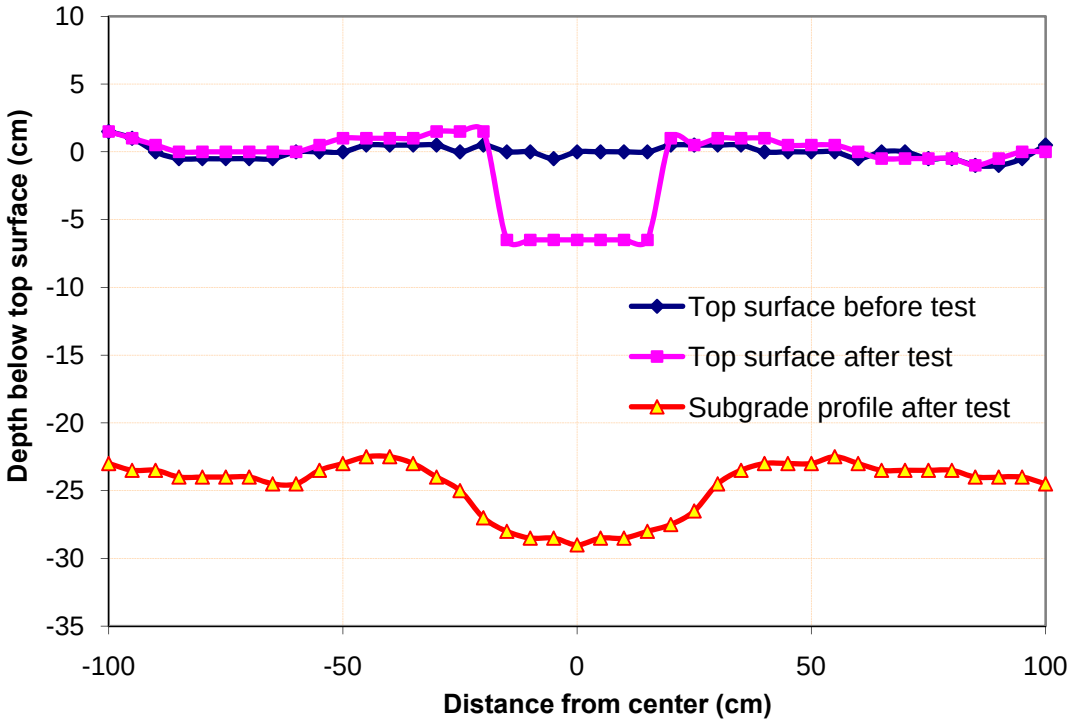

Figure 3.40 Surface profile for 23 cm thick unreinforced base (subgrade CBR=3%)

3.4.7 23 cm thick base reinforced with T1 geogrid

Figures 3.41, 3.42, 3.43, and 3.44 show the results of DCP penetration index profiles, the permanent displacement of the loading plate versus the number of cycle, the maximum vertical stress at the center and the interface between the base and the subgrade, and the surface profiles of the 23 cm thick T1 geogrid-reinforced base over the weak subgrade.

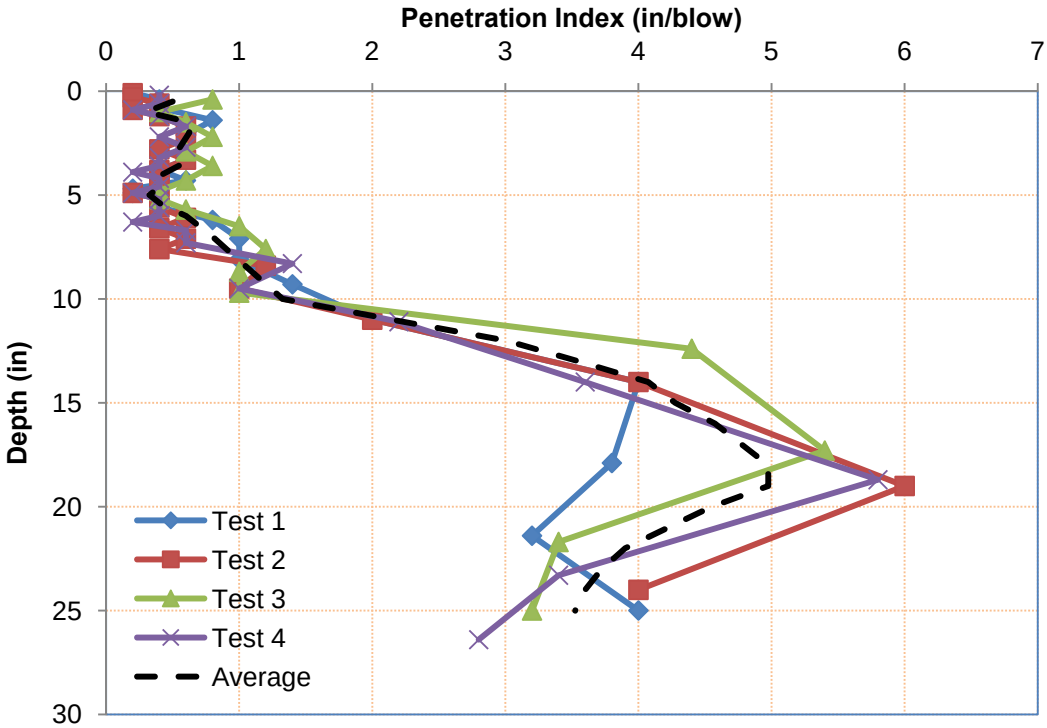

Figure 3.41 DCP test data for 23 cm thick T1 geogrid-reinforced base

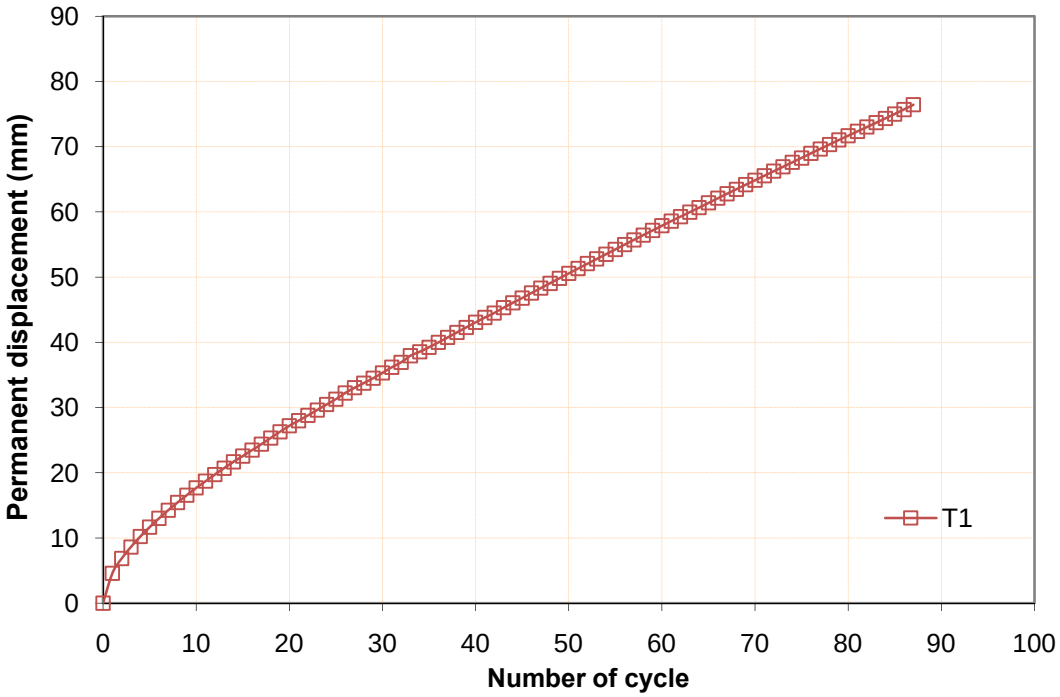

Figure 3.42 Permanent displacement of the loading plate versus the number of cycle for 23 cm thick T1 geogrid-reinforced base

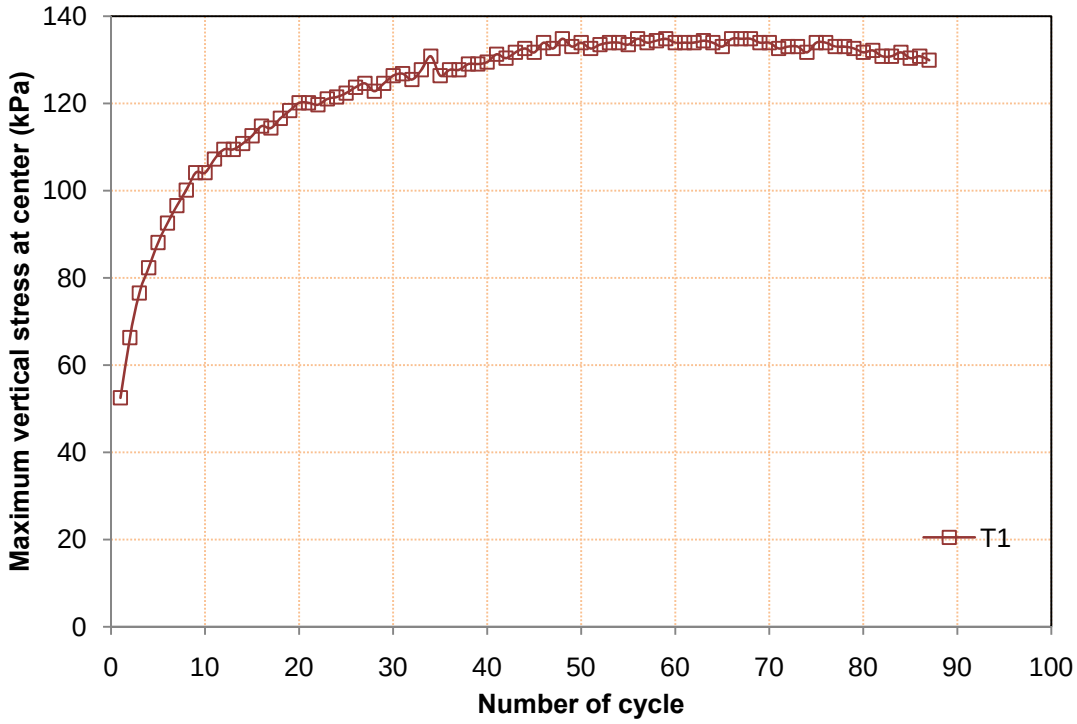

Figure 3.43 Maximum vertical stresses at the center and the interface between the base and the subgrade versus the number of cycle for 23 cm thick T1 geogrid-reinforced base

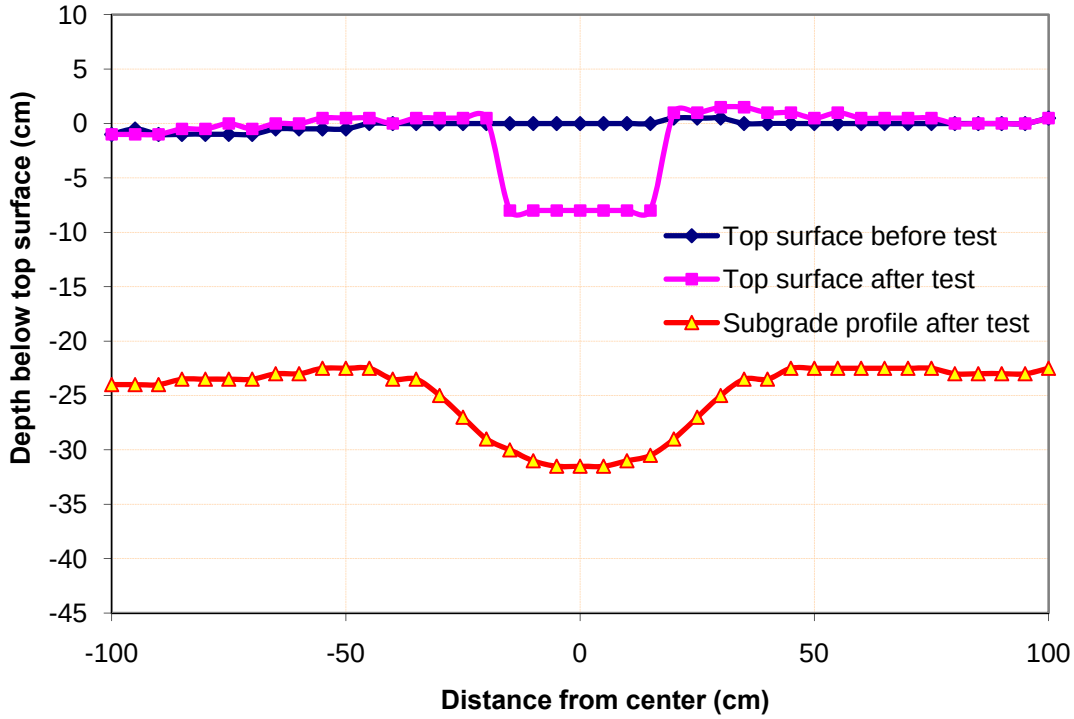

Figure 3.44 Surface profiles for 23 cm thick T1 geogrid-reinforced base

3.4.8 23 cm thick base reinforced with T1 geogrid (higher CBR subgrade)

Figures 3.45, 3.46, 3.47, and 3.48 show the results of DCP penetration index profiles, the permanent displacement of the loading plate versus the number of cycle, the maximum vertical stress at the center and the interface between the base and the subgrade, and the surface profiles of the 23 cm thick T1 geogrid-reinforced base over the weak subgrade at approximately 3% CBR.

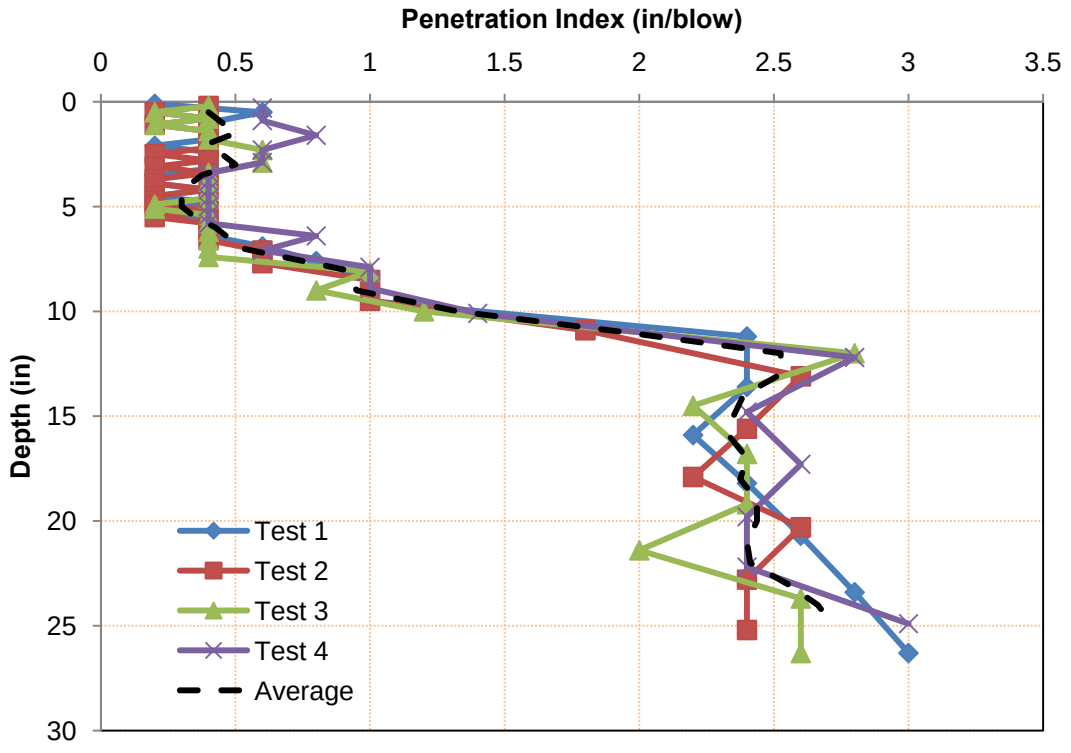

Figure 3.45 DCP test data for 23 cm thick T1 geogrid-reinforced base (higher CBR subgrade)

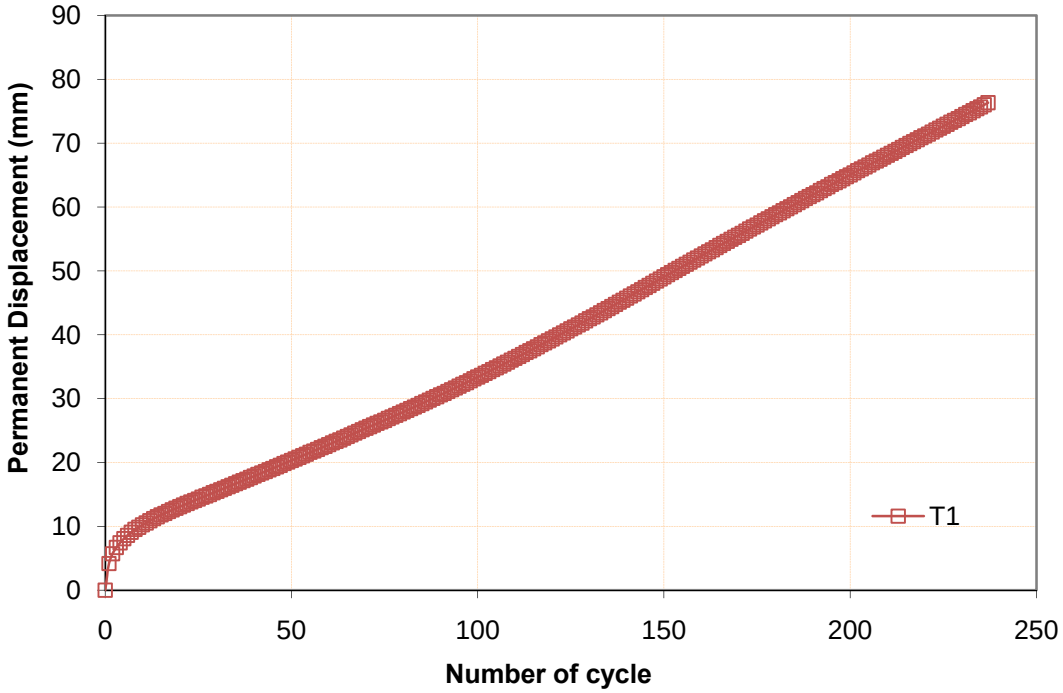

Figure 3.46 Permanent displacement of the loading plate versus the number of cycle for 23 cm thick T1 geogrid-reinforced base (higher CBR subgrade)

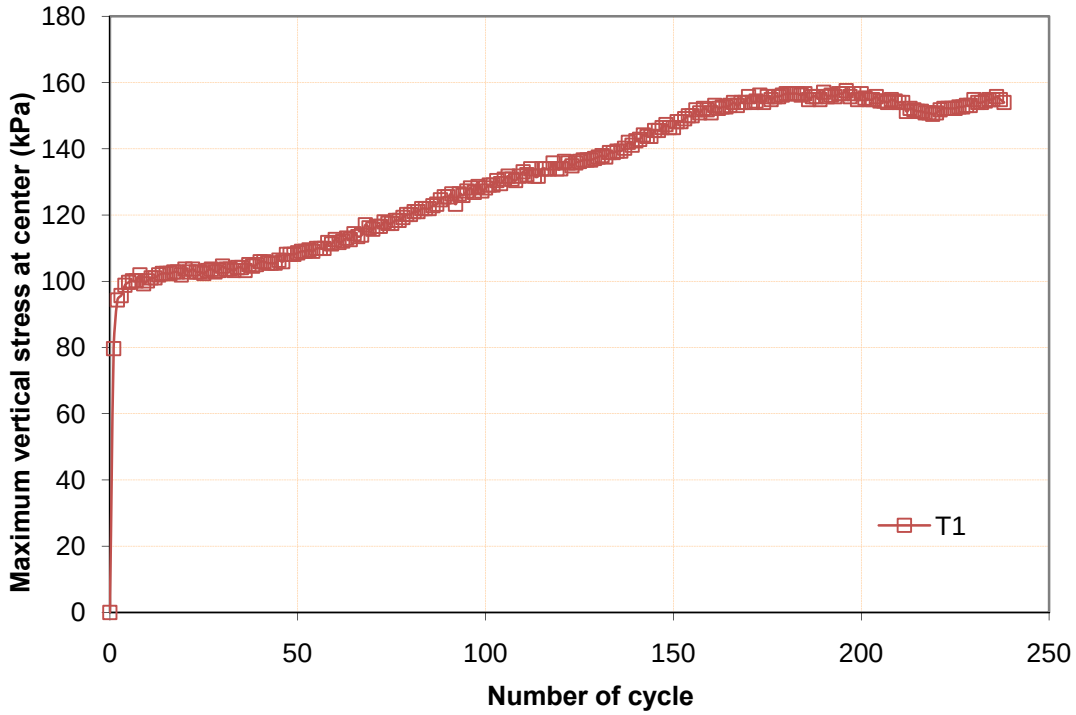

Figure 3.47 Maximum vertical stresses at the center and the interface between the base and the subgrade versus the number of cycle for 23 cm thick T1 geogrid-reinforced base (higher CBR subgrade)

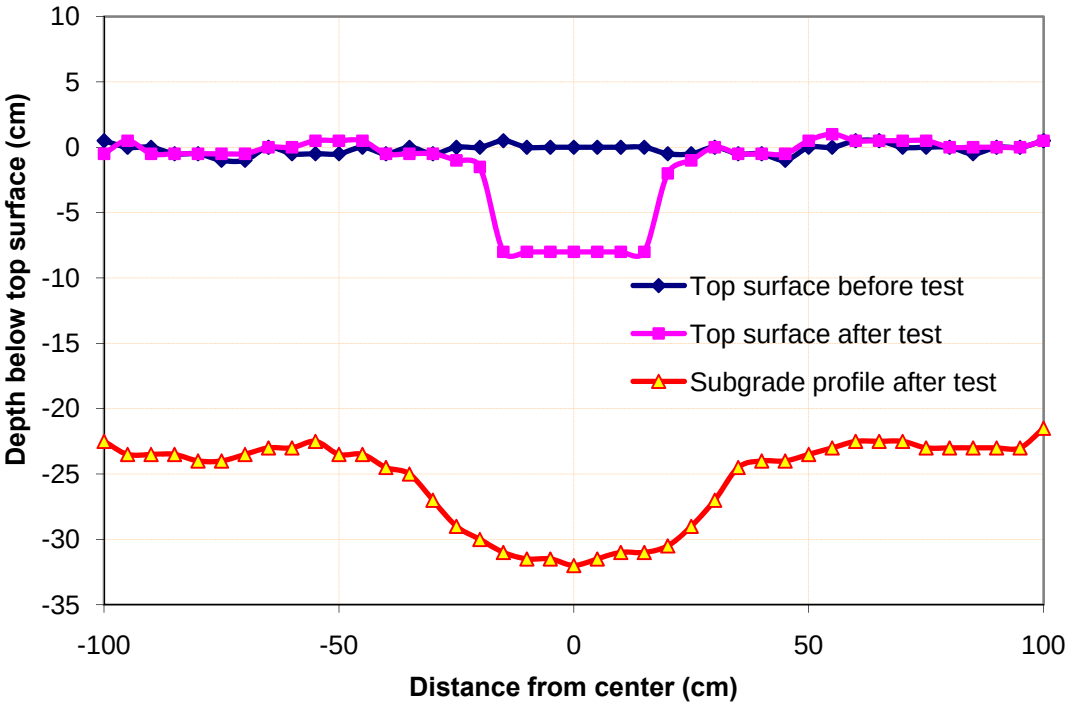

Figure 3.48 Surface profiles for 23 cm thick T1 geogrid-reinforced base (higher CBR subgrade)

3.4.9 23 cm thick base reinforced with T2 geogrid

Figures 3.49, 3.50, 3.51, and 3.52 show the results of DCP penetration index profiles, the permanent displacement of the loading plate versus the number of cycle, the maximum vertical stress at the center and the interface between the base and the subgrade, and the surface profiles of the 23 cm thick T2 geogrid-reinforced base over the weak subgrade.

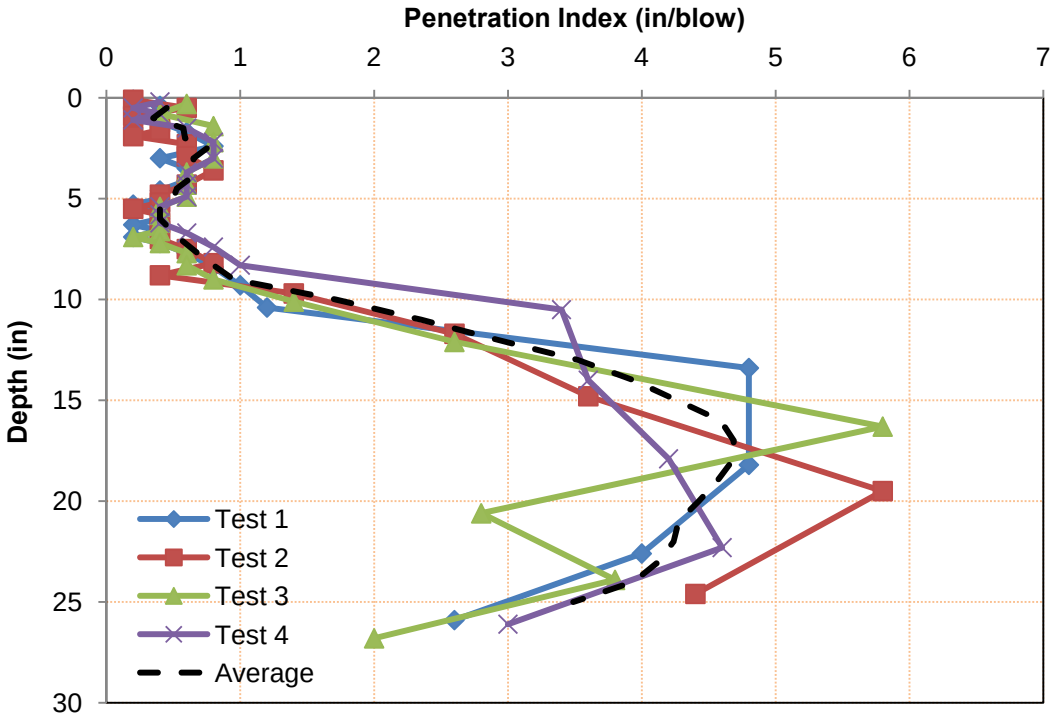

Figure 3.49 DCP test data for 23 cm thick T2 geogrid-reinforced base

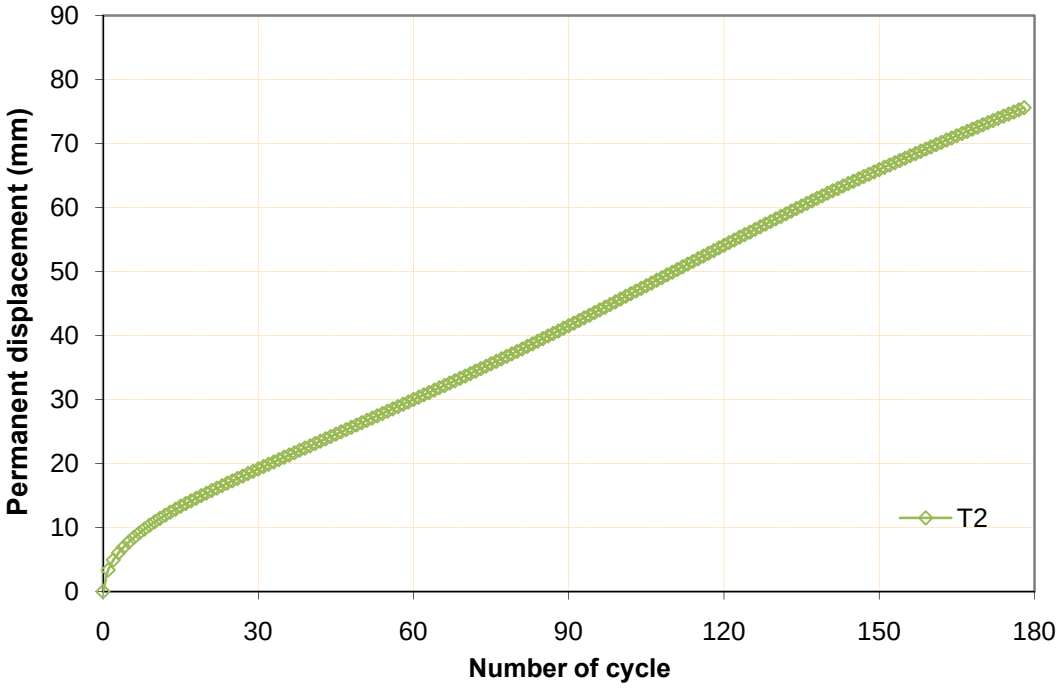

Figure 3.50 Permanent displacement of the loading plate versus the number of cycle for 23 cm thick T2 geogrid-reinforced base

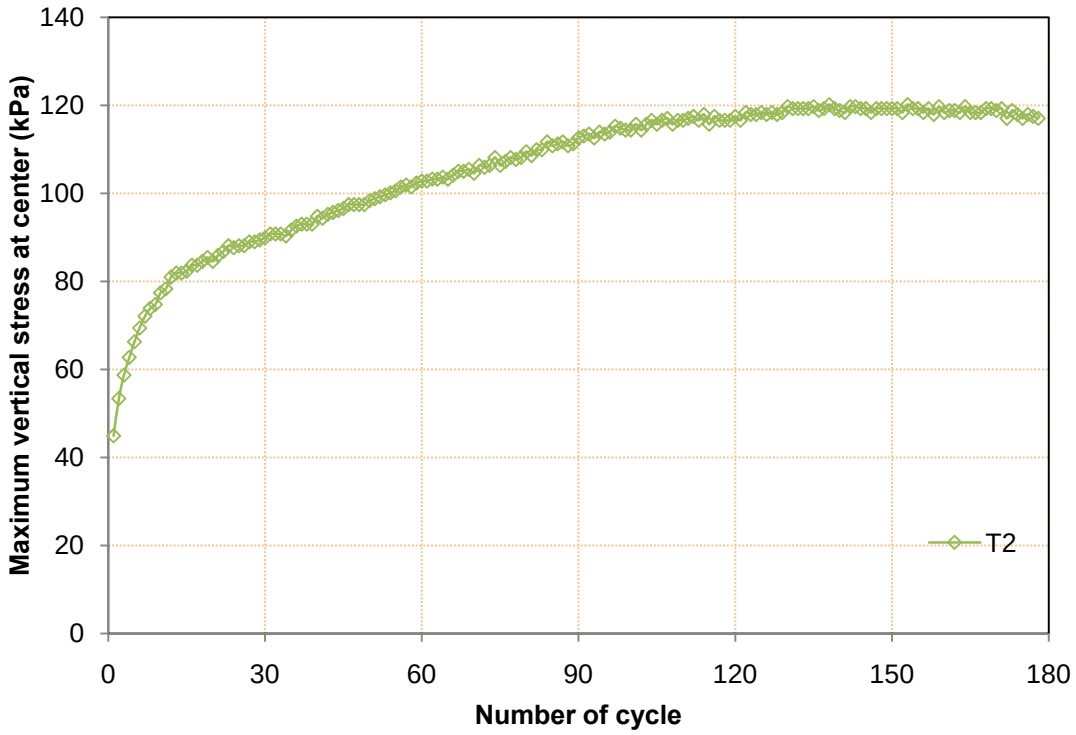

Figure 3.51 Maximum vertical stresses at the center and the interface between the base and the subgrade for 23 cm thick T2 geogrid-reinforced base

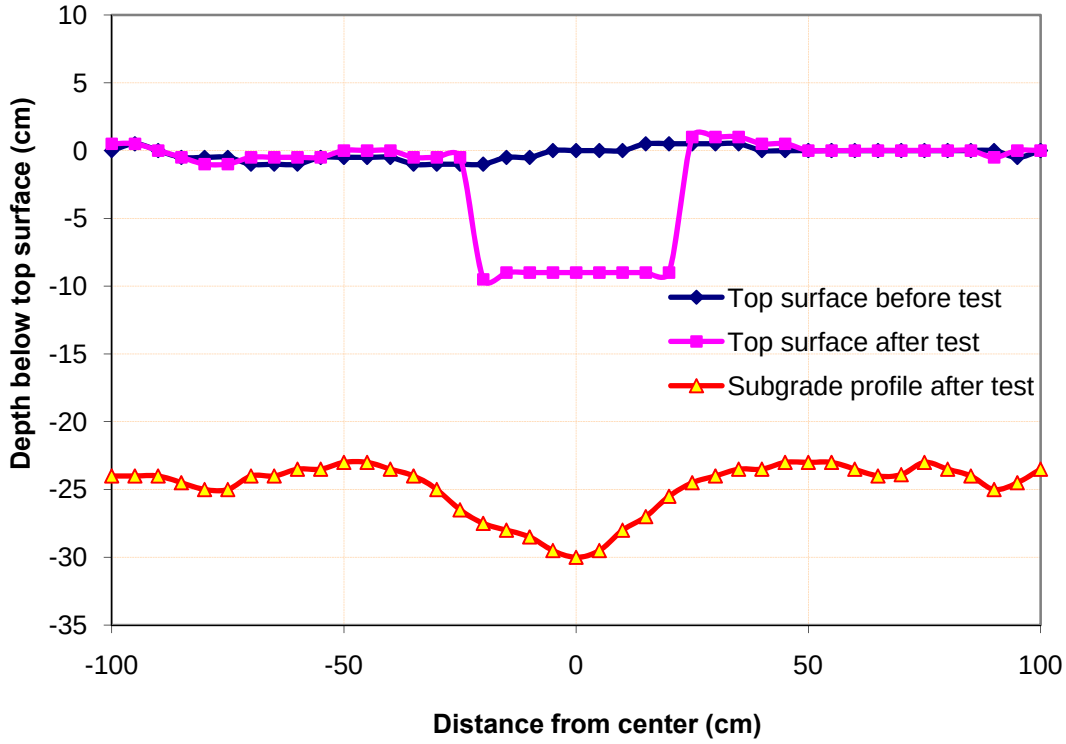

Figure 3.52 Surface profiles for 23 cm thick T2 geogrid-reinforced base

3.4.10 23 cm thick base reinforced with T3 geogrid

Figures 3.53, 3.54, 3.55, and 3.56 show the results of DCP penetration index profiles, the permanent displacement of the loading plate versus the number of cycle, the maximum vertical stress at the center and the interface between the base and the subgrade, and the surface profiles of the 23 cm thick T3 geogrid-reinforced base over the weak subgrade.

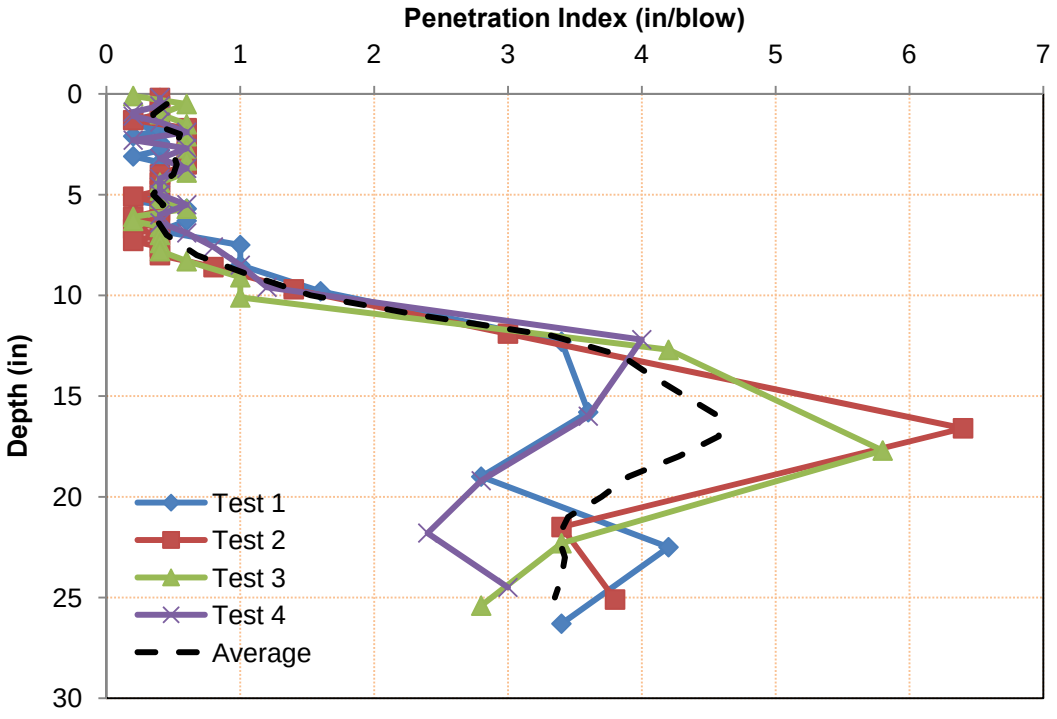

Figure 3.53 DCP test data for 23 cm thick T3 geogrid-reinforced base

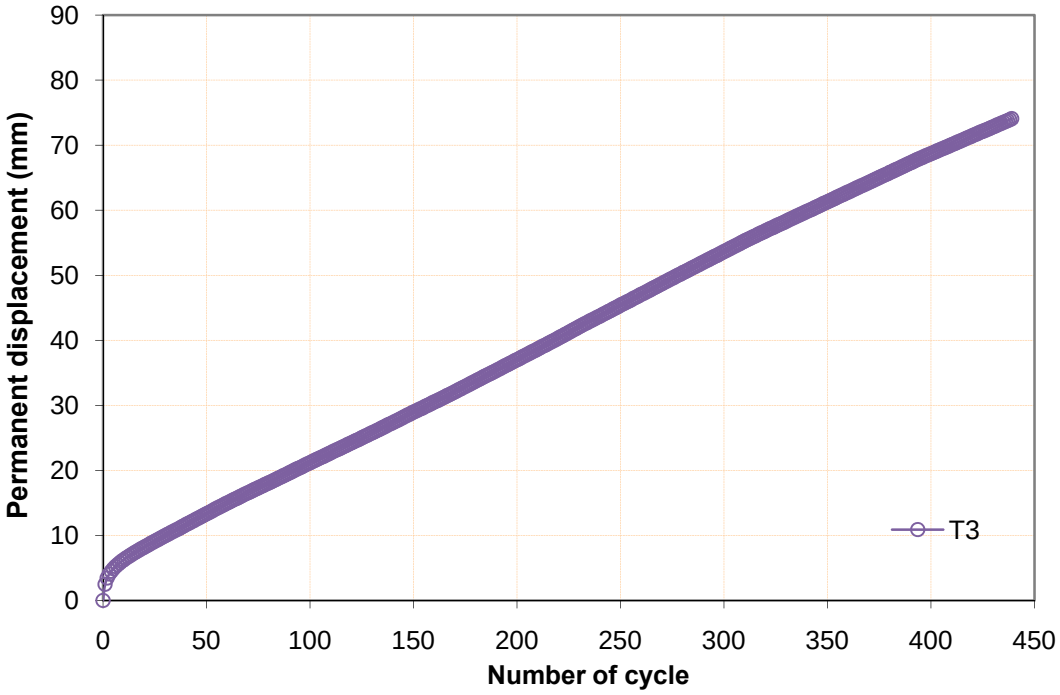

Figure 3.54 Permanent displacement of the loading plate versus the number of cycle for 23 cm thick T3 geogrid-reinforced base

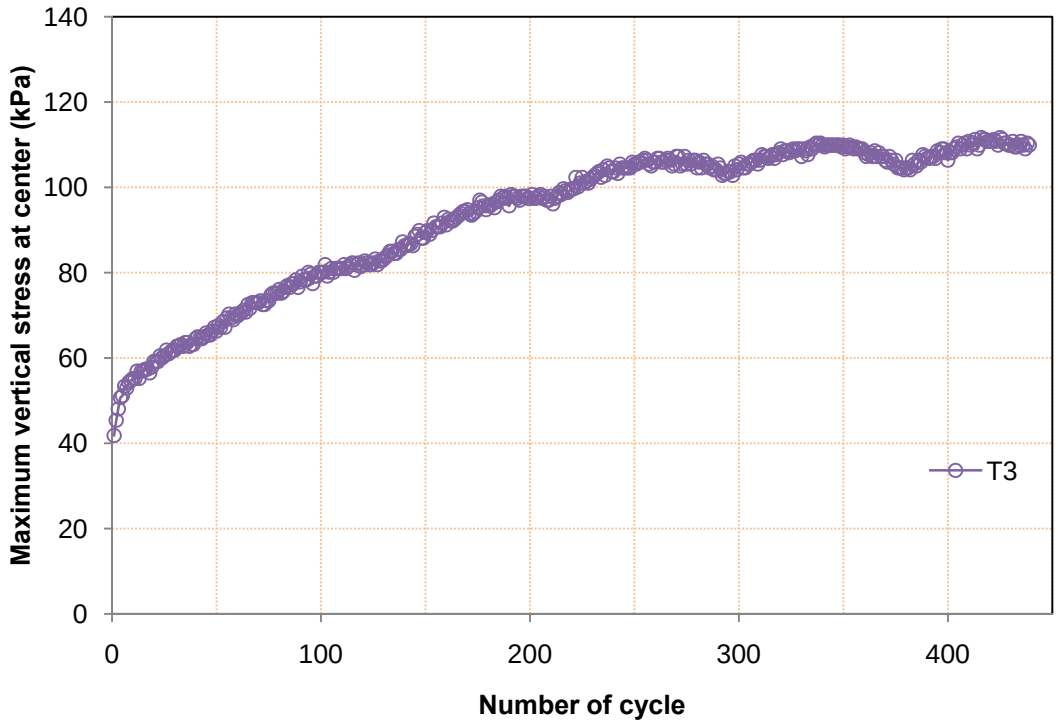

Figure 3.55 Maximum vertical stresses at the center and the interface between the base and the subgrade for 23 cm thick T3 geogrid-reinforced base

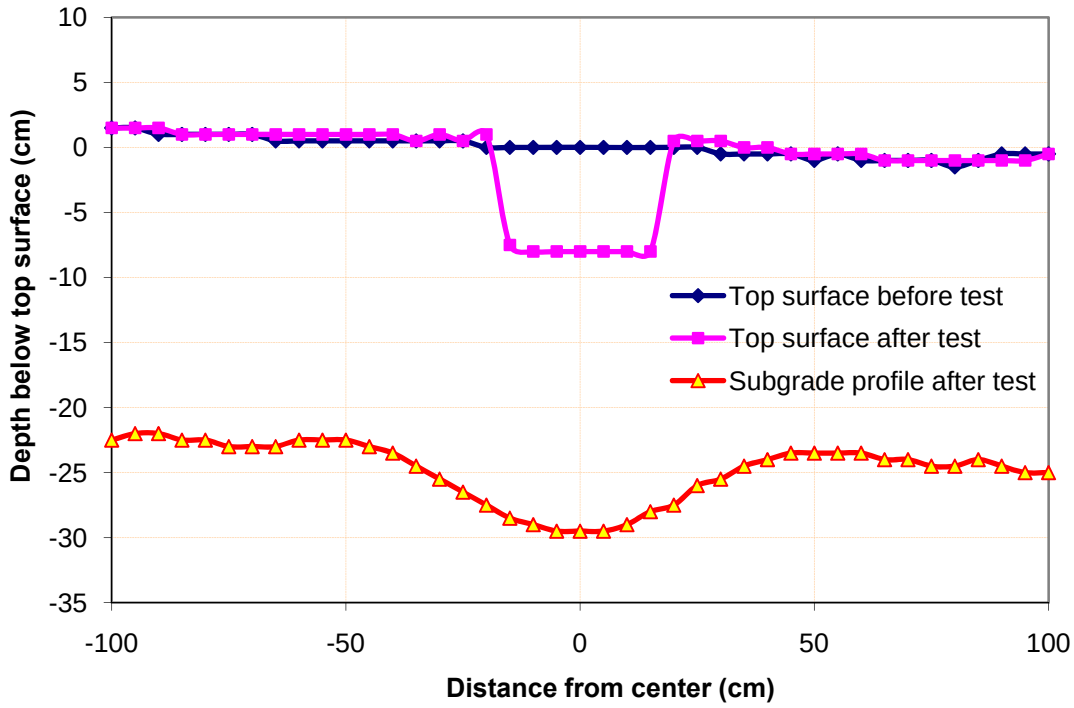

Figure 3.56 Surface profiles for 23 cm thick T3 geogrid-reinforced base

3.4.11 30 cm thick unreinforced base

Figures 3.57, 3.58, 3.59, and 3.60 show the results of DCP penetration index profiles, the permanent displacement of the loading plate versus the number of cycle, the maximum vertical stress at the center and the interface between the base and the subgrade, and the surface profiles of the 30 cm thick unreinforced base over the weak subgrade.

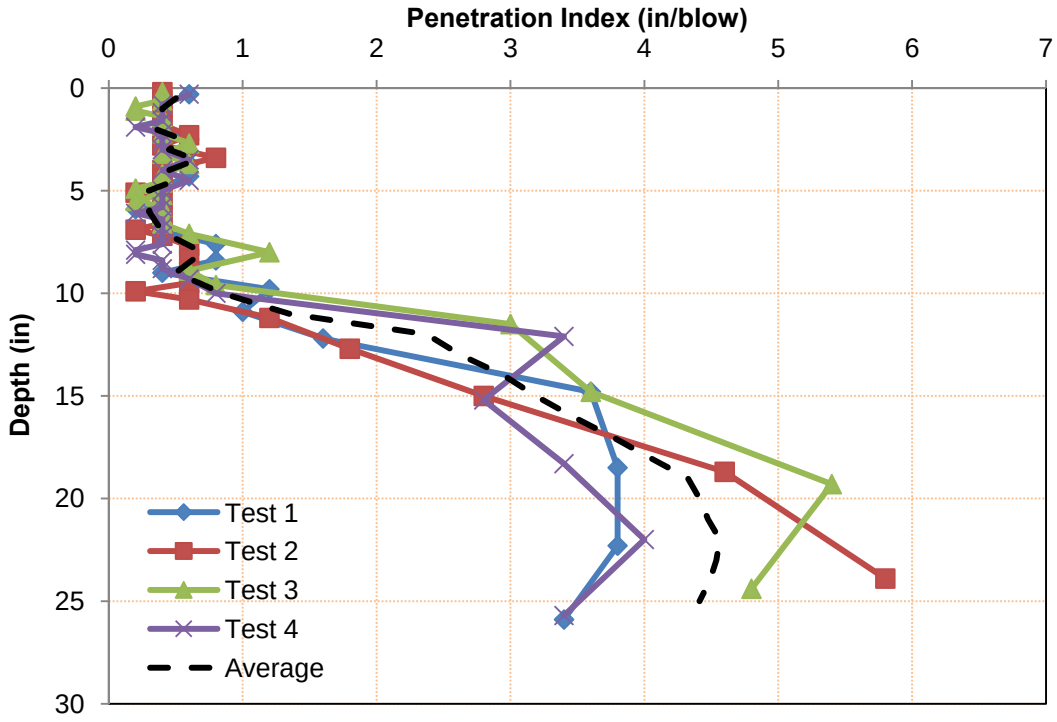

Figure 3.57 DCP test data for 30 cm thick unreinforced base

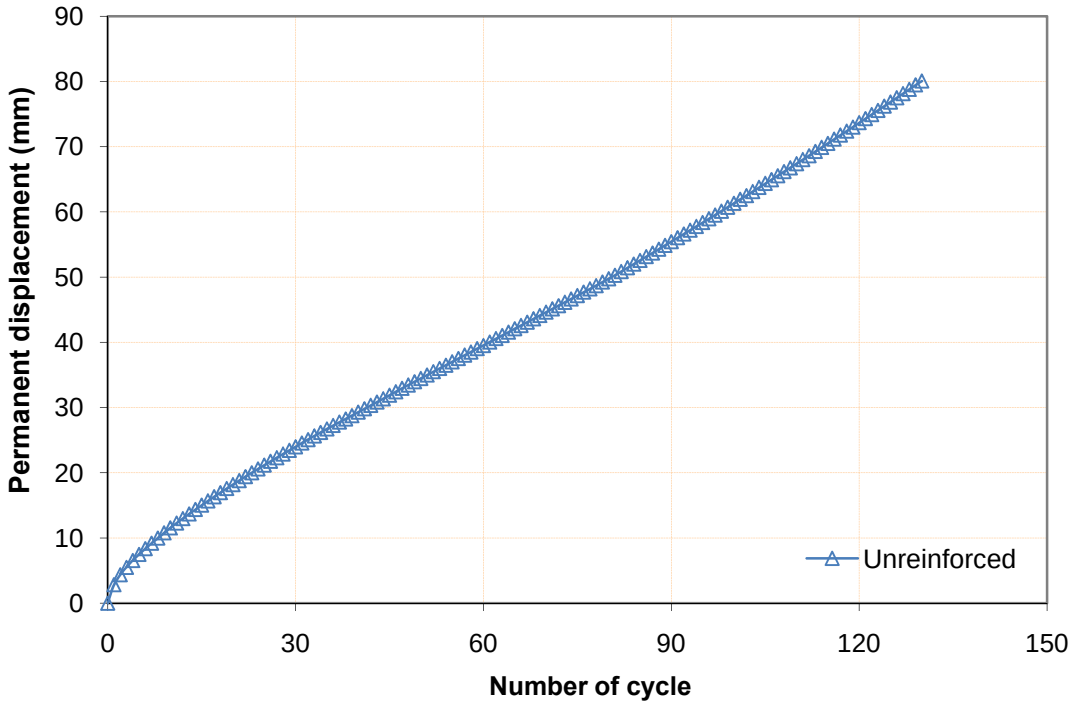

Figure 3.58 Permanent displacement of the loading plate vs. the number of cycle for 30 cm thick unreinforced base

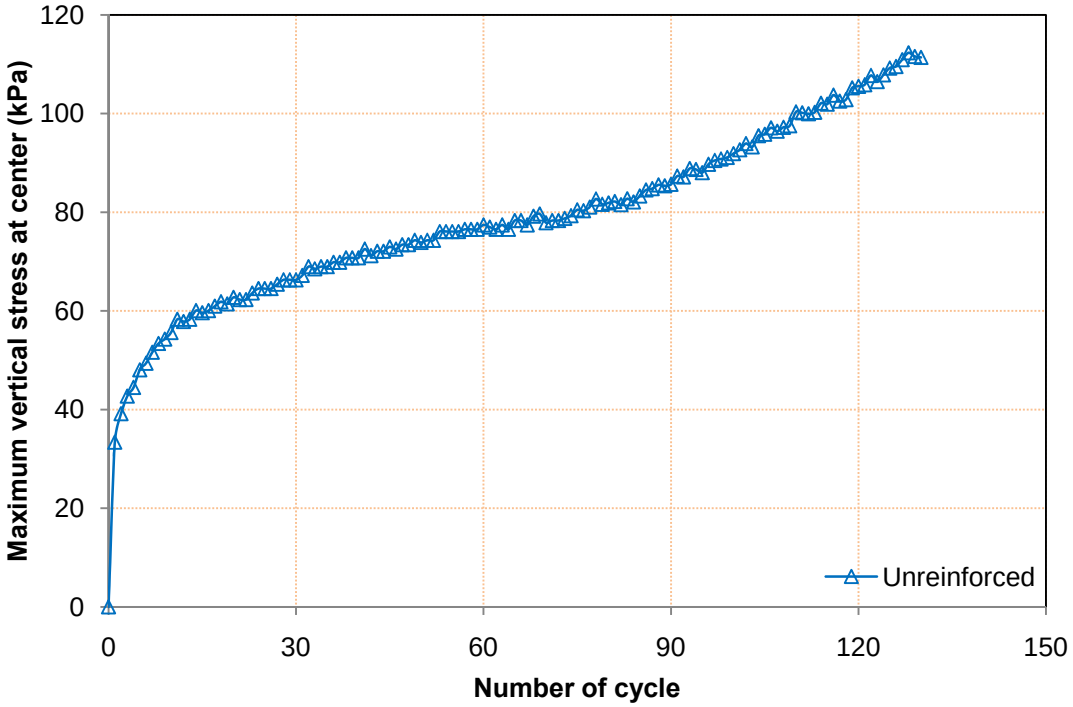

Figure 3.59 Maximum vertical stresses at the center and the interface between the base course and the subgrade for 30 cm thick unreinforced base

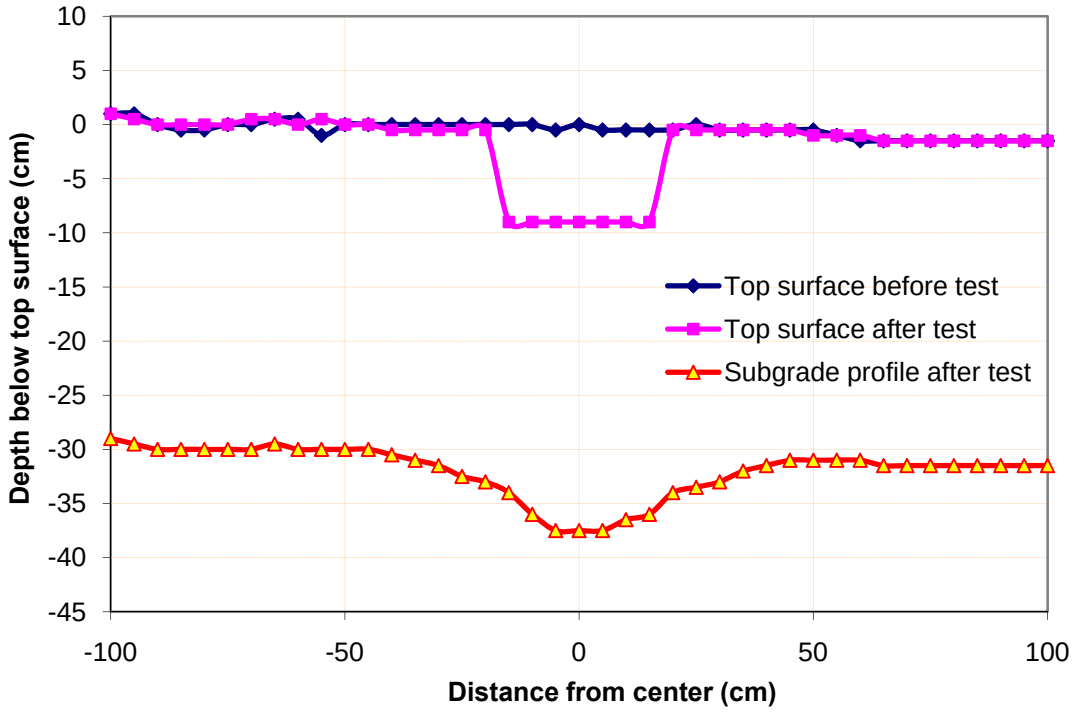

Figure 3.60 Surface profiles for 30 cm thick unreinforced base

3.4.12 30 cm thick base reinforced with T1 geogrid

Figures 3.61, 3.62, 3.63, and 3.64 show the results of DCP penetration index profiles, the permanent displacement of the loading plate versus the number of cycle, the maximum vertical stress at the center and the interface between the base and the subgrade, and the surface profiles of the 30 cm thick T1 geogrid-reinforced base over the weak subgrade.

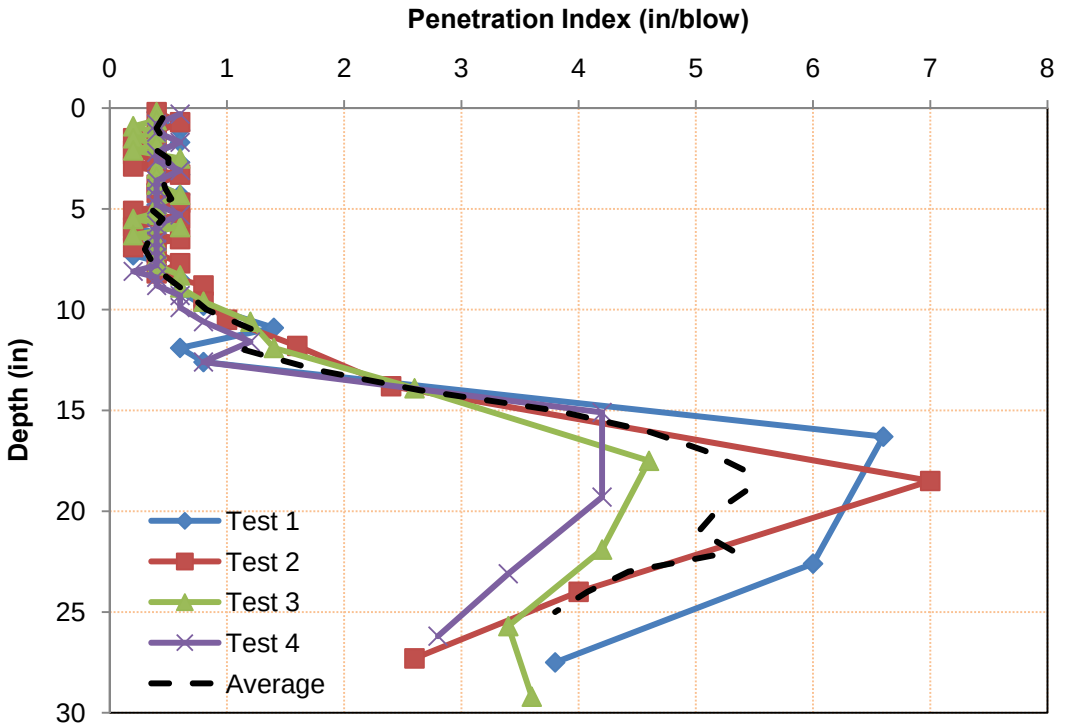

Figure 3.61 DCP test data for 30 cm thick T1 geogrid-reinforced base

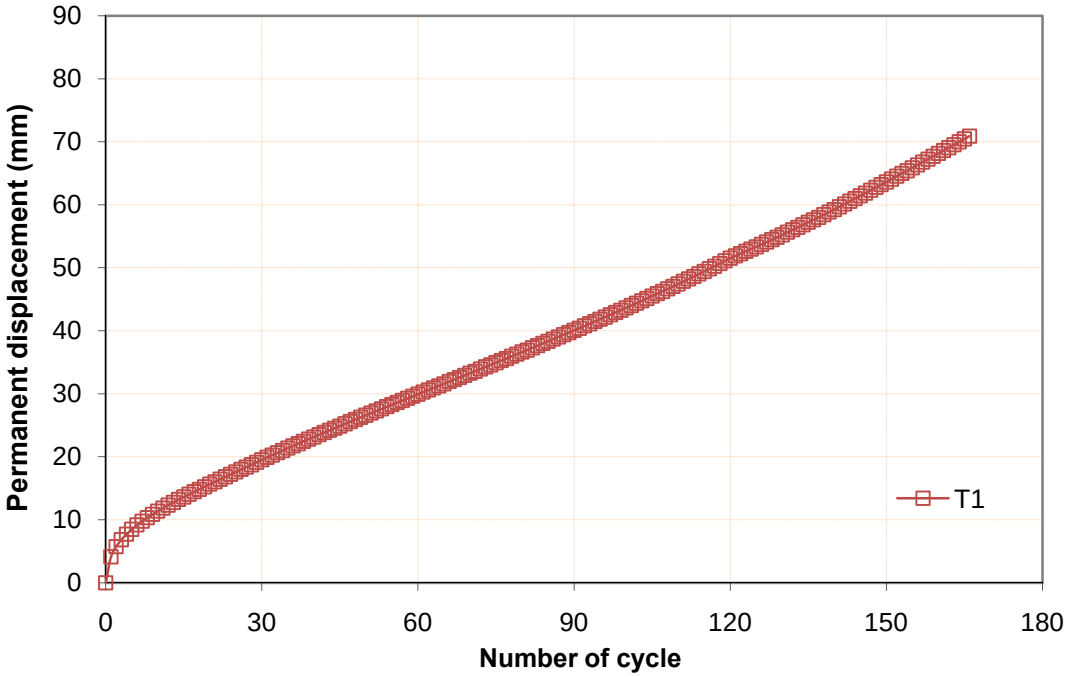

Figure 3.62 Permanent displacement of the loading plate versus the number of cycle for 30 cm thick T1 geogrid-reinforced base

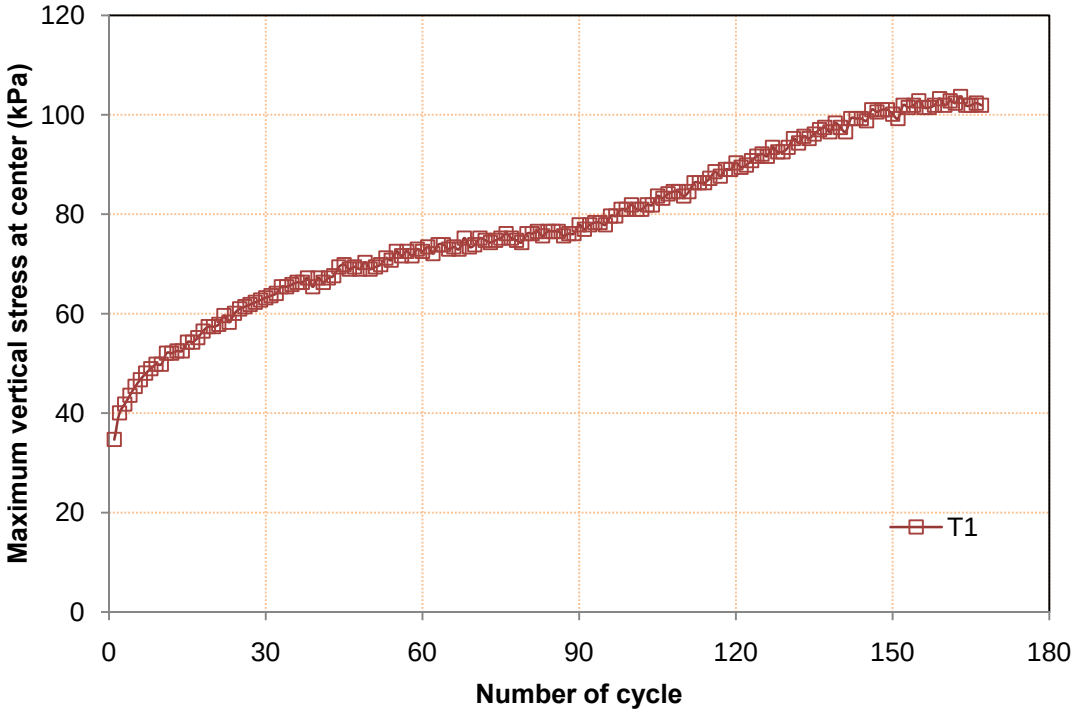

Figure 3.63 Maximum vertical stresses at the center and the interface between the base and the subgrade for 30 cm thick T1 geogrid-reinforced base

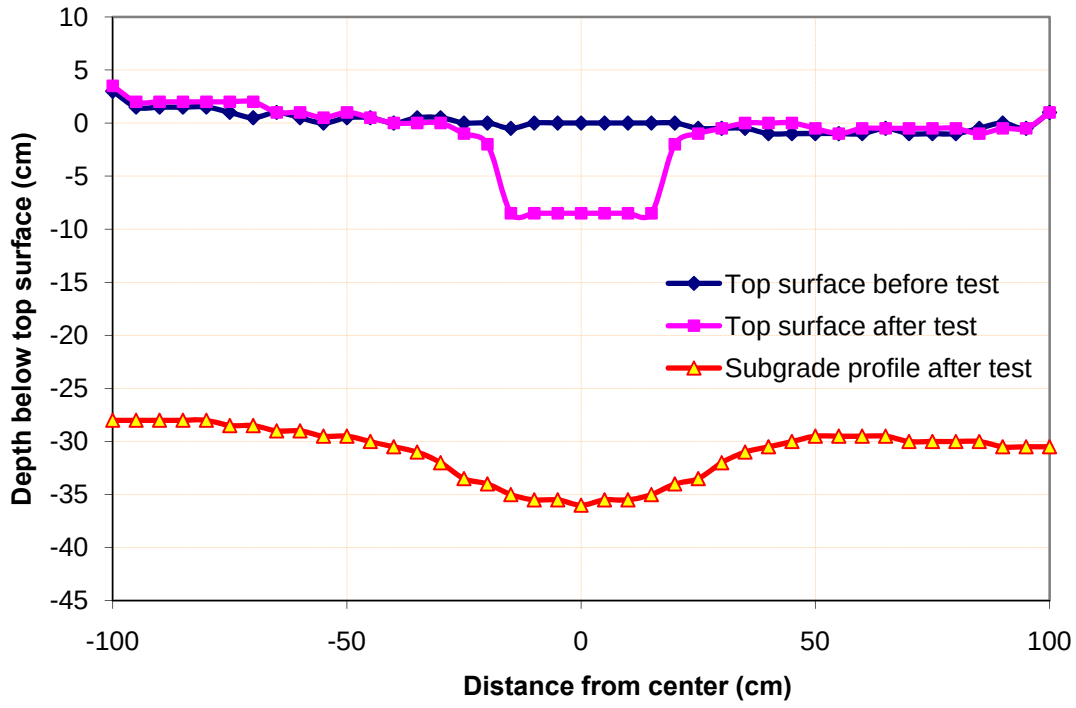

Figure 3.64 Surface profiles for 30 cm thick T1 geogrid-reinforced base

3.4.13 30 cm thick base reinforced with T2 geogrid

Figures 3.65, 3.66, 3.67, and 3.68 show the results of DCP penetration index profiles, the permanent displacement of the loading plate versus the number of cycle, the maximum vertical stress at the center and the interface between the base and the subgrade, and the surface profiles of the 30 cm thick T2 geogrid-reinforced base over the weak subgrade.

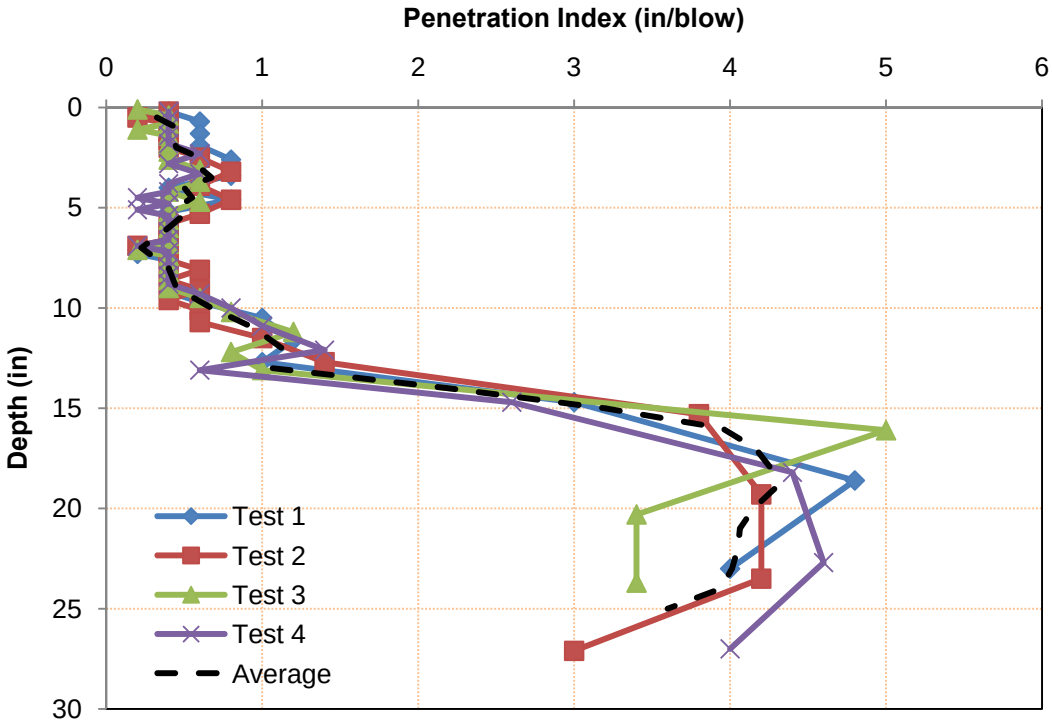

Figure 3.65 DCP test data for 30 cm thick T2 geogrid-reinforced base

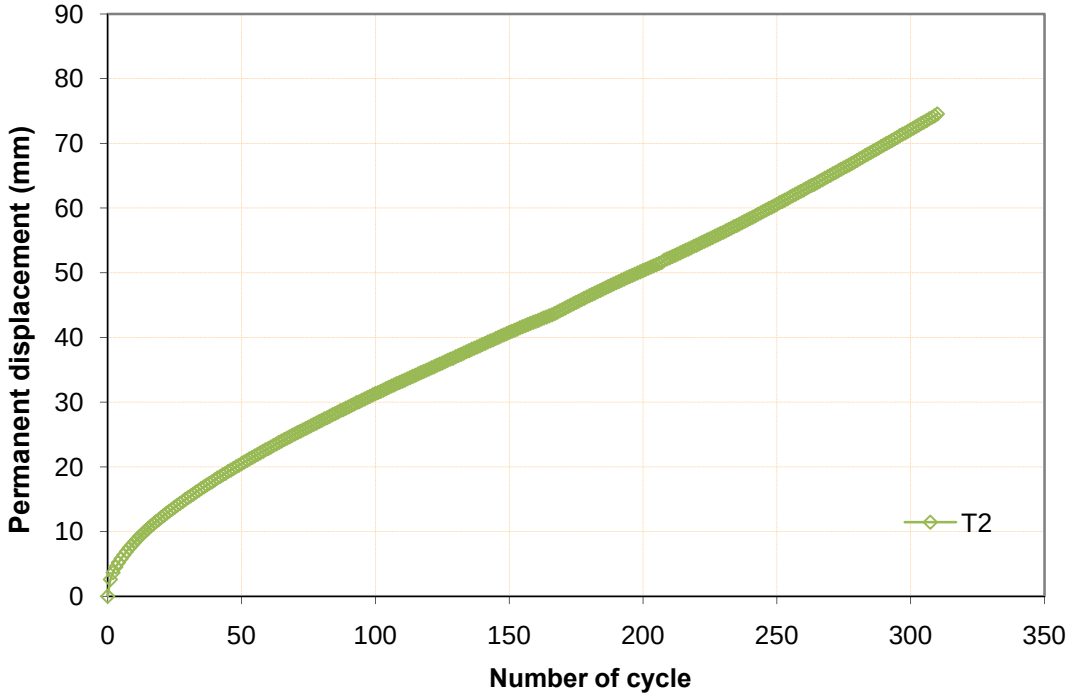

Figure 3.66 Permanent displacement of the loading plate versus the number of cycle for 30 cm thick T2 geogrid-reinforced base

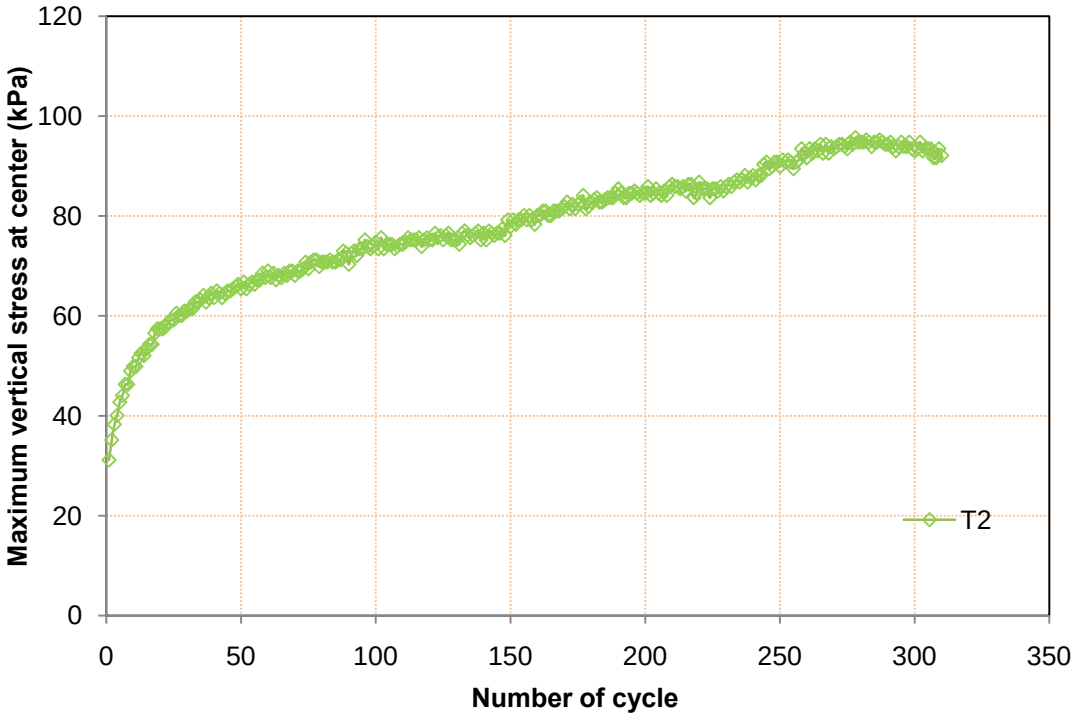

Figure 3.67 Maximum vertical stresses at the center and the interface between the base and the subgrade for 30 cm thick T2 geogrid-reinforced base

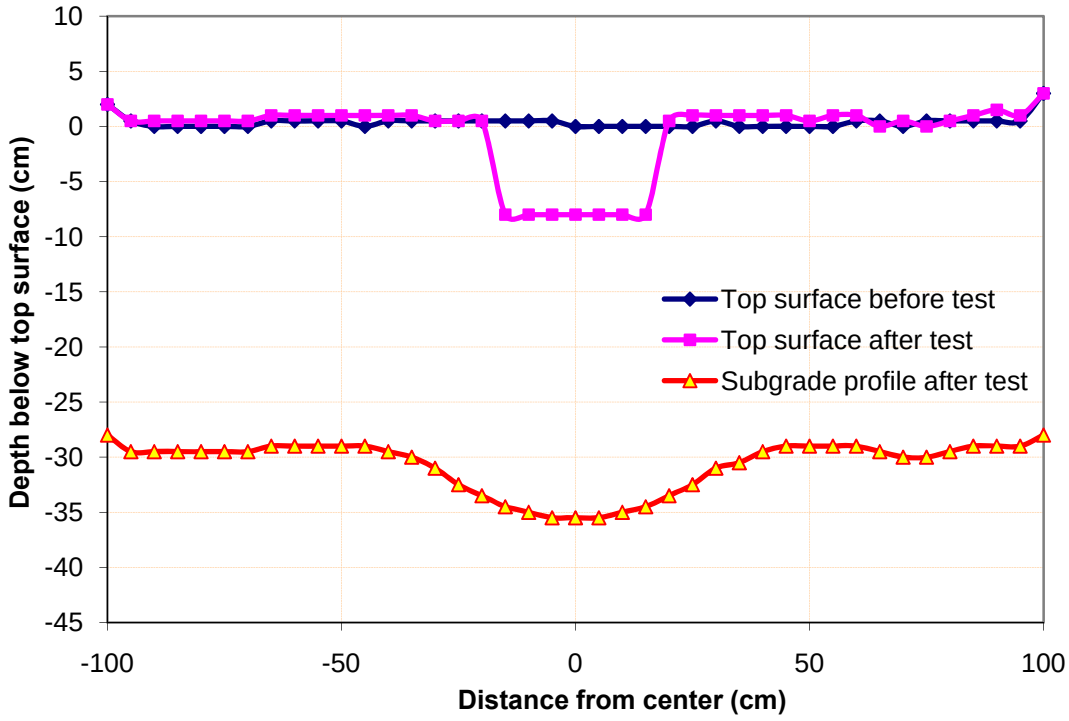

Figure 3.68 Surface profile for 30 cm thick T2 geogrid-reinforced base

3.4.14 30 cm thick base reinforced with T3 geogrid

Figures 3.69, 3.70, 3.71, and 3.72 show the results of DCP penetration index profiles, the permanent displacement of the loading plate versus the number of cycle, the maximum vertical stress at the center and the interface between the base and the subgrade, and the surface profiles of the 30 cm thick T3 geogrid-reinforced base over the weak subgrade.

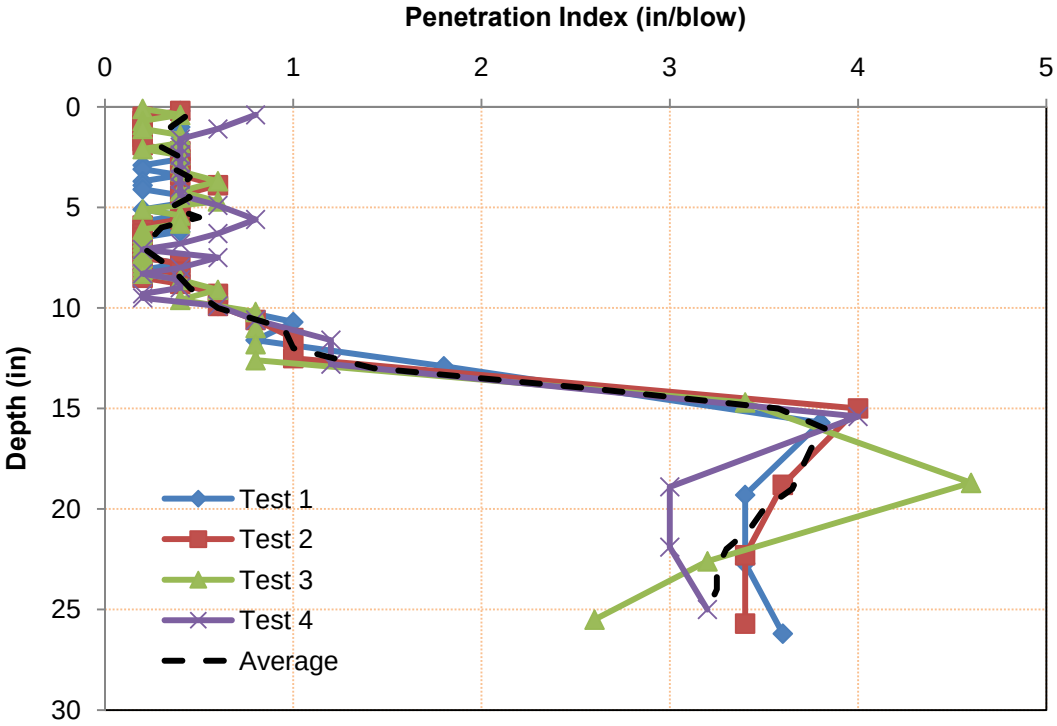

Figure 3.69 DCP test data for 30 cm thick T3 geogrid-reinforced base

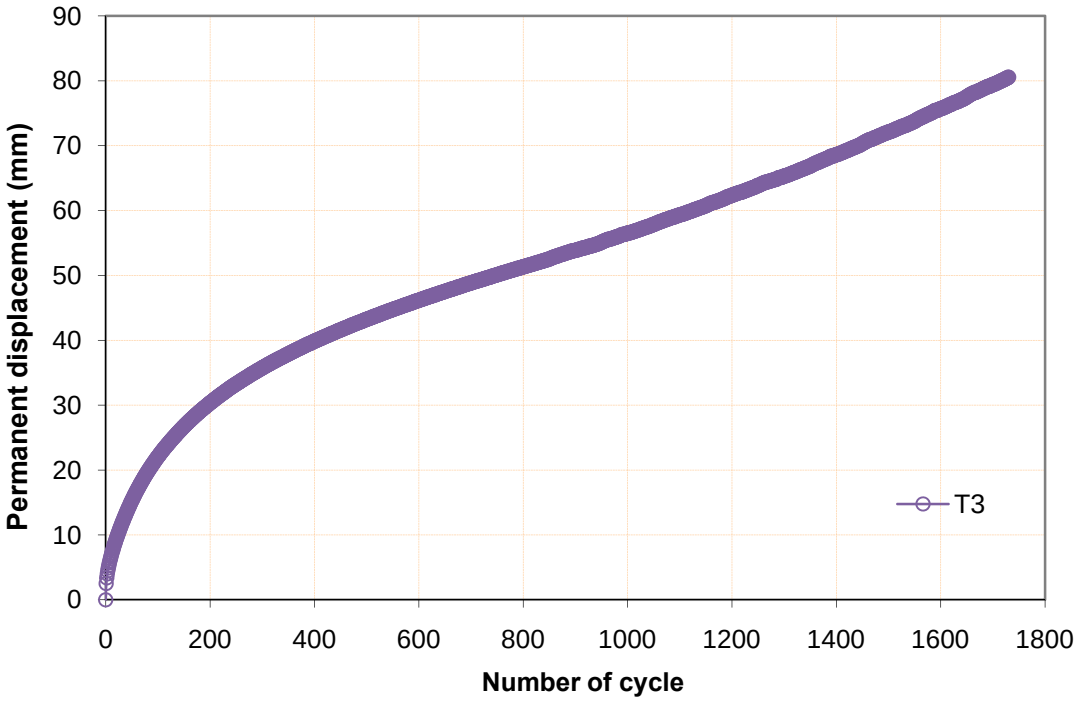

Figure 3.70 Permanent displacement of the loading plate versus the number of cycle for 30 cm thick T3 geogrid-reinforced base

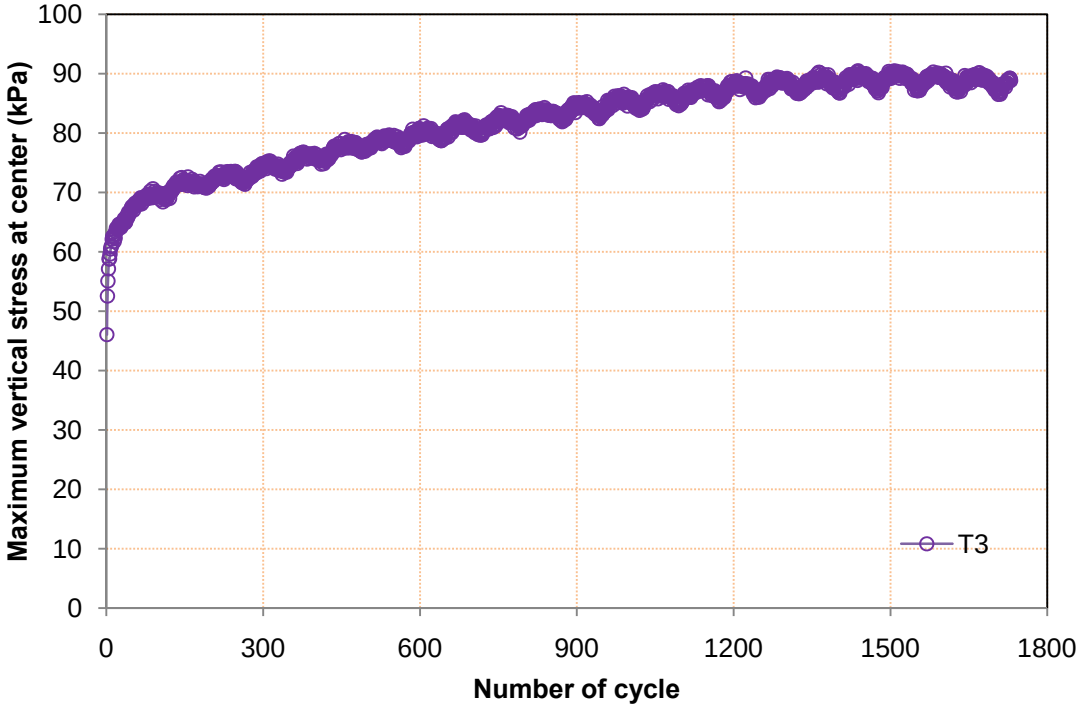

Figure 3.71 Maximum vertical stresses at the center and the interface between the base and the subgrade for 30 cm thick T3 geogrid-reinforced base

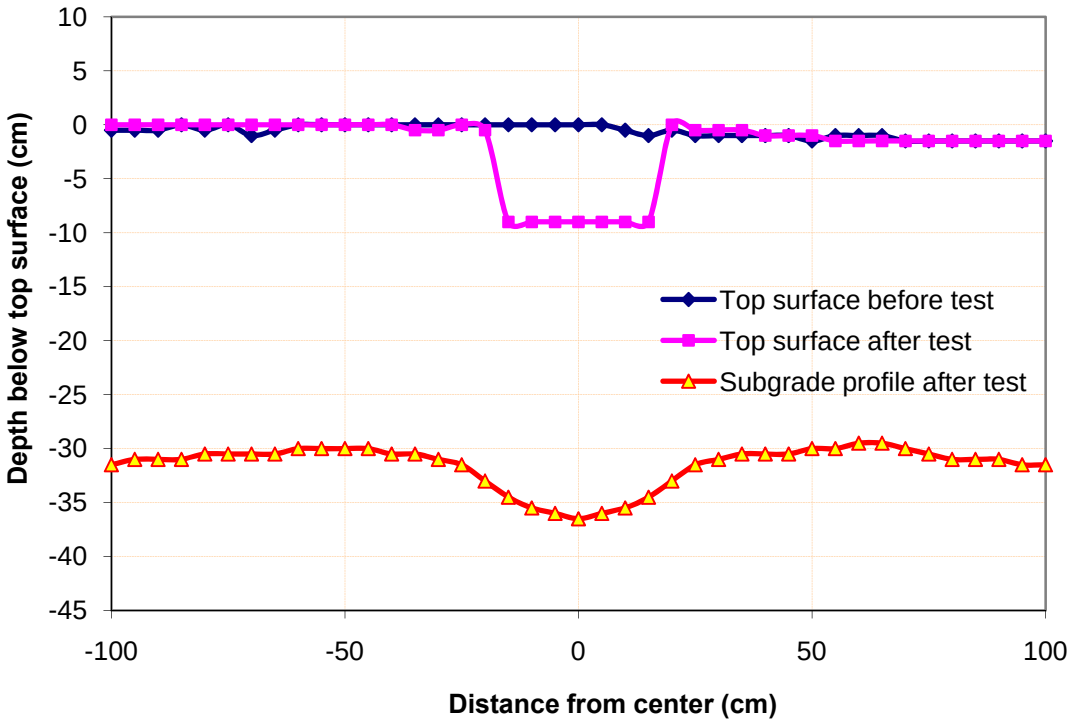

Figure 3.72 Surface profiles for 30 cm thick T3 geogrid-reinforced base

Test data for other tests will be provided in Chapter 4.

Chapter 4 DATA ANALYSIS

4.1 CBR Calculations

The California Bearing Ratios (CBR) for the bases and the subgrades in the box tests were estimated based on the DCP penetration indices using Eq. (3.2)

4.2 Repeatability

In order to verify the repeatability of the test method, three repeated experiments were conducted for two reinforced sections with T1 and T2 geogrids at 23 cm and 30 cm thick base courses, respectively. The density and stiffness of base courses and subgrade were controlled by DCP and vane shear tests. Figures 4.1 and 4.2 show the comparisons of the CBR profiles and the curves of the permanent displacement vs. the number of cycle between the original and repeated experiments for 23cm thick T1 geogrid-reinforced bases. Figure 4.1 shows that the CBR values for both sections are close. The curves of the permanent displacement vs. the number of cycle for these two sections are also close. In the repeated experiment for 23 cm thick T1 geogrid-reinforced bases, the pressure cell placed at center was broken, so the comparison between maximum vertical stress vs. the number of cycle for the repeated test and original test is not possible.

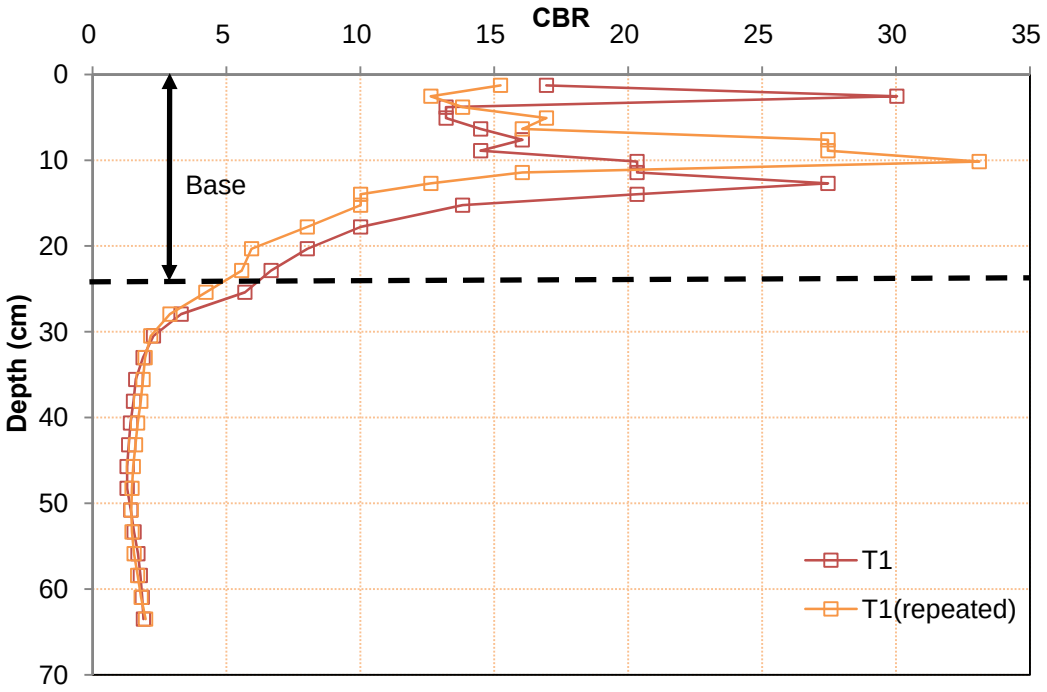

Figure 4.1 CBR profiles for 23cm thick T1 geogrid-reinforced base courses

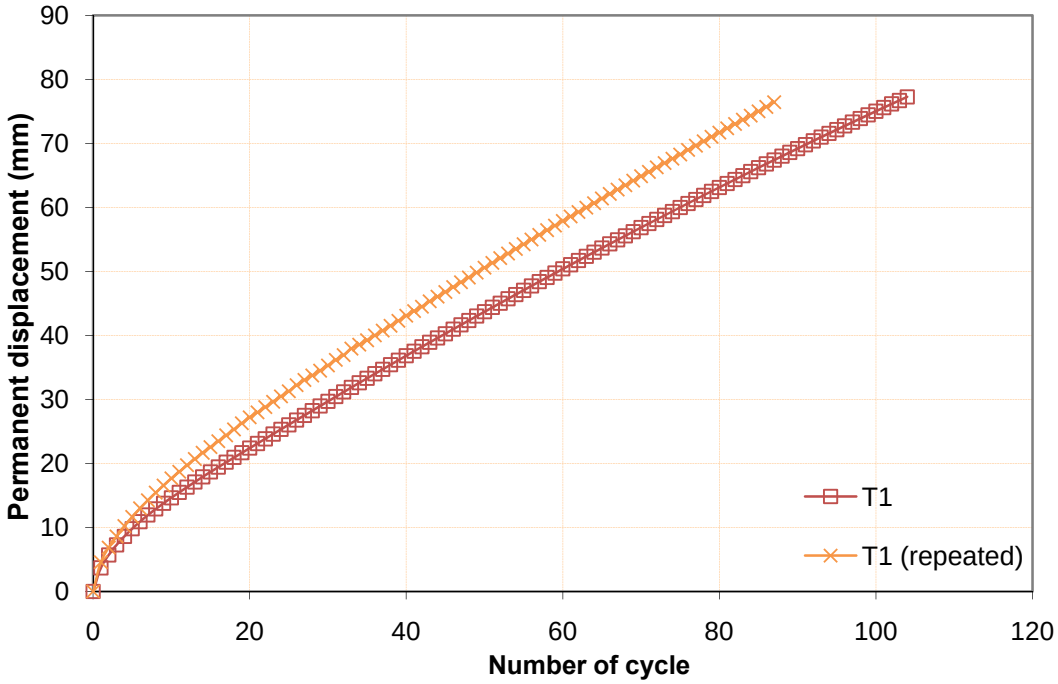

Figure 4.2 Permanent displacements of the loading plate versus the number of cycles for 23cm thick T1 geogrid-reinforced base courses

Figures 4.3, 4.4, and 4.5 show the comparisons of the CBR profiles, the curves of the permanent displacement vs. the number of cycle, and the maximum vertical stresses at the center between the original and repeated experiments for 30cm thick T1 geogrid-reinforced bases. These figures show that all the test results are close for the original and repeated experiments.

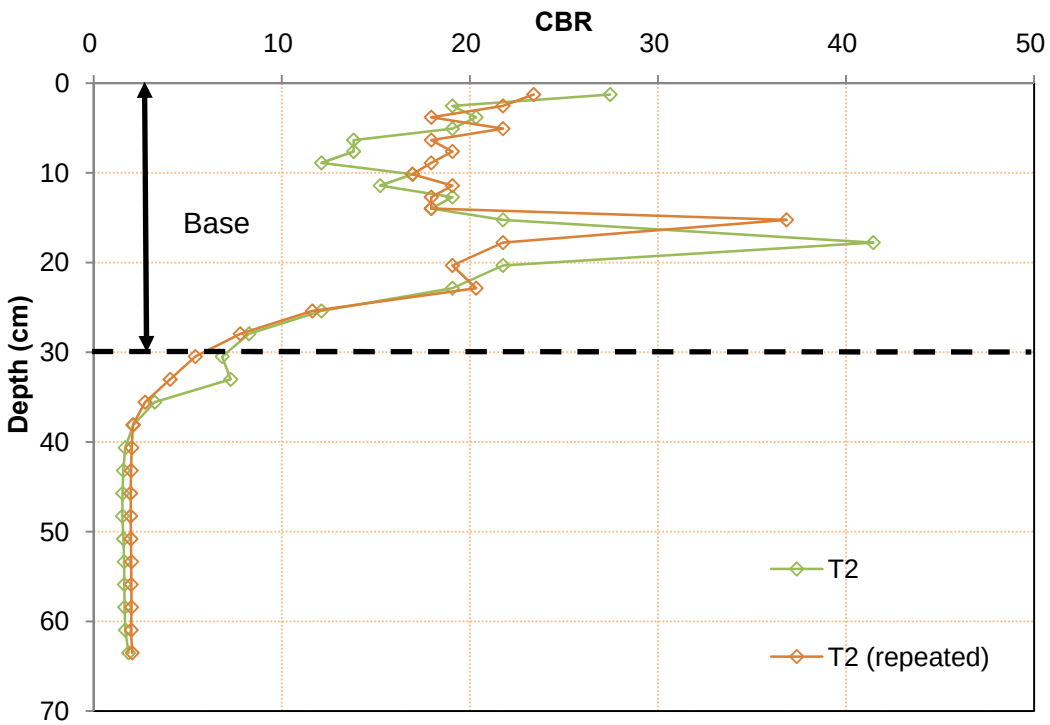

Figure 4.3 CBR profile for T2-reinforced base course at 30 cm thickness

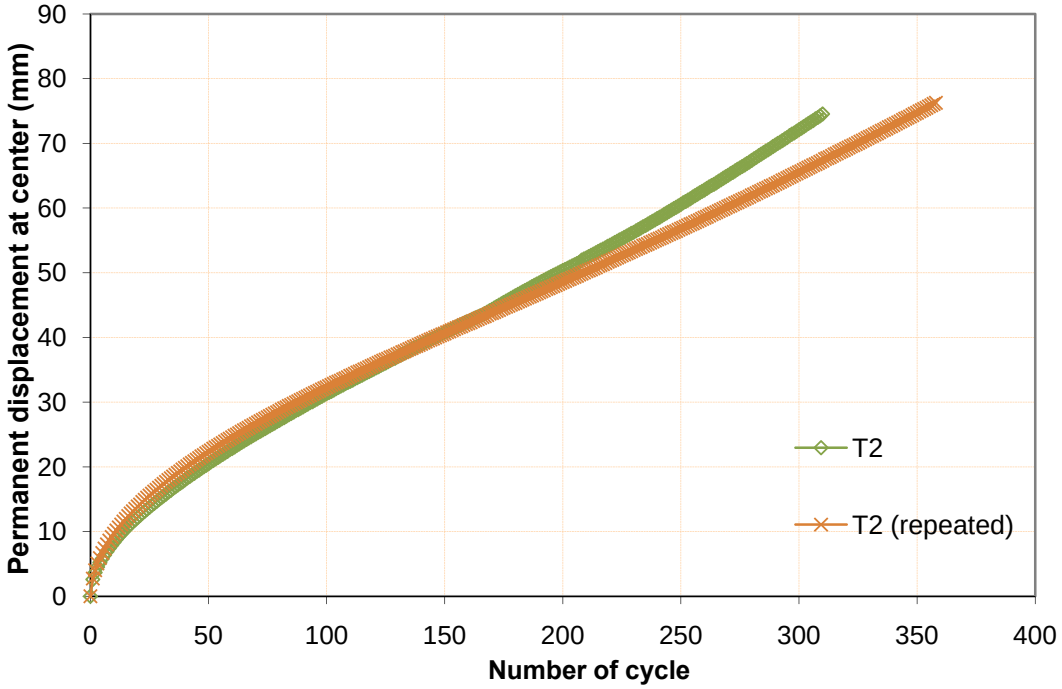

Figure 4.4 Permanent displacement of the loading plate versus the number of cycles for T2-reinforced 30 cm thick base course

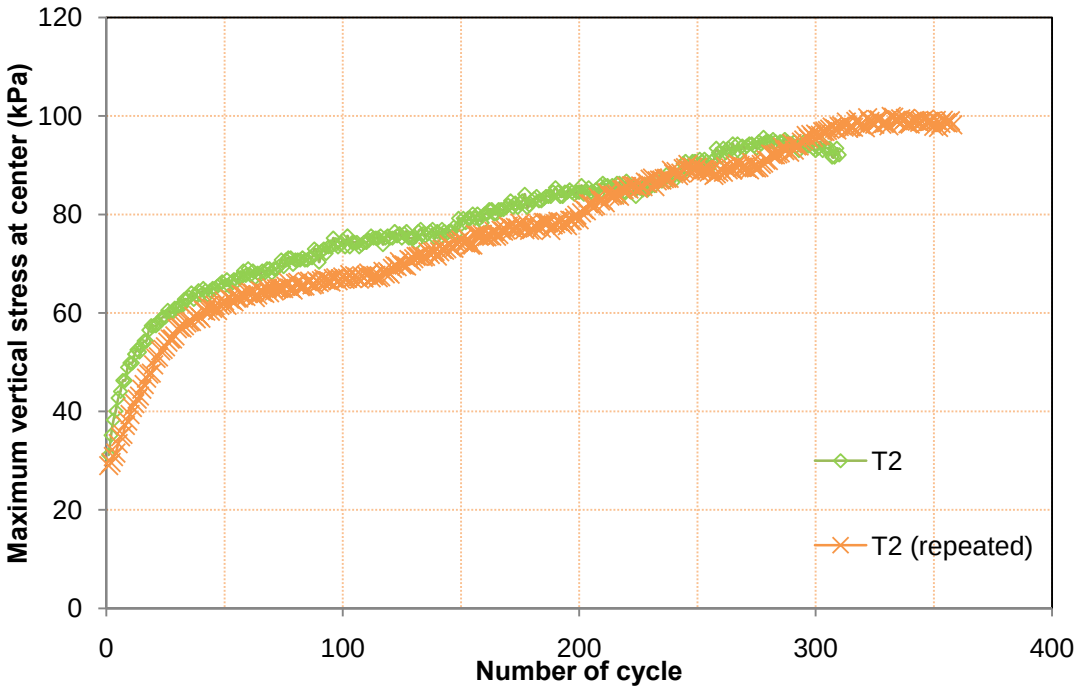

Figure 4.5 Maximum vertical stresses at center versus the number of cycles for T2-reinforced 30 cm thick base course

The comparisons of the above two pairs of original and repeated tests demonstrate that the test method used in this study is appropriate and repeatable. When the CBR values of the base course and the subgrade for two tests are close, the performance of these two test sections is similar. The small difference in the permanent displacement and/or the maximum vertical stress can be explained by the deviation of the CBR value in the base and/or the subgrade. The base course with a higher CBR value could sustain more loading cycles and transferred less vertical stress onto the subgrade as compared with the base course with a lower CBR value.

4.3 Consistency of CBR Profiles

It was designed that the test sections would have a 20% CBR base course over a 2% CBR subgrade except for those used for investigating the effects of base and subgrade CBR values. Figures 4.6, 4.7, and 4.8 provide the CBR profiles for those tests having the same base thickness (15, 23, or 30cm). All three figures show that the average CBR values for the bases were approximately 20% and those for the subgrades were approximately 2%. The base materials within 5cm above the top of the subgrade had lower CBR values because the subgrade was too weak to ensure the proper compaction within this range.

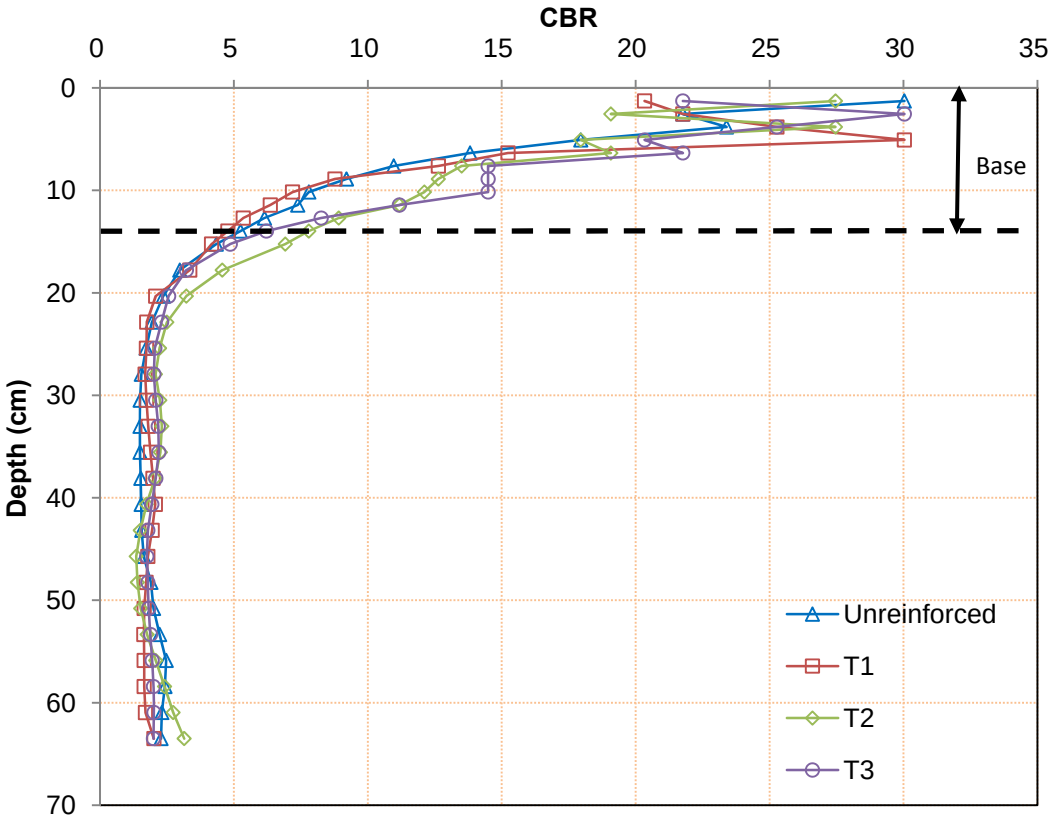

Figure 4.6 CBR profiles for 15 cm thick base courses

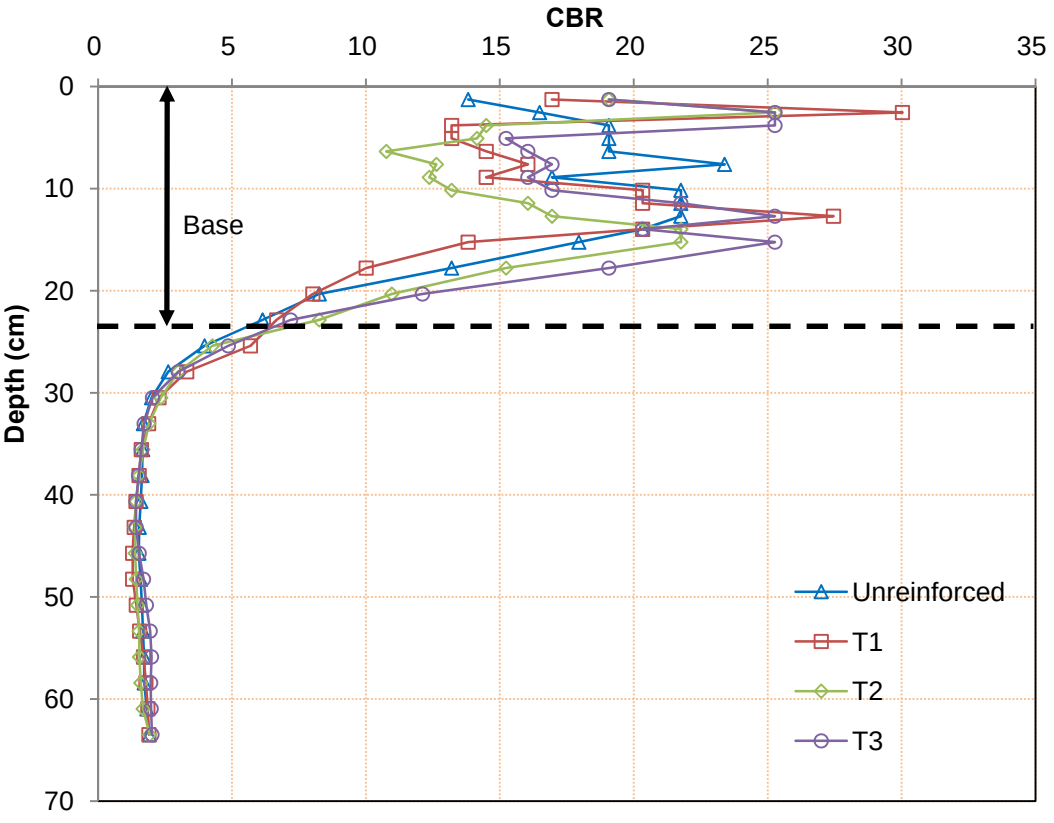

Figure 4.7 CBR profiles for 23 cm thick base courses

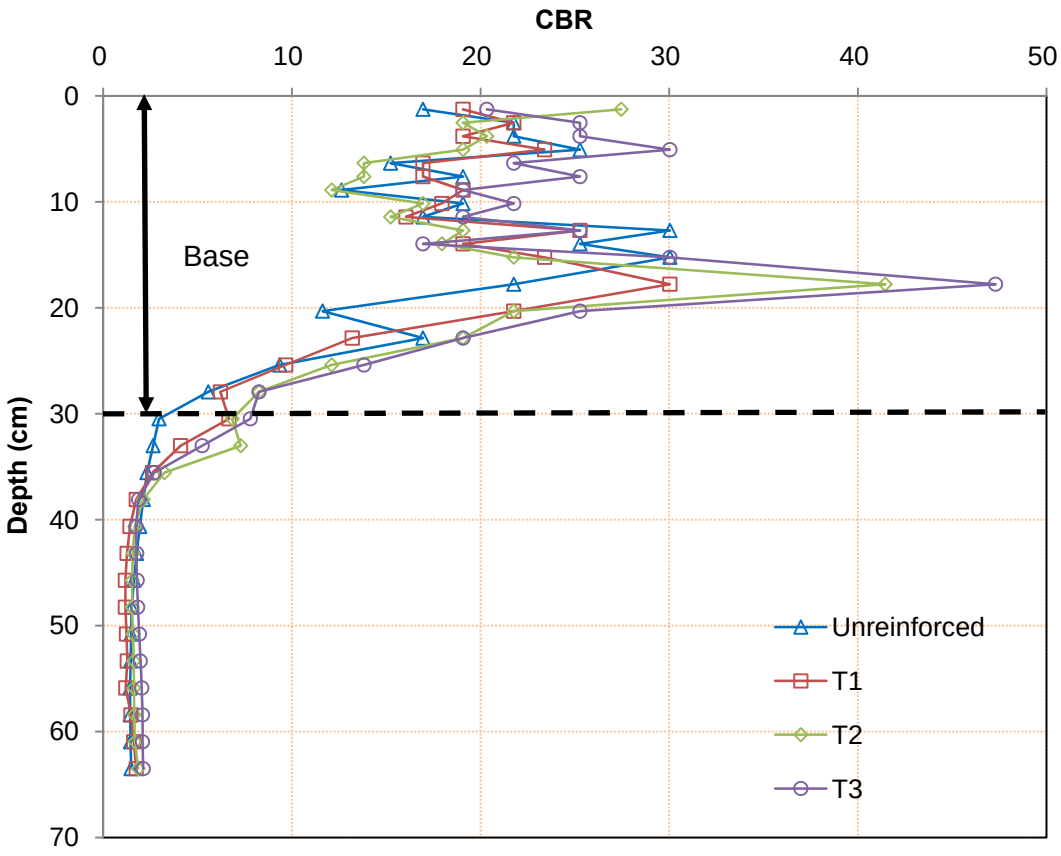

Figure 4.8 CBR profiles for 30 cm thick base courses

4.4 Displacement Analysis

4.4.1 Permanent displacement

A permanent displacement of 75 mm for the loading plate was used as the criterion to terminate the cyclic loading test. Figures 4.9, 4.10, and 4.11 present the permanent displacements of the loading plate versus the number of loading cycles for the unreinforced and reinforced bases by T1, T2, and T3 geogrids at the base course thickness of 15, 23, and 30 cm, respectively. It is shown that the permanent displacement increased with the number of cycles. At the same thickness, the reinforced bases had less permanent deformation than the unreinforced bases at the

same cycle. The permanent deformation increased more slowly for the reinforced bases than the unreinforced bases. The heavy-duty geogrid, T3, was more effective in reducing the permanent deformation and the rate of deformation increase than the medium-duty geogrid, T2, and regular-duty geogrid, T1 geogrid and the unreinforced bases. It is also shown that the permanent displacements for all the bases are similar at the initial few cycles because the geogrid was not mobilized at small displacements. With an increase of the number of loading cycles, the benefit of geogrids became more obvious.

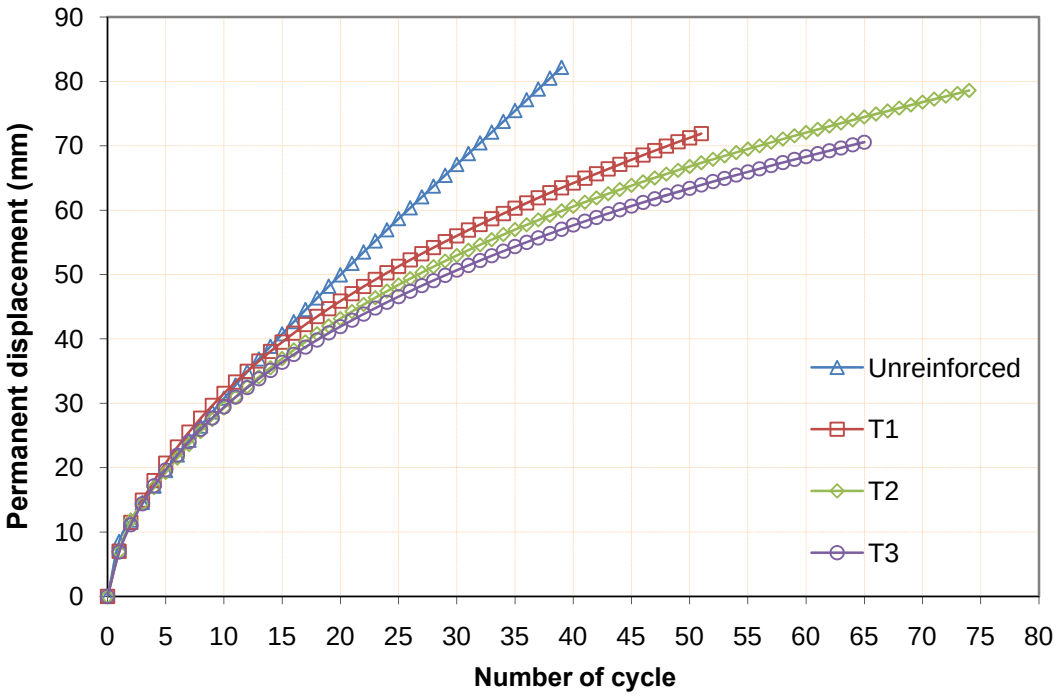

Figure 4.9 Permanent displacement of the loading plate versus the number of cycle (base thickness = 15 cm)

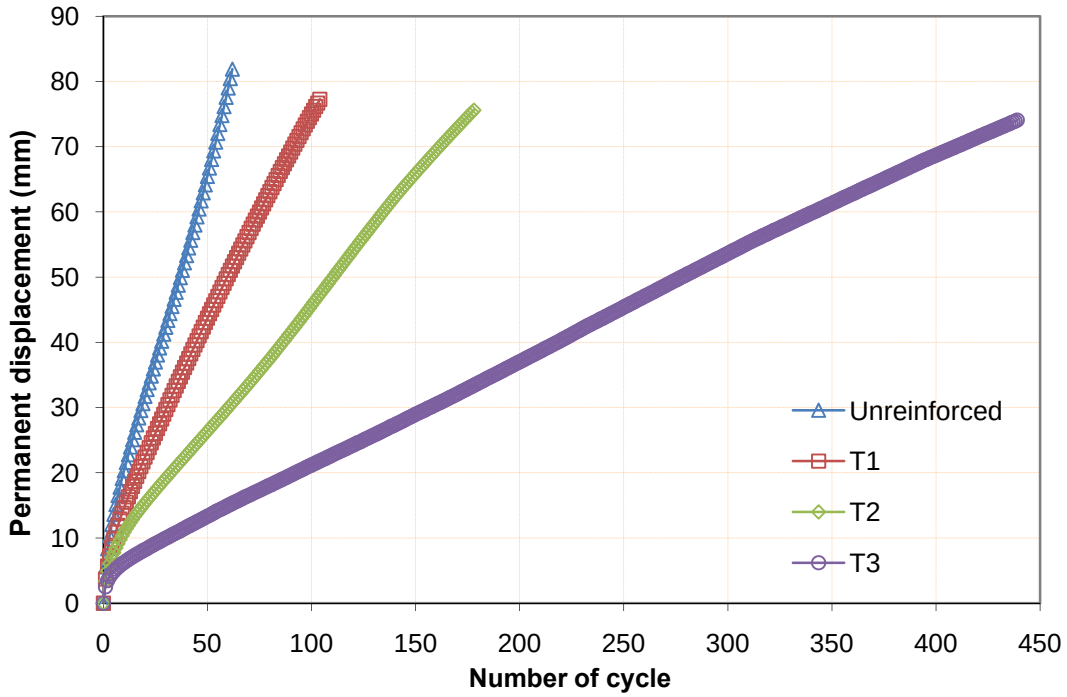

Figure 4.10 Permanent displacement of the loading plate versus the number of cycle (base thickness = 23 cm)

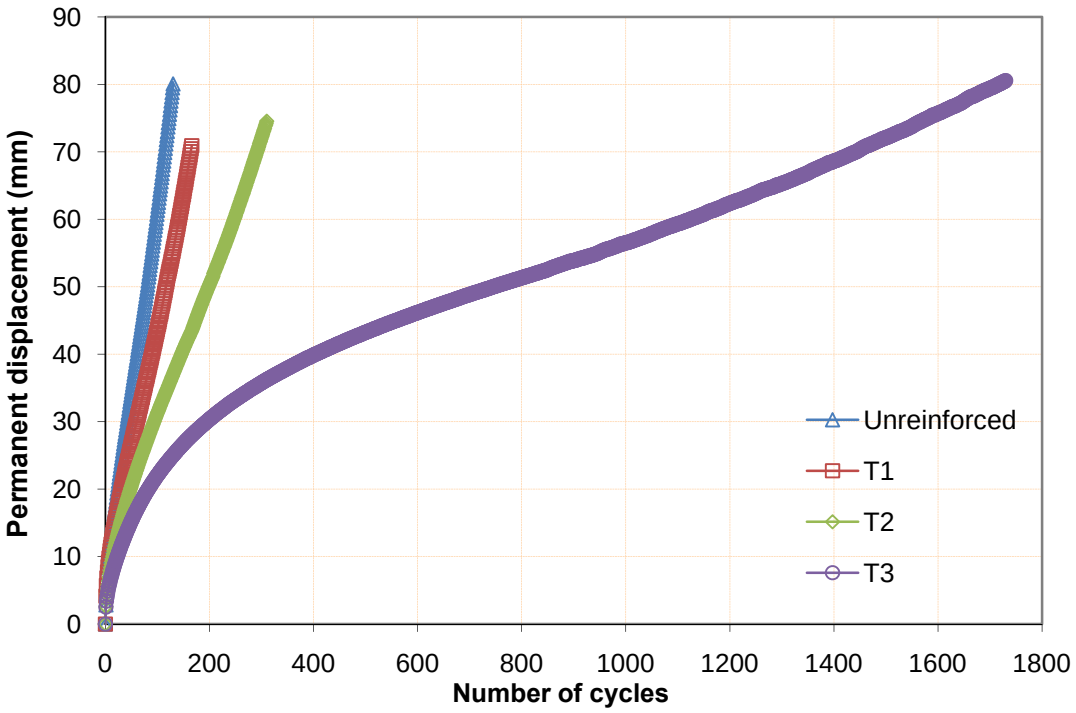

Figure 4.11 Permanent displacement of the loading plate versus the number of cycle (base thickness = 30 cm)

In order to demonstrate the benefit of the geogrids, an improvement factor is defined here as the ratio of the number of cycles for the reinforced base over the number of cycles for the unreinforced base at the same permanent displacement of 75 mm. The improvement factor can be expressed as below:

$$Improvement\ f = \frac{N_{\text{reinforced}}}{\text{N}_{\text{unreinforced}}} \quad (4.1)$$

where $N_{\text{reinforced}}$ = the number of cycles for the reinforced base at the permanent displacement of 75 mm; $N_{\text{unreinforced}}$ = the number of cycles for the unreinforced base at the permanent displacement of 75 mm.

At 15 cm base thickness, the numbers of cycles for the unreinforced, T1, T2, and T3, geogrid-reinforced bases at the permanent displacement of 75 mm were 35, 55, 66, and 78, respectively. Therefore, the improvement factors for the T1, T2, and T3, geogrids were 1.57, 1.88, and 2.23, respectively.

At 23 cm base thickness, the numbers of cycles for the unreinforced, T1, T2, and T3 geogrid-reinforced bases at the permanent displacement of 75 mm were 57, 85, 176, and 447, respectively. Therefore, the improvement factors for T1, T2, and T3 geogrids were 1.49, 3.09, and 7.84, respectively.

At 30 cm base thickness, the numbers of cycles for the unreinforced, T1, T2, and T3

geogrid-reinforced bases at the permanent displacement of 75 mm were 122, 177, 312, and 1580, respectively. Therefore, the improvement factors for T1, T2, and T3 geogrids were 1.45, 2.56, and 12.95, respectively.

Overall, T3 geogrid performed the best for all three base thicknesses. The performance of the geogrids from the best to the least is T3, T2, and T1, which is the same order as the levels of robustness, unit weight, rib thicknesses, and mechanical properties of these geogrids, and as expected for this specific family of geogrid products.

4.4.2 Resilient displacement

Figures 4.12, 4.13, and 4.14 present the percentage of resilient displacement at each loading cycle for the unreinforced and reinforced bases. The percentage of resilient displacement was calculated as the rebound divided by the total displacement in each cycle. Overall, the percentage of resilient displacement increased nonlinearly for both unreinforced and reinforced bases. For geogrid-reinforced bases, the percentage of resilient displacement reached as high as 90% to 99% of the total displacement for each cycle. However, for unreinforced bases, the percentage of resilient displacement was much lower. Therefore, the geogrids significantly increased the percentage of resilient displacement as compared with the unreinforced base. In other words, the reinforced bases are more resilient than the unreinforced base.

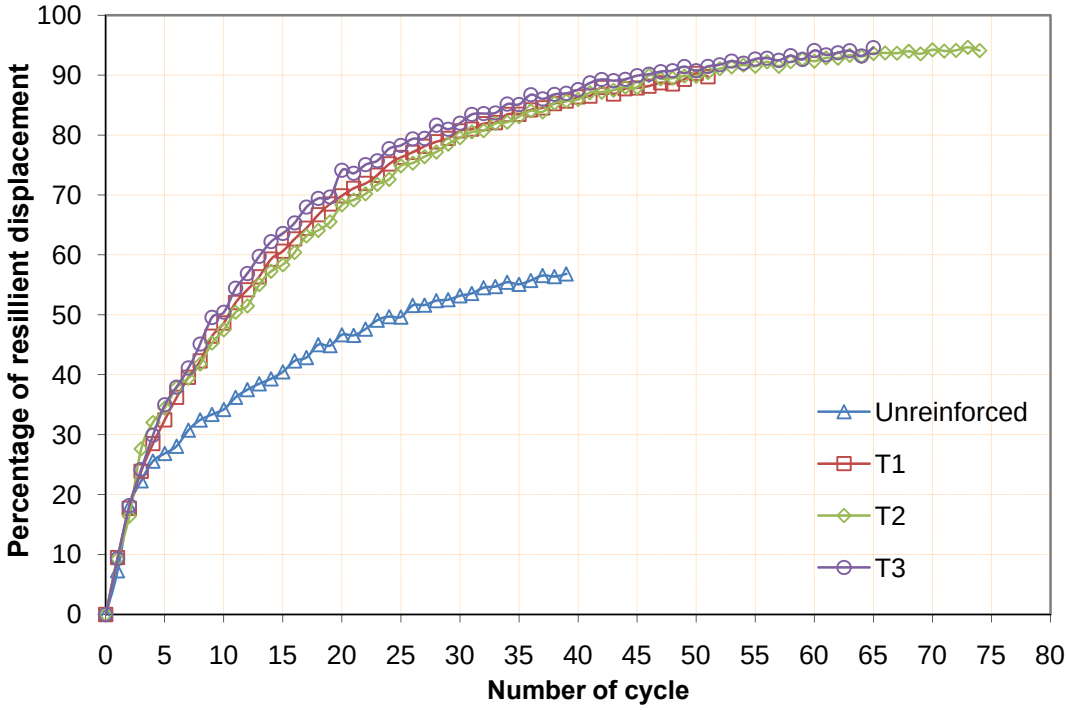

Figure 4.12 Percentage of resilient displacement of the loading plate versus the number of cycles (base thickness = 15 cm)

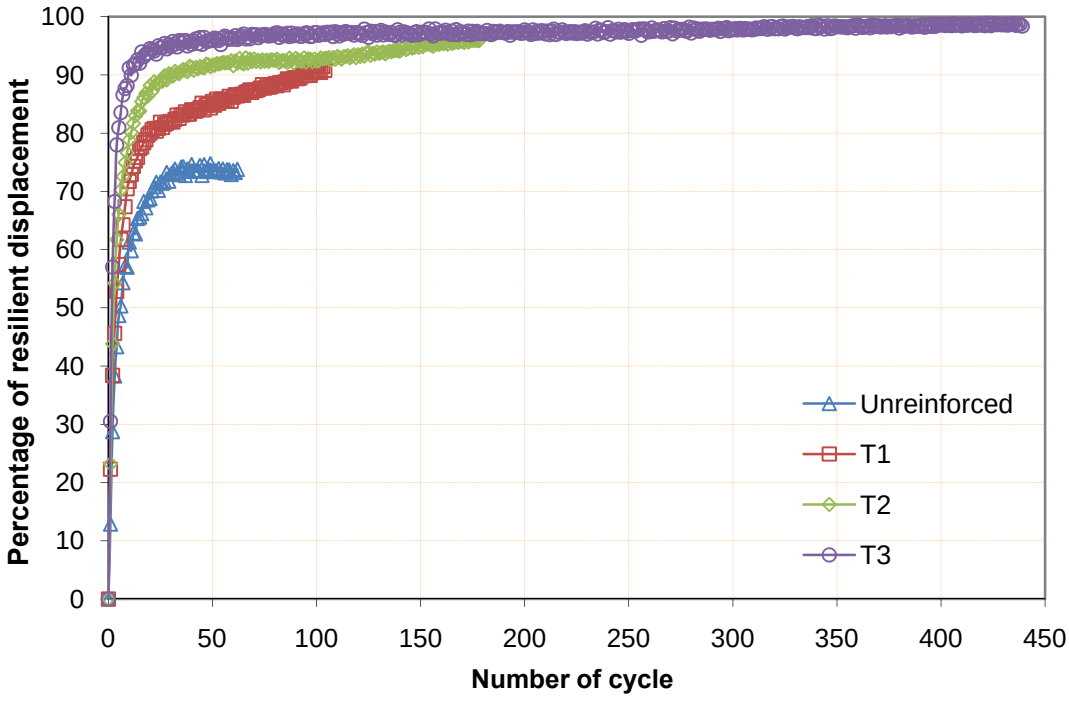

Figure 4.13 Percentage of resilient displacement of the loading plate versus the number of cycles (base thickness = 23 cm)

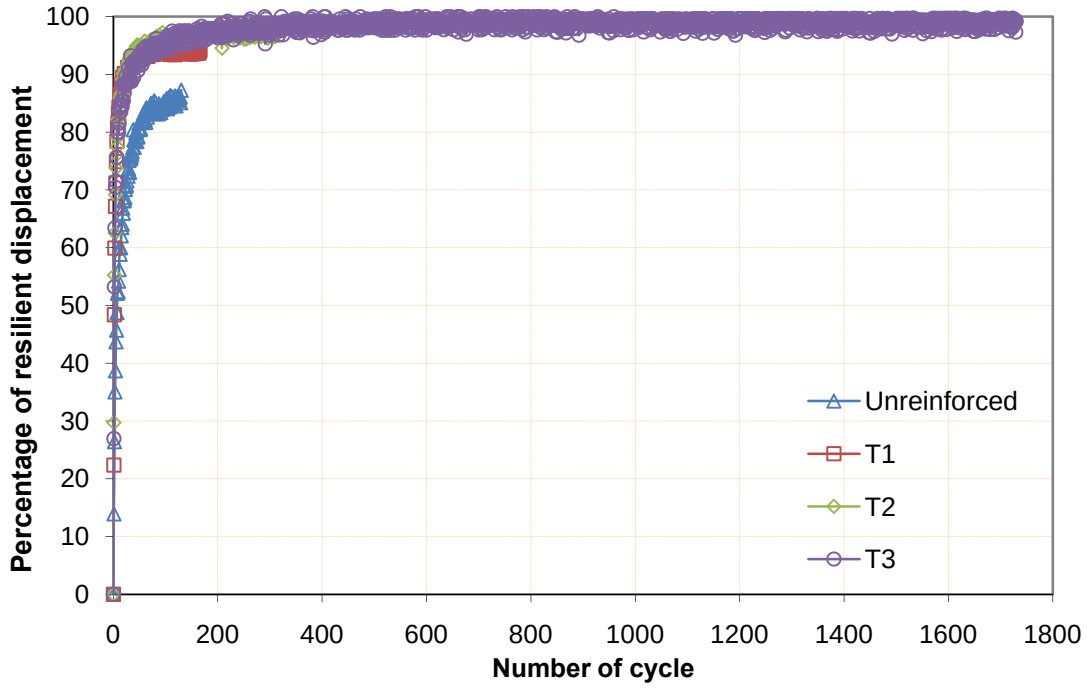

Figure 4.14 Percentage of resilient displacement of the loading plate versus the number of cycles (base thickness = 30 cm)

4.5 Stress Analysis

4.5.1 Maximum vertical stress

For each test, vertical stresses at the interface between the base course and the subgrade were measured at four different distances from the center, 0, 25, 50, and 75 cm. Figures 4.15, 4.16, and 4.17 presents the measured maximum vertical stresses located along the center of the loading plate. It is clear that the initial maximum vertical stresses for all tests were close to each other. However, the maximum vertical stresses increased faster for the unreinforced bases than the reinforced bases. When the more robust, thicker and higher mechanical property geogrid was used, the maximum vertical stresses increased more slowly than when the less robust, thinner and lower mechanical property geogrid was used. It should be noted though that

there is likely a point of optimum for all of the various geogrid properties and the property compatibility between the geogrid and the soil being reinforced is important. The test results also show that the unreinforced base had the highest maximum vertical stress at each base thickness. The lower maximum vertical stresses in the reinforced bases are attributed to the benefit of the geogrids on increasing the stress distribution angle. The base reinforced by the T3 geogrid had a larger distribution angle than that reinforced by the T2 geogrid, which had a larger distribution angle than that reinforced by the T1 geogrid. More discussion on the stress distribution will be presented later. Figures 4.15, 4.16, and 4.17 also show that the maximum vertical stresses increased with the number of cycles, which is in good agreement with the finding by Gabr (2001). The increase in the maximum vertical stress with the number of cycles was explained by Giroud and Han (2004a) as the reduction of the stress distribution angle due to the deterioration of the base course.

It is also found in Figure 4.15 that the maximum vertical stresses decreased after reaching the peak values (around 20 to 30 cycles) for all the reinforced bases. This reduction may result from the establishment of a stabilized composite between the geogrid and the base materials. The stabilized composite has improved stiffness and load spread capabilities, and significantly enhanced ductility which leads to decreased stress on the subgrade. Another contributing factor may be the tensioned membrane effect provided by the geogrid alone. However, the tensioned membrane effect only influences the performance of the reinforced base after large displacements, such as

100 mm or more (Giroud and Han, 2004b) and does not govern performance in the low deformation ranges. However, this effect may play a greater role at a smaller displacement when the base course is relatively thin. When the base course is thicker, the influence of the tensioned membrane effect becomes less. Figures 4.16 and 4.17 do not show obvious peaks of the maximum vertical stresses for the unreinforced and reinforced bases. In other words, when the base course was thicker, the tensioned membrane effect became less significant to reduce the vertical stress and the stabilized composite effects dominate.

Figures 4.16 and 4.17 also show that the maximum vertical stresses increased rapidly after a certain loading cycle. This phenomenon may be because that the base course deteriorated to a certain stage and the base course itself could not sustain the vertical stress anymore. After this cycle, the unpaved section approached to the failure quickly. A further study is needed to verify this phenomenon.

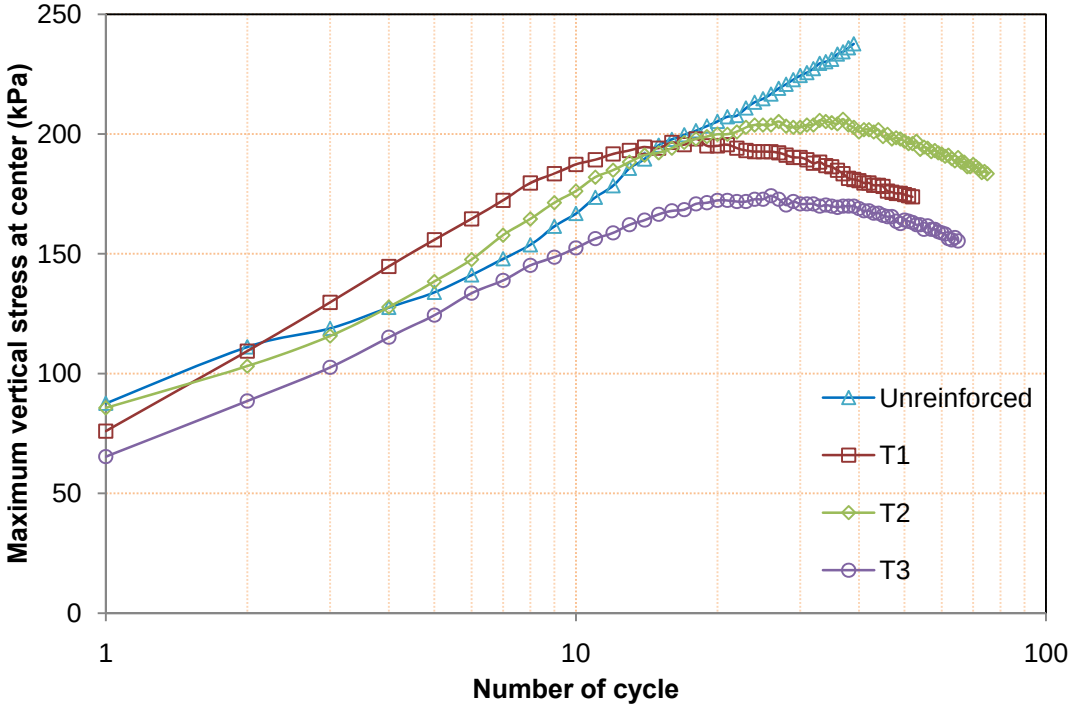

Figure 4.15 Maximum vertical stresses at the interface between the base and the subgrade (base thickness = 15 cm)

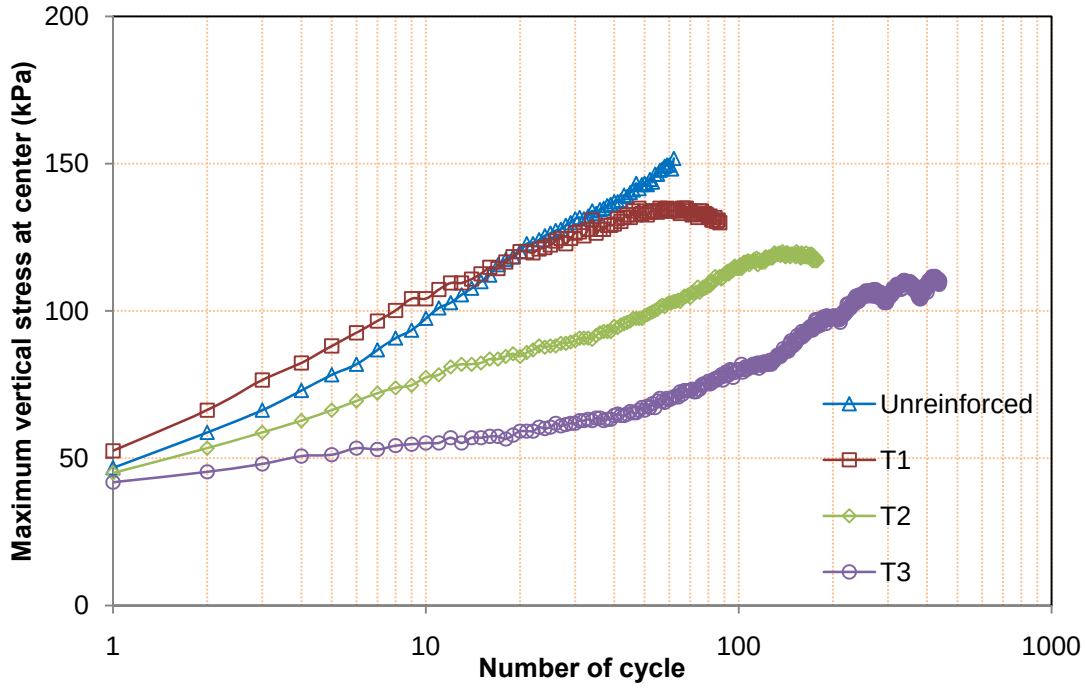

Figure 4.16 Maximum vertical stresses at the interface between the base and the subgrade (base thickness = 23 cm)

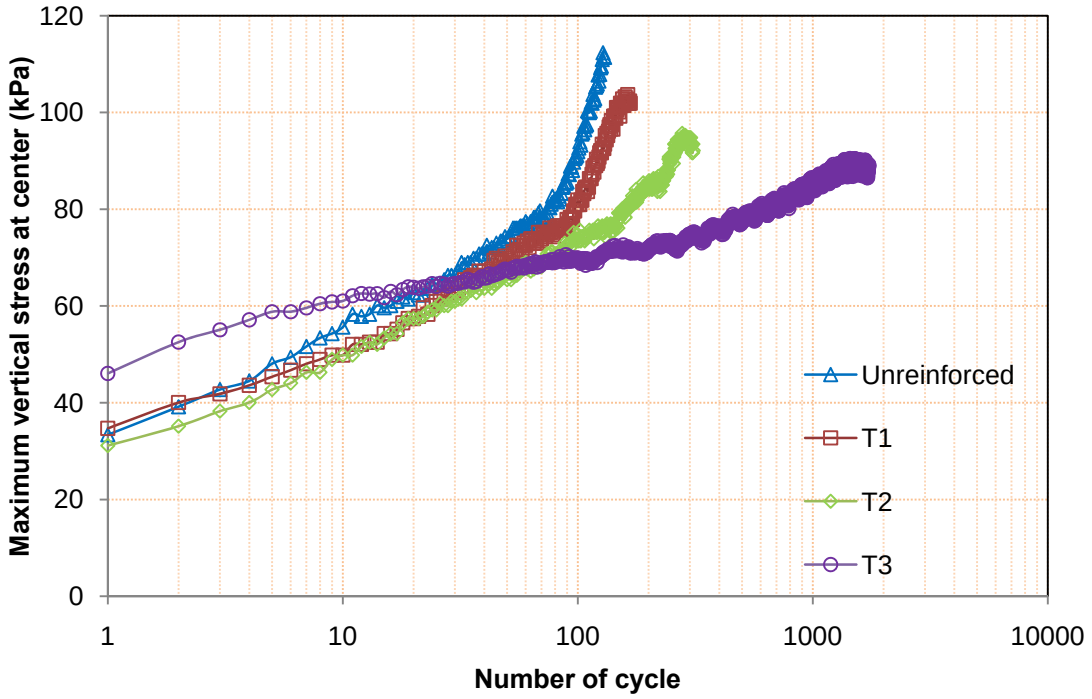

Figure 4.17 Maximum vertical stresses at the interface between the base and the subgrade (base thickness = 30 cm)

4.5.2 Stress distribution

The measured vertical stresses at different distances from the center during cyclic loading can be plotted to show their distributions. Figures 4.18, 4.19, and 4.20 present the distributions of the vertical stresses at the interface between the base and the subgrade for the unreinforced and T1, T2, and T3 geogrid-reinforced base courses at base thicknesses of 15, 23, and 30cm, respectively. It is shown that the geogrids reduced the maximum vertical stresses at the center and transferred the vertical load to a wider area as compared with the unreinforced bases.

The test results show that the different grades of geogrids within the triangular aperture geogrid family affected the stress distribution. The more robust, thicker and higher mechanical property geogrids helped distribute the stresses more uniformly

thus reducing the maximum vertical stresses and resulting in less displacement of the subgrade.

Stress distribution was also influenced by the properties of the base course. The stiffer base course (i.e., higher CBR) could distribute the load to a wider area. Further discussion on the influence of the stiffness of the base course will be addressed later in this chapter.

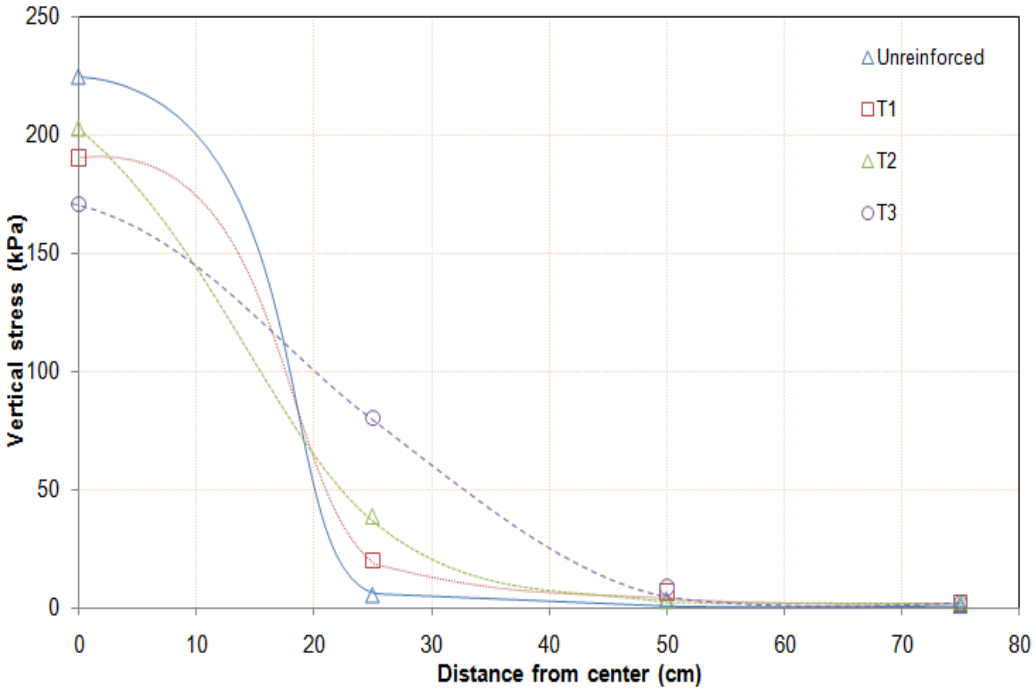

Figure 4.18 Vertical stress distributions at 30th load cycle (base thickness = 15 cm)

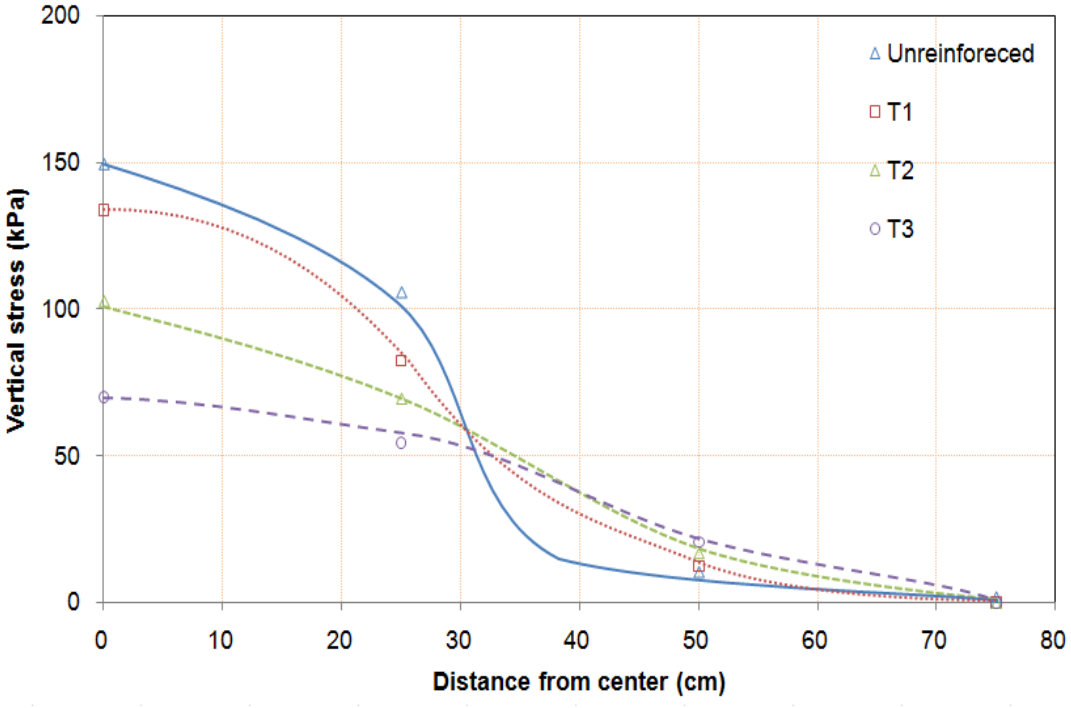

Figure 4.19 Vertical stress distributions at 60th load cycle (base thickness = 23 cm)

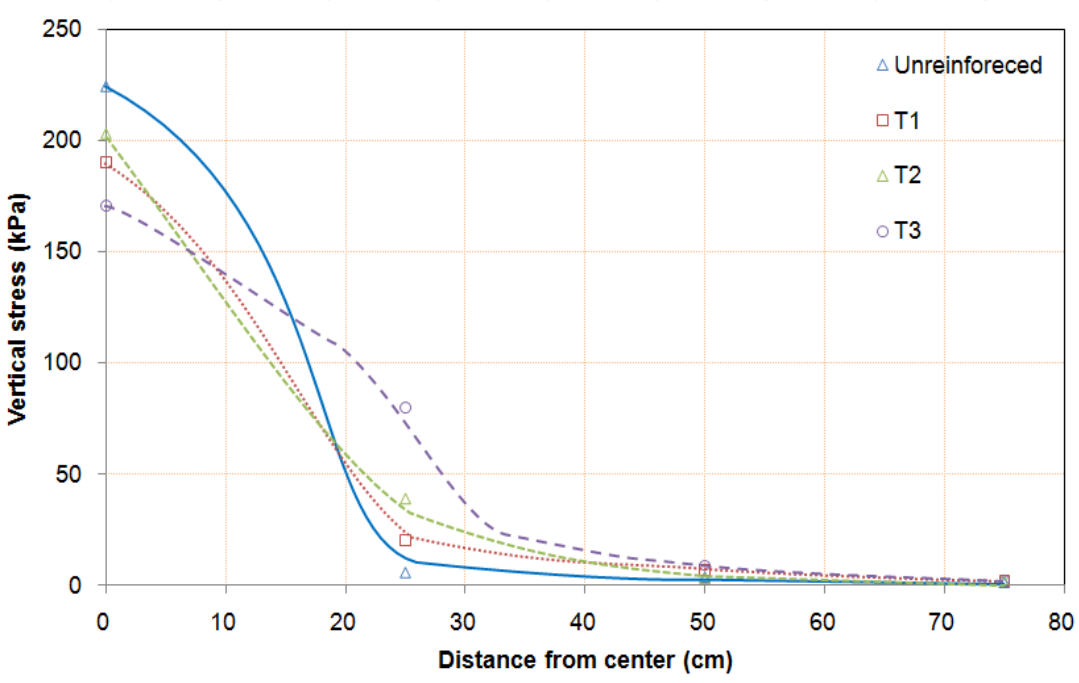

Figure 4.20 Vertical stress distributions at 90th load cycle (base thickness = 30 cm)

Figures 4.21 to 4.24 present the change of stress distribution during the cyclic loading for the 15cm thick unreinforced and T1 geogrid-reinforced base courses, the 23cm thick T2 and T3 geogrid-reinforced base courses, respectively.

During the cyclic loading, the stress distribution became less uniform and more concentrated in a smaller area for all the tests. This phenomenon is in agreement with the model in the Giroud and Han method (Giroud and Han 2004a), i.e., the base course would deteriorate during the cyclic loading. Within an increase in the number of cycles, the stress distribution angle becomes smaller, therefore, the vertical stresses concentrate onto a smaller center area. One of the functions of the geogrid is to maintain the quality of the base course and slow down the reduction of the stress distribution angle.

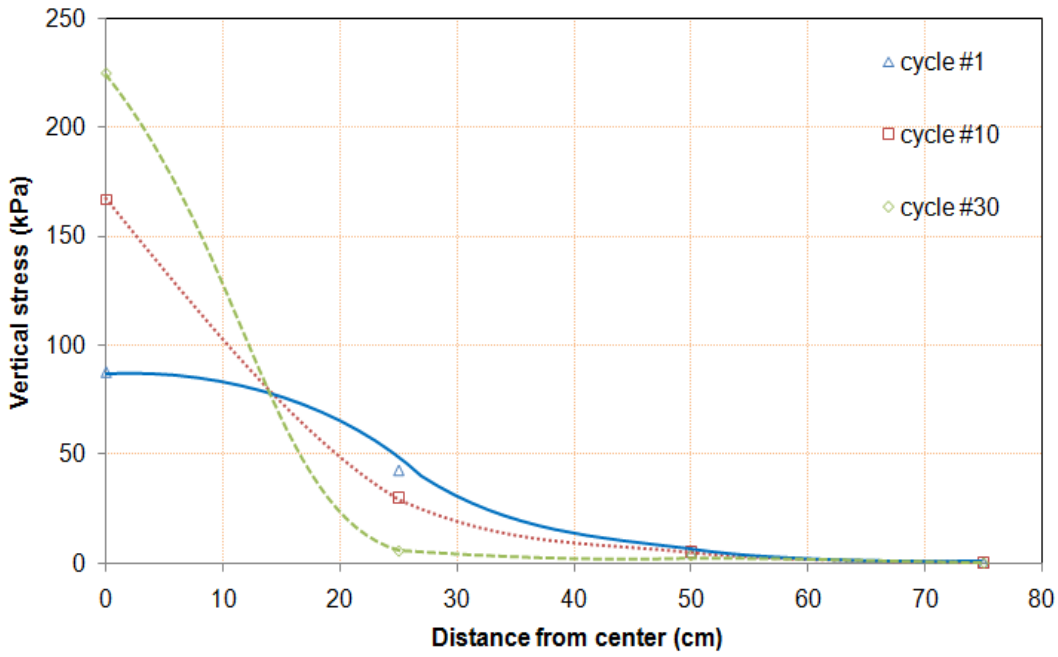

Figure 4.21 Vertical stress distributions at the interface between the base course and the subgrade for 15 cm thick unreinforced base course

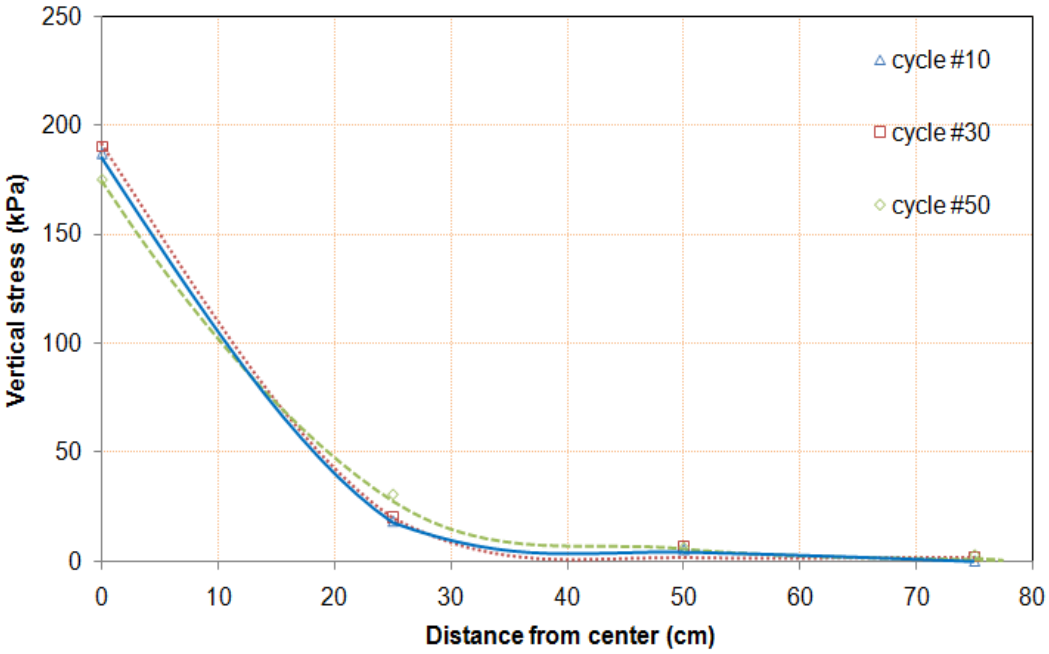

Figure 4.22 Vertical stress distributions at the interface between the base course and the subgrade for 15 cm thick T1 geogrid-reinforced base course

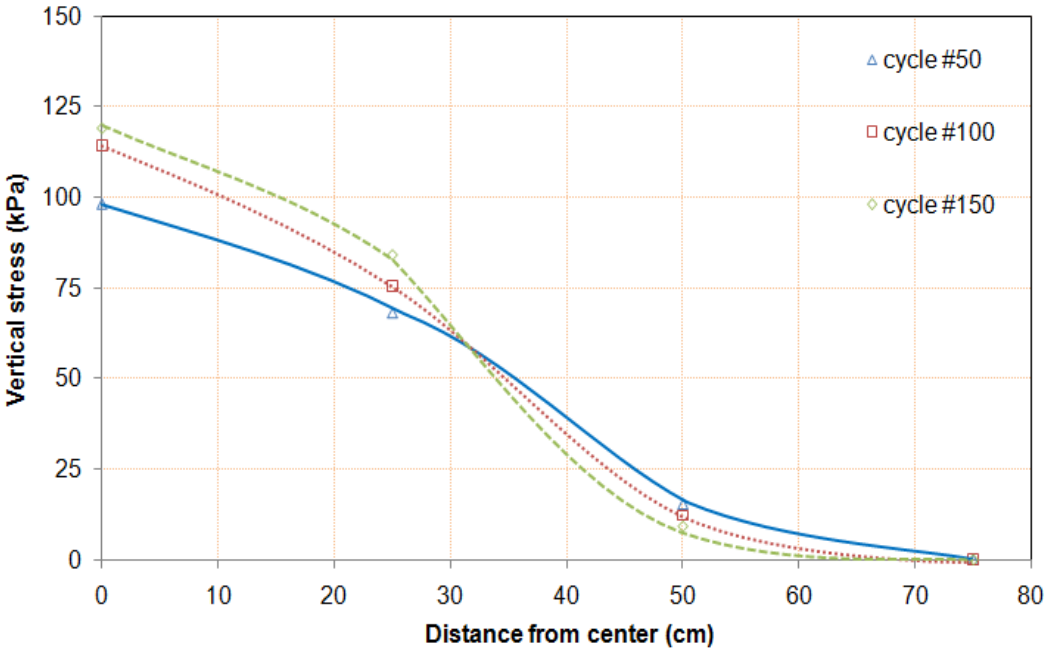

Figure 4.23 Vertical stress distributions at the interface between the base course and the subgrade for 23 cm thick T2 geogrid-reinforced base course

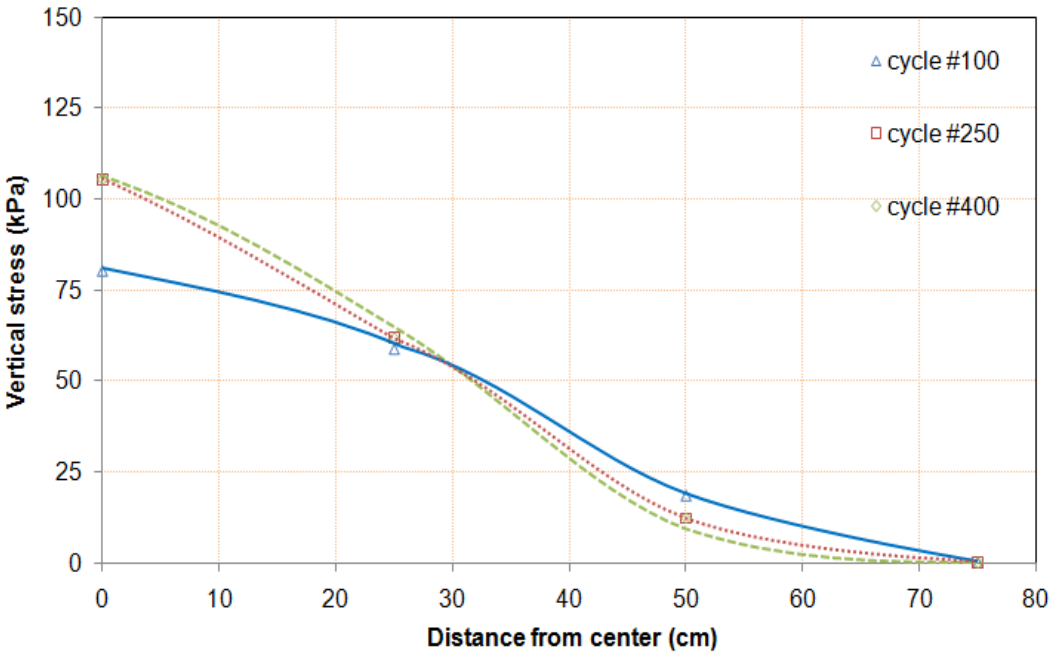

Figure 4.24 Vertical stress distributions at the interface between the base course and the subgrade for 23 cm thick T3 geogrid-reinforced base course

4.5.3 Stress distribution angle

It is necessary to discuss the stress distribution angle further since it plays an essential role in the stress distribution. Assuming a wheel load, P, is applied uniformly upon a circular area having a radius, r. The vertical stresses are distributed to a depth, h, at a stress distribution angle, α. The vertical stress (pressure), p_i, at the interface between the base course and the subgrade can be estimated using the following equation (Giroud and Han, 2004a):

$$p_i = \frac{P}{\pi(r + h\tan\alpha)^2} \tag{4.2}$$

where *pi* = the distributed vertical stress at the interface between the base course and the subgrade (kPa); *P* = the wheel load (kN); *r* = the radius of the circular area.

According to the measured maximum vertical stress at the interface, the applied wheel load, and the plate diameter, the stress distribution angle can be calculated for each cycle during the cyclic loading tests. Figures 4.25, 4.26, and 4.27 show the relationships between the reciprocal of the tangential values of the stress distribution angles and the number of cycles. The initial values of 1/tan (α) for all the tests are close to one and increase nearly linearly with the increase of the number of cycles. The deviation of the initial value of 1/tan (α) may be caused by the slight difference in the initial stiffness of the base course and the subgrade. The contribution of the geogrid to the initial stress distribution angle is minimal because the base course is not fully engaged within the apertures of the geogrid. These figures show that the base courses with greater thicknesses had higher initial stress distribution angles. The unreinforced base course had the similar initial stress distribution angle as the geogrid-reinforced base courses. However, the stress distribution angles for the unreinforced bases decreased with the number of cycles faster than those for the reinforced bases. In this case the vertical stress for the unreinforced base course was concentrated near the center of the plate, which is consistent with the results discussed earlier in the stress analysis. In addition, the heavy-duty geogrid T3 reduced the rate of reduction in the stress distribution angle, which led to the slow increase in the vertical stress at the center. The reduction of the value of 1/tan (α) presented in Figure 4.25 can be explained by the mechanically stabilized layer effect and the tensioned membrane effect as discussed in Section 4.3.1.

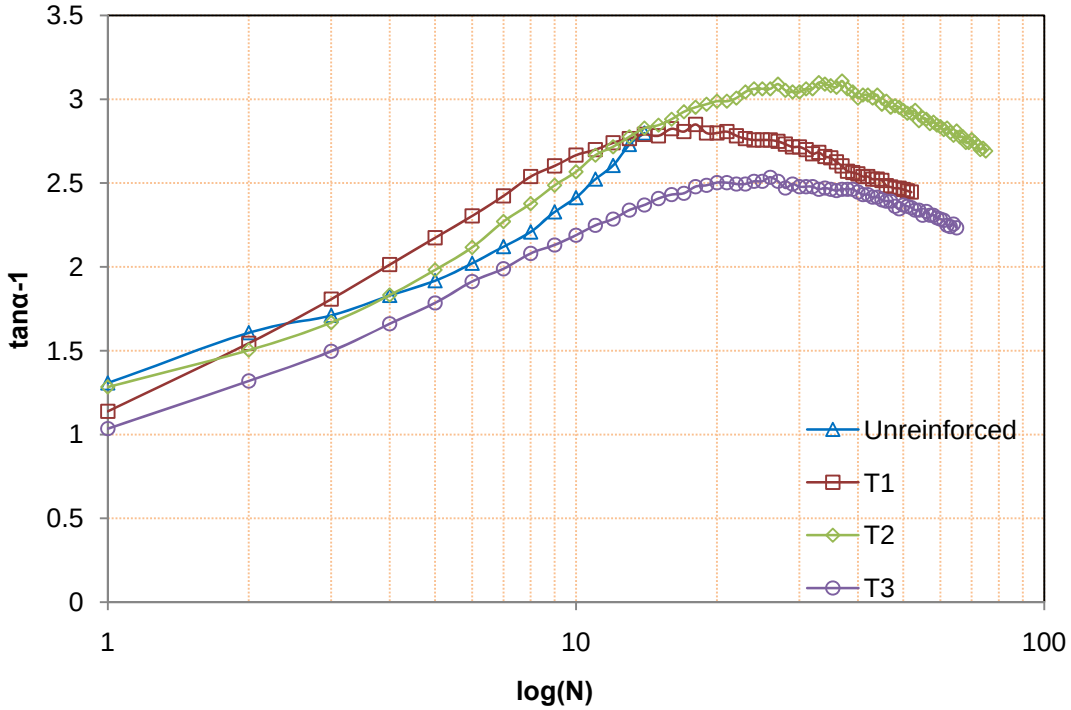

Figure 4.25 Relationship between the stress distribution angle and the number of cycles (base thickness = 15 cm)

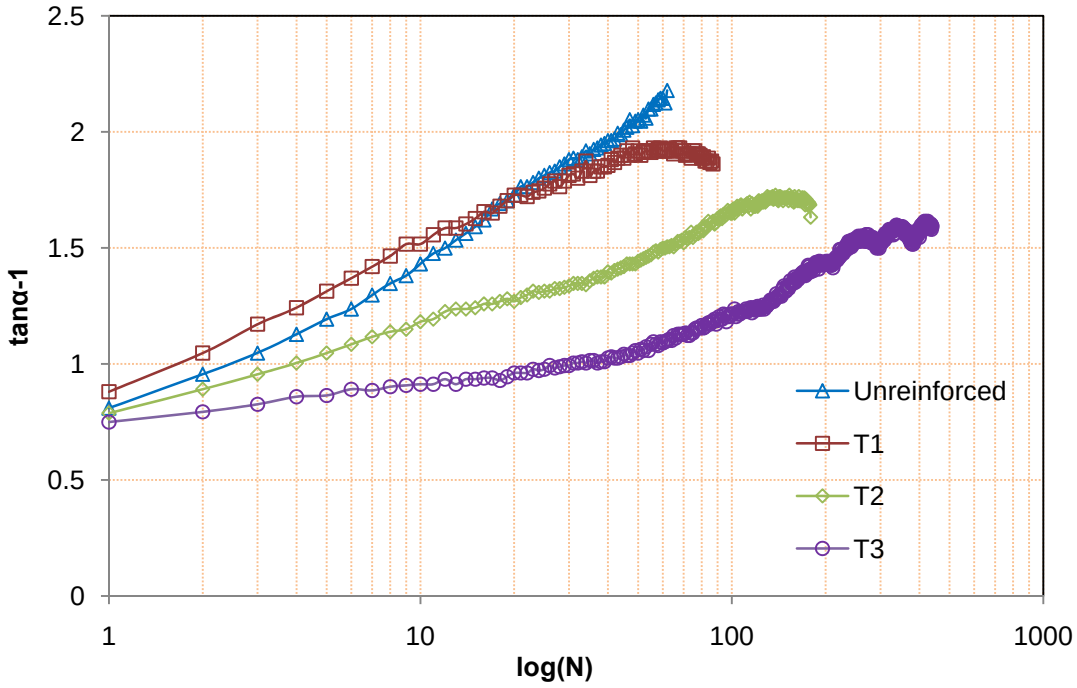

Figure 4.26 Relationship between the stress distribution angle and the number of cycles (base thickness = 23 cm)

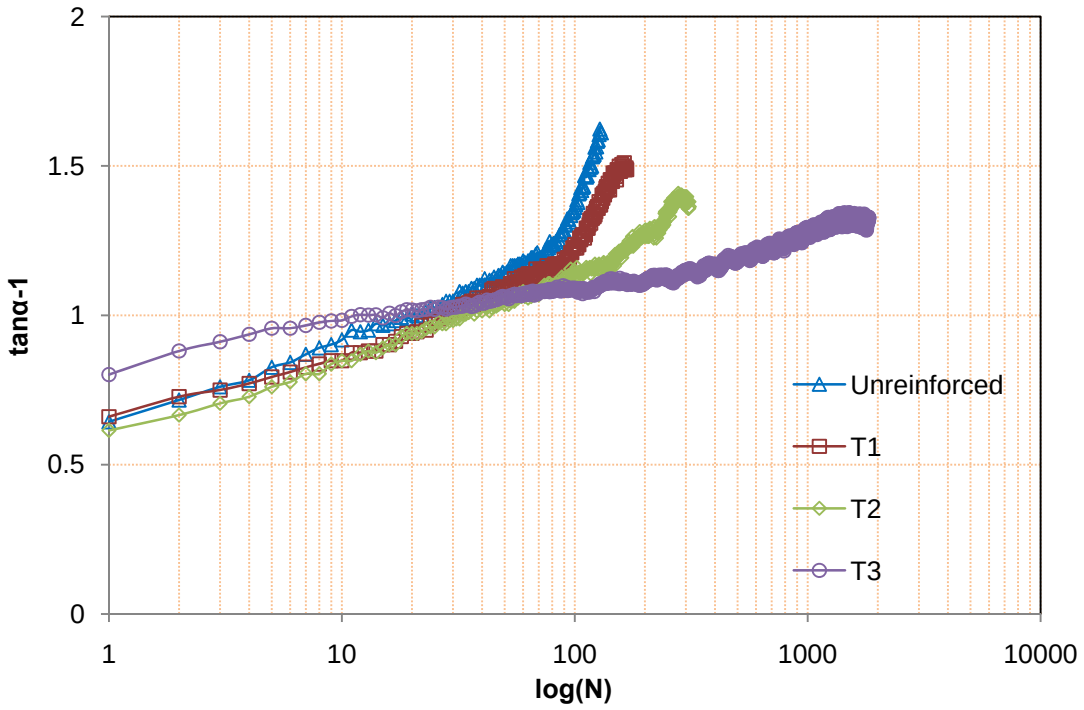

Figure 4.27 Relationship between the stress distribution angle and the number of cycles (base thickness = 30 cm)

4.5.4 Modulus analysis

The above analyses show that during the cyclic loading, the quality of the base course deteriorated thus resulting in a reduction in the stress distribution angle. A further study on the deterioration of the base course is presented below. Some previous studies considered the geosynthetic reinforcement being equivalent to the increase in the thickness of the base course (for example, Giroud and Noiray, 1981). In this study, however, the benefit from the geosynthetic reinforcement is considered increasing the modulus of the base course. Before Boussinesq's solution is used, Odemark's method (Ullidtz, 1987) can be employed to transform a two-layer system (i.e., the base course and the subgrade) into an equivalent homogenous system. From the following formula, the equivalent thickness can be calculated:

$$h_e = h[\frac{E_{bc}(1-{\mu_2}^2)}{E_{sg}(1-{\mu_1}^2)}\}^{\frac{1}{3}} \quad (4.3)$$

where, h = the thickness of the base course; h_e = the equivalent thickness; E_{bc} = the elastic modulus of the base course; E_{sg} = the elastic modulus of the subgrade; μ_1= Poisson's ratio of the base course (μ_1= 0.3 was chosen in this study); and μ_2= Poisson's ratio of subgrade (μ_2= 0.5 was chosen in this study).

Based on the measured vertical stress at the center and the interface between the base course and the subgrade, the equivalent thickness of the base course can be calculated using the following Boussinesq solution and then the modulus of the base course can be estimated using Eq. (4.3) if the modulus of the subgrade is known.

$$\sigma_c = p[1 - \frac{{h_e}^3}{(r^2 + {h_e}^2)^{1.5}}] \quad (4.4)$$

where, σ_c = the vertical stress at the interface between the base course and the subgrade (kPa); h_e = the equivalent thickness; p = the contact pressure on the the surface (kPa); and r = the radius of the equivalent tire contact area (m).

To obtain the modulus of the subgrade, four cyclic loading tests were conducted with the same test equipment and material for the subgrade. Figures 4.28 to 4.31 show

the test results for these tests. In these cyclic loading tests, there were no base course and geogrid. The load was applied directly upon the subgrade by the 30cm diameter rigid plate to investigate the resilient modulus of the subgrade. The resilient modulus of the subgrade was calculated using the elastic solution presented in Harr (1966):

$$\delta = \frac{p_i B I (1 - \nu^2)}{E_{sg}} \tag{4.5}$$

where, δ = the elastic displacement, i.e., the rebound in each load cycle (m); p_i = the vertical stress applied on the subgrade (kPa); ν = Poisson's ratio of the subgrade; B = the diameter of the loading plate (m); I = the displacement influence factor; and E_{sg} = the resilient modulus of the subgrade.

Each test was cyclically loaded until the modulus reached the constant. According to all four tests, the average value of the resilient modulus of the subgrade was 37.16 MPa. Since the load was applied by a rigid plate, the resilient modulus under flexible loading should be multiplied by a factor of 0.79, as indicated by Yoder and Witczak (1975). Thus, the corrected resilient modulus of the subgrade is 29.36 MPa.

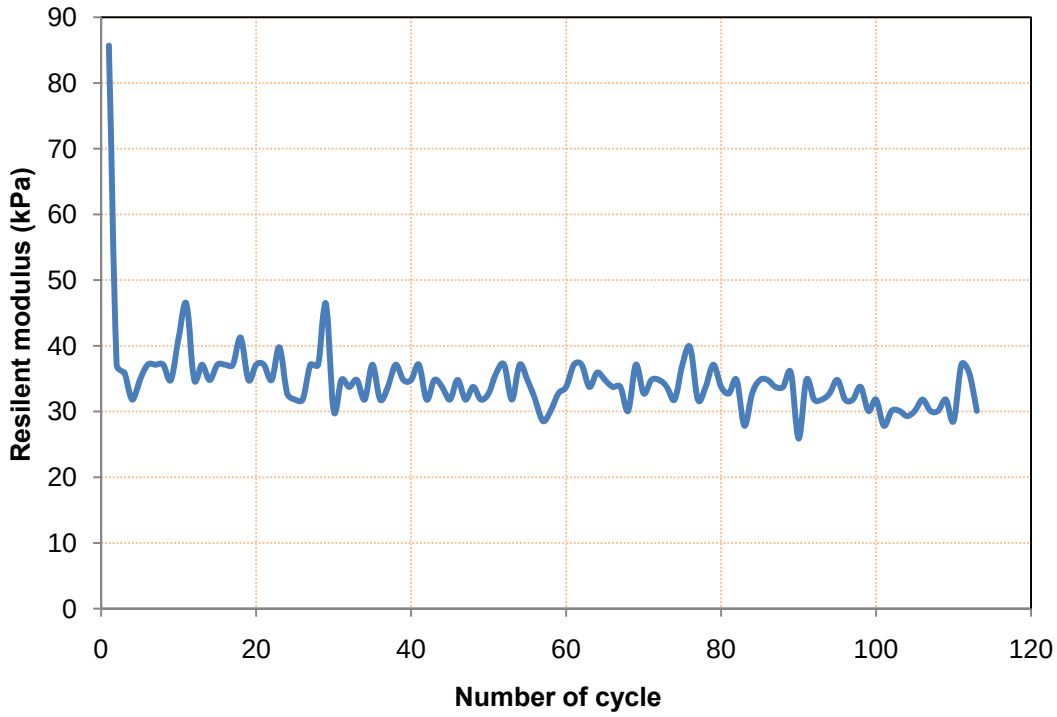

Figure 4.28 Resilient modulus of the subgrade versus the number of cycles under cyclic loading of 4 kN

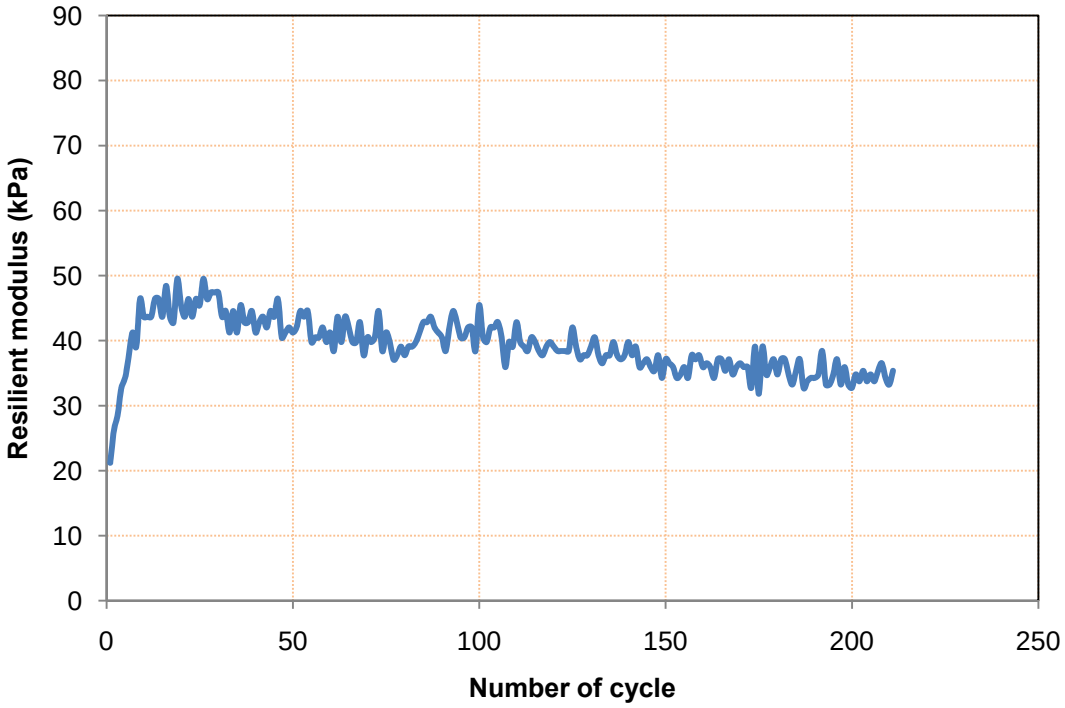

Figure 4.29 Resilient modulus of the subgrade versus the number of cycles under cyclic loading of 8 kN

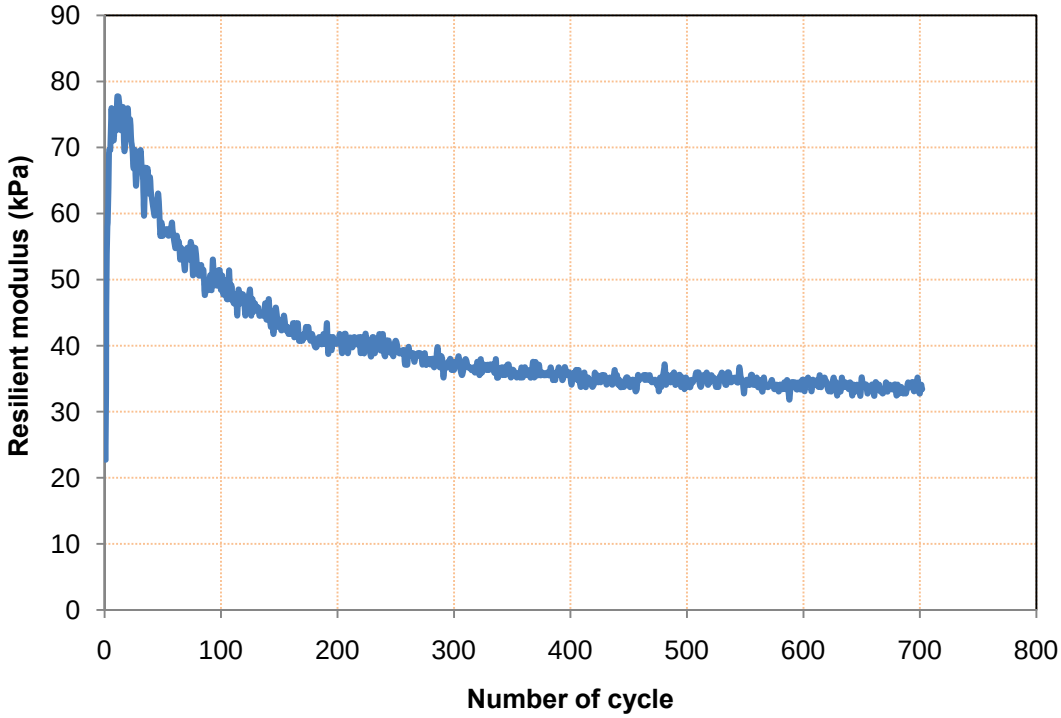

Figure 4.30 Resilient modulus of the subgrade versus the number of cycles under cyclic loading of 12 kN

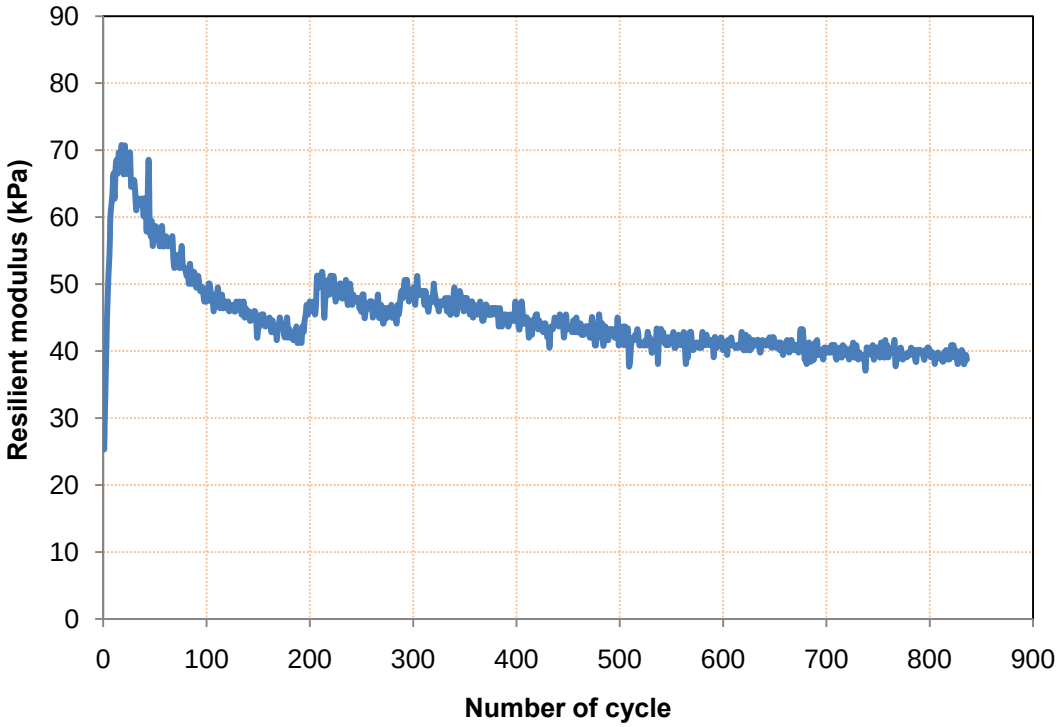

Figure 4.31 Resilient modulus of the subgrade versus the number of cycles under cyclic loading of 16 kN

To use the method of equivalent thickness, the following two requirements should be met: (1) the upper layer should have a higher modulus than the lower layer. The modulus ratio of the upper layer to the lower layer is recommend to be larger than 2. (2) the equivalent thickness is preferred to be greater than the radius of the loading plate to make the method more accurate (Ullidtz, 1987). The test conditions in this study meet the preferred requirements for Odemark's method. The calculated modulus ratios versus the number of cycles are shown in Figures 4.32, 4.33, and 4.34 for base courses at the thicknesses of 15cm, 23cm, and 30cm, respectively.

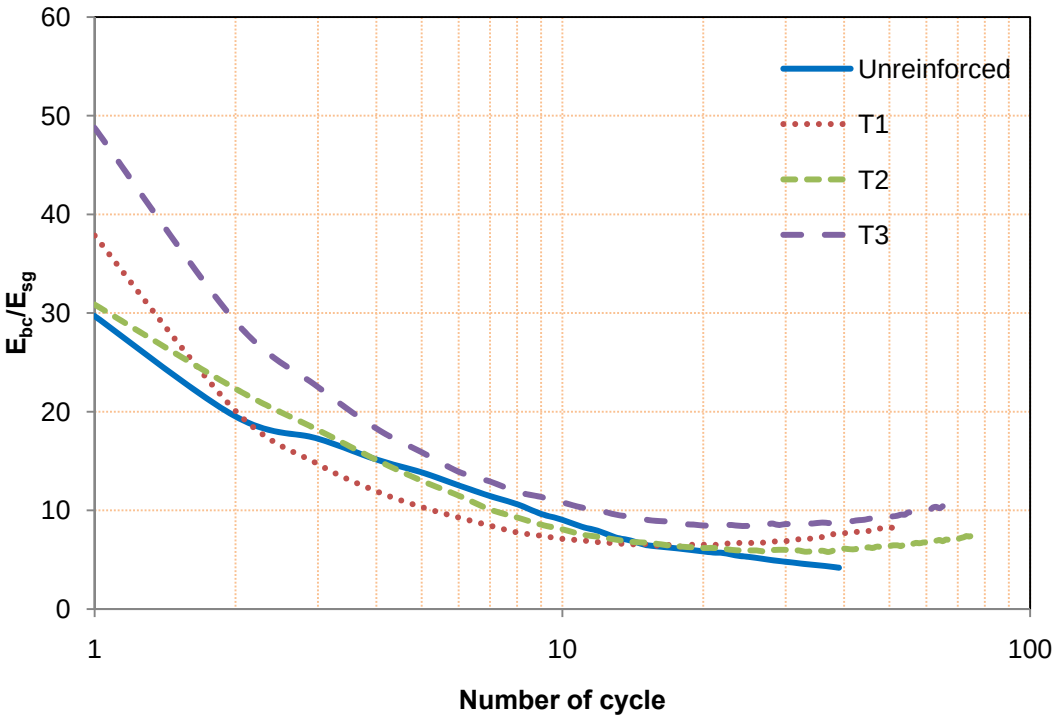

Figure 4.32 Modulus ratio of the base course over the subgrade versus the number of cycles (base course thickness = 15 cm)

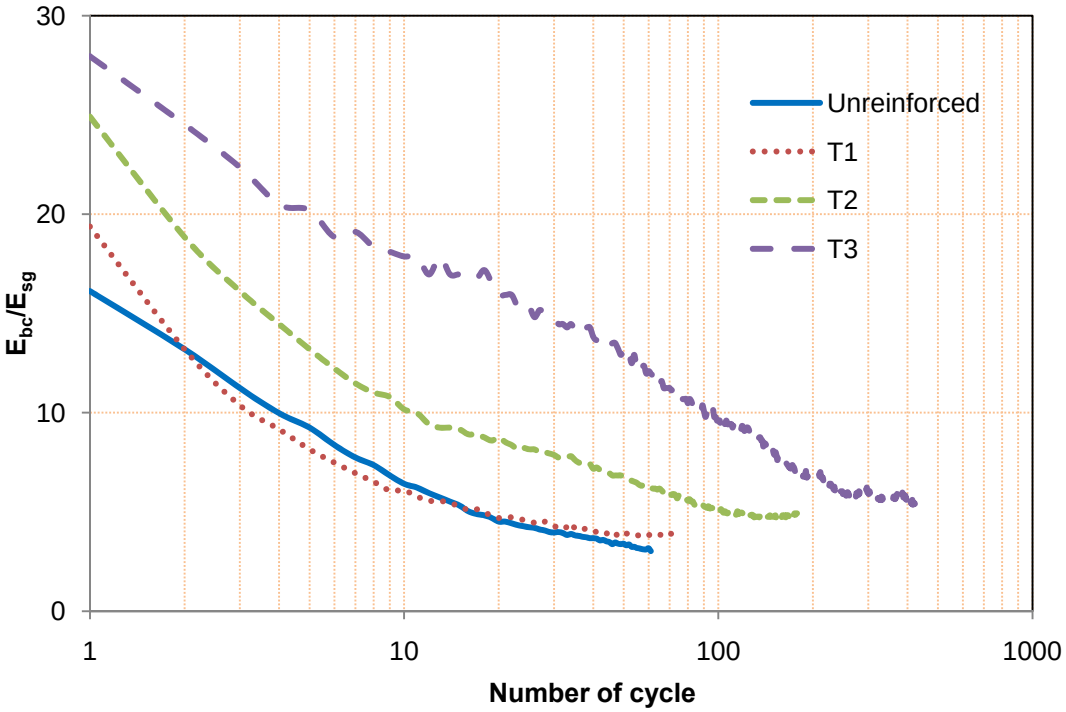

Figure 4.33 Modulus ratio of the base course over the subgrade versus the number of cycles (base course thickness = 23 cm)

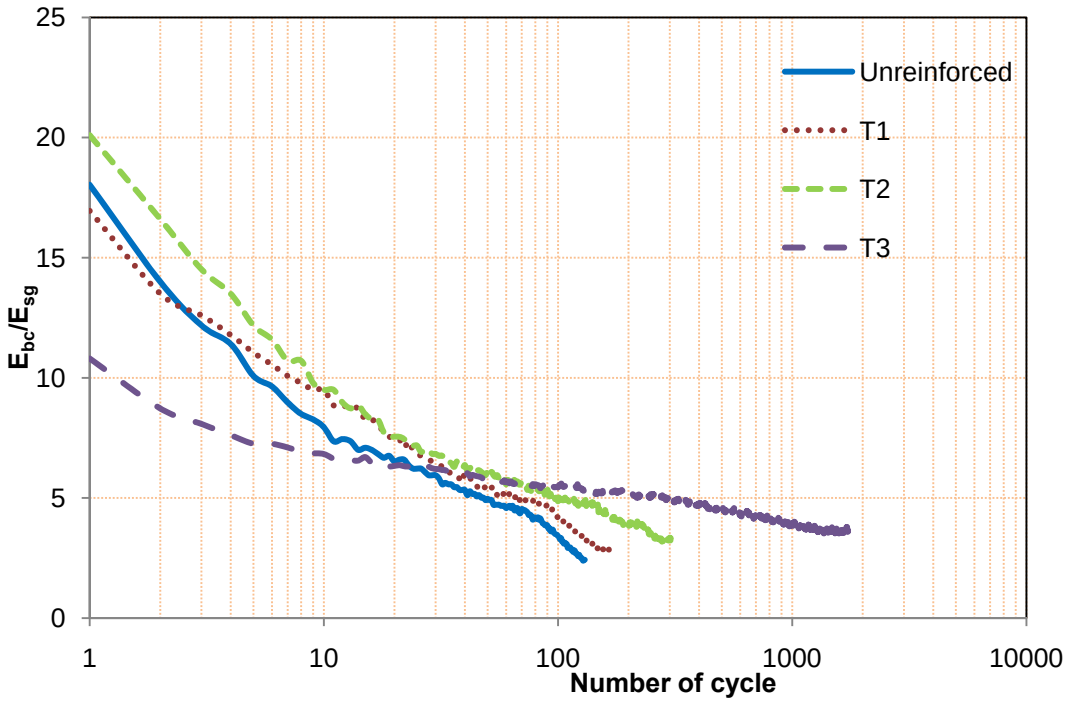

Figure 4.34 Modulus ratio of the base course over the subgrade versus the number of cycles (base course thickness = 30 cm)

4.5.5 Effect of the properties of base course and subgrade soil on stress distribution

Unpaved roads usually have a base course and a subgrade. The resilient modulus of the base course is mostly higher than that of the subgrade. As demonstrated by Burmister (1958) using the theory of elasticity, the vertical stress at the interface of the base course and the subgrade decreases with the increase of the ratio of modulus of the base course over the subgrade. In the Giroud and Han method (2004a), the vertical stress at the interface between base course and subgrade was estimated based on the Burmister solution for a two-layer system. The vertical stress increases with the number of loading cycles due to the deterioration of the base course, which leads to narrowing of the stress distribution area. However, the relationship between the reduction of the stress distribution angle and the decrease of the modulus of the base course needs a further investigation especially considering the use of triangular aperture geogrids.

Figures 4.35, 4.36, and 4.37 present the correlation between the stress distribution angle ratio and the modulus ratio during the cyclic loading for each test. Using the statistical method, the influence of the ratio of modulus and the base course thickness, the following correlation can be obtained:

$$\frac{\tan \alpha_N}{\tan \alpha_1} = e^{c-1.78} R_E^{0.47} R_H^{0.7} \quad (4.6)$$

where $\tan\alpha_N$ = the tangential value of the distribution angle in cycle N; $\tan\alpha_1$ = the tangential value of the distribution angle in first cycle; e = the base of exponential function; c = the compaction influence factor, $c \approx 1 - \frac{\mathrm{CBR_{bc}}}{\mathrm{CBR_{un}}}$, $\mathrm{CBR_{bc}}$= the CBR value of the base course, $\mathrm{CBR_{un}}$ = the CBR value of the unreinforced base course; $\mathrm{R_E} = \frac{\mathrm{E_{bc}}}{\mathrm{E_{sg}}}$, E_{bc} = the resilient modulus of the base course; E_{sg} = the resilient modulus of the subgrade; $\mathrm{R_H} = \frac{\mathrm{H}}{\mathrm{H_0}}$, H = the thickness of the base course; $\mathrm{H_0}$ = 15 cm. The R square value for Equation (4.6) is 0.94.

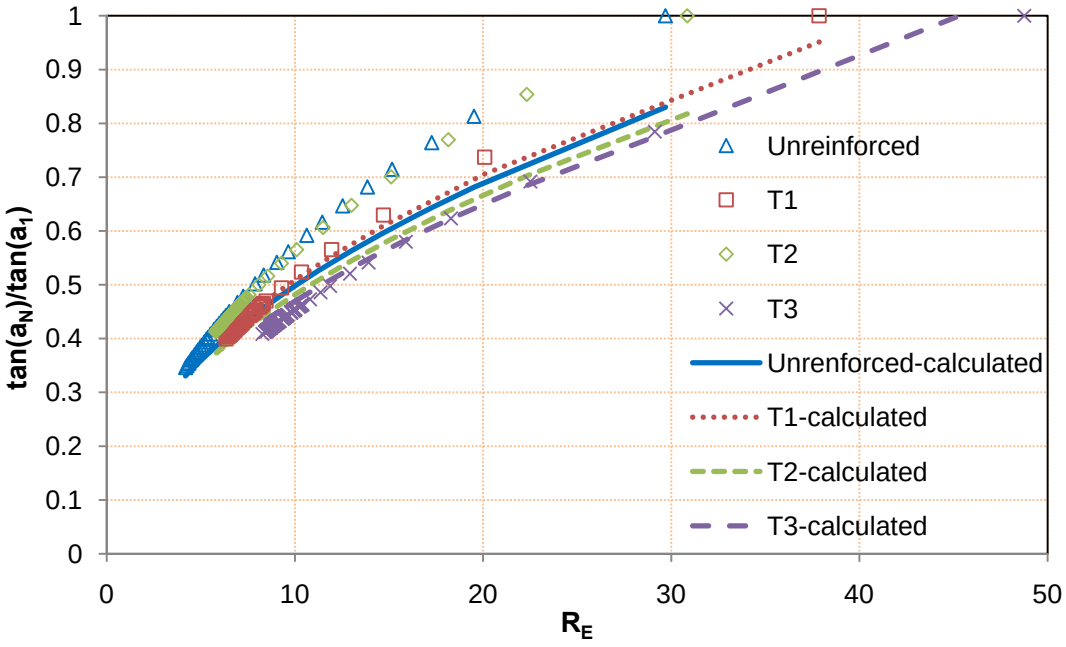

Figure 4.35 Relationship between the stress distribution angle and the modulus ratio (base course thickness = 15cm)

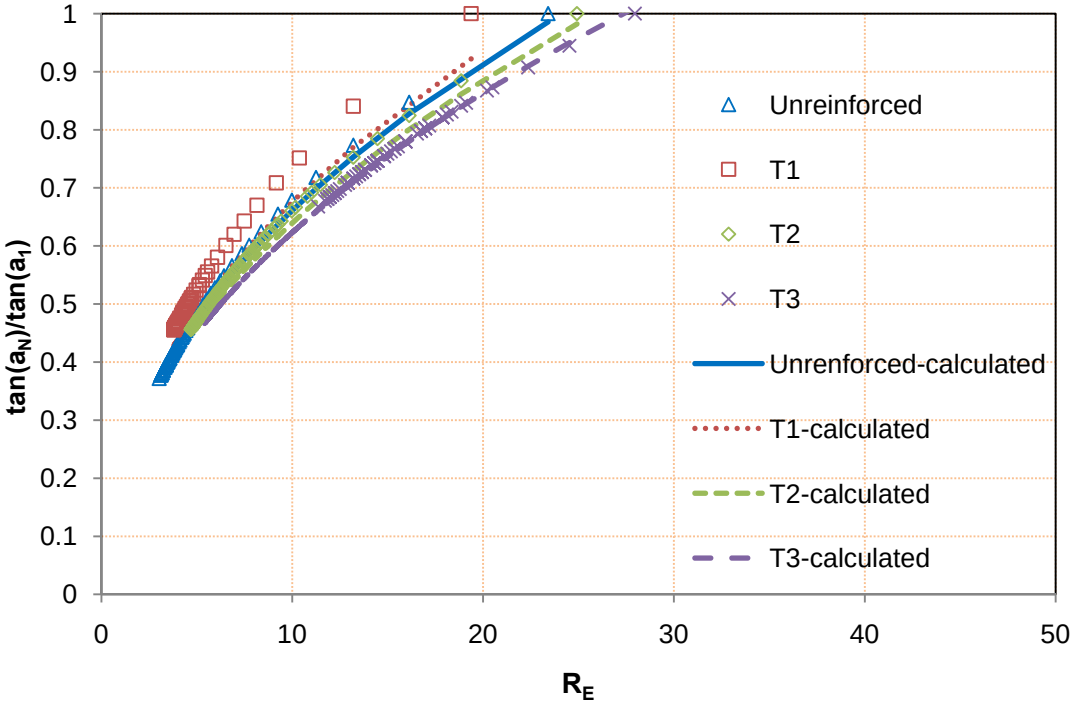

Figure 4.36 Relationship between the stress distribution angle and the modulus ratio (base course thickness = 23cm)

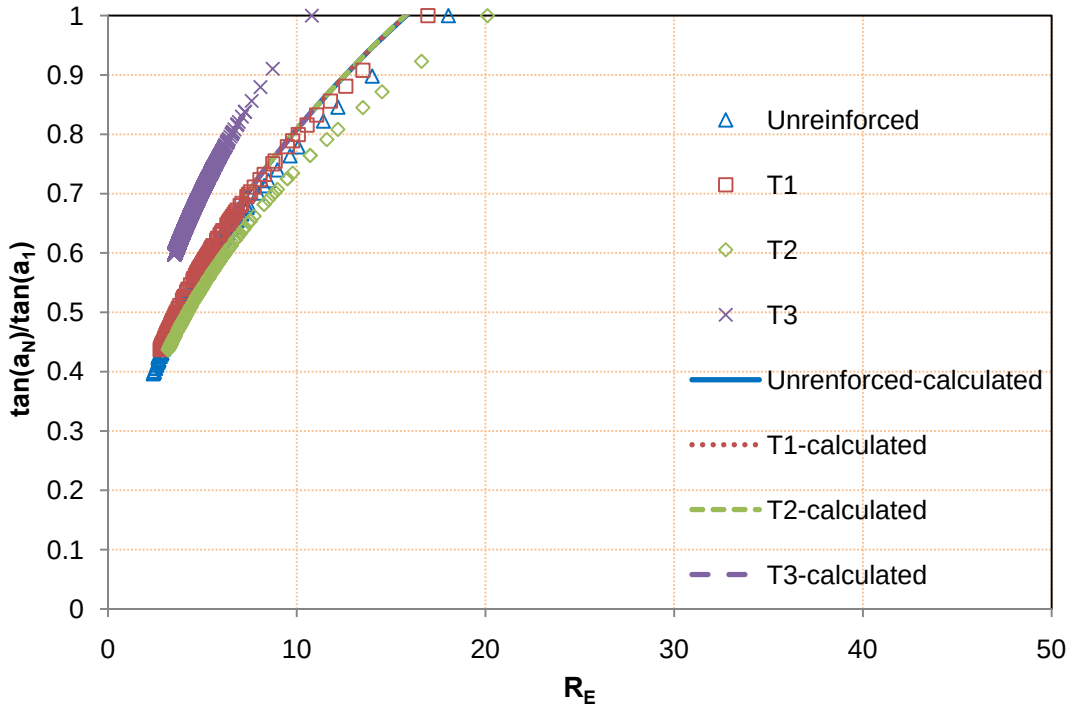

Figure 4.37 Relationship between the stress distribution angle and the modulus ratio (base course thickness = 30cm)

4.6 Influence of stiffness of base course on performance

In order to investigate the influence of the initial stiffness of the base course on the performance, three additional tests were conducted for unreinforced, T2, and T3 geogrid-reinforced base courses. The thickness of all these base courses was 15cm. The main difference between these three tests and other tests was that the base course in these tests was compacted to approximately 5% CBR value while other tests had 20% CBR for the base courses. The comparisons of the test results are shown in Figures 4.38, 4.39, and 4.40.

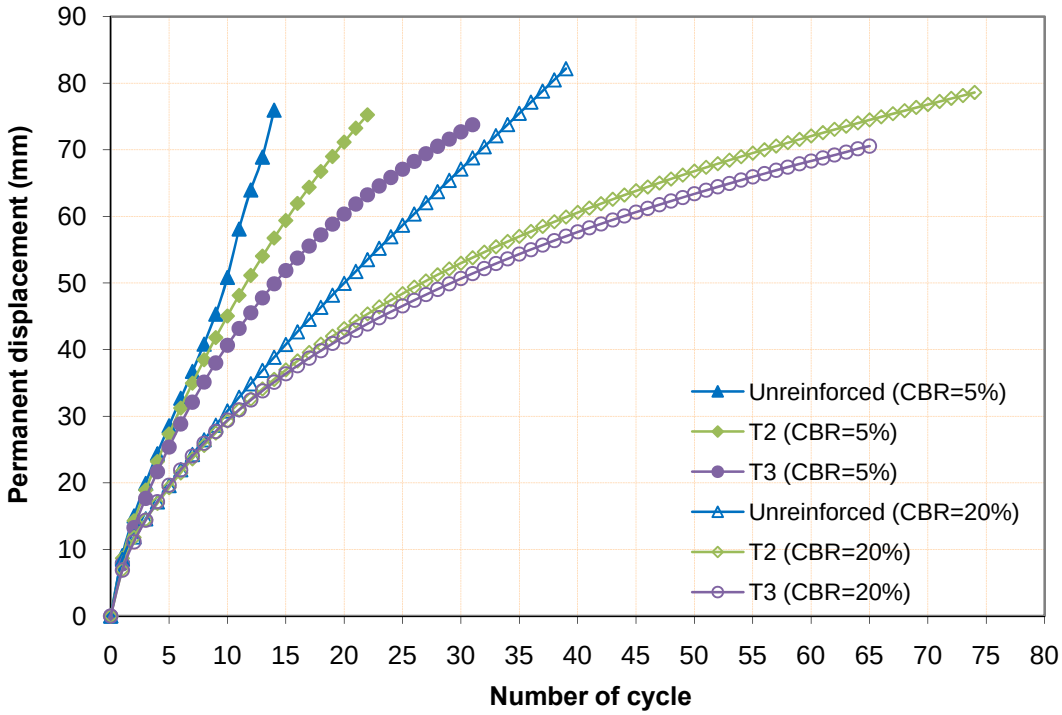

Figure 4.38 Permanent displacement of the loading plate versus the number of cycles for 15cm thick base courses with CBR=5% or 20%

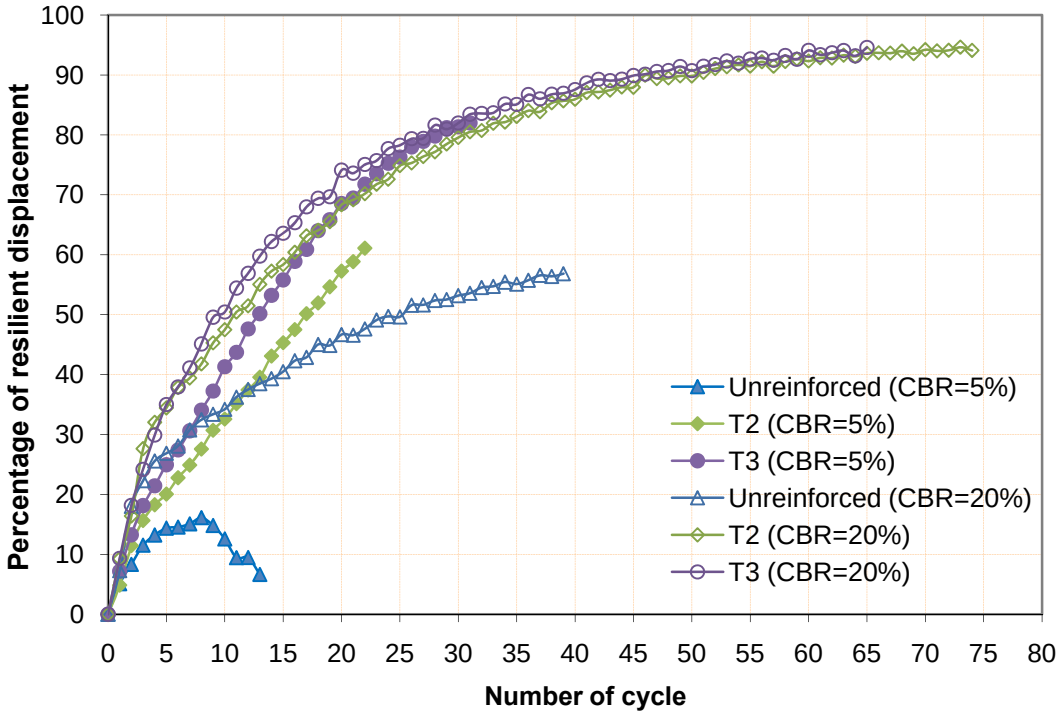

Figure 4.39 Percentage of resilient displacement of the loading plate versus the number of cycles for 15cm thick base courses with CBR=5% or 20%

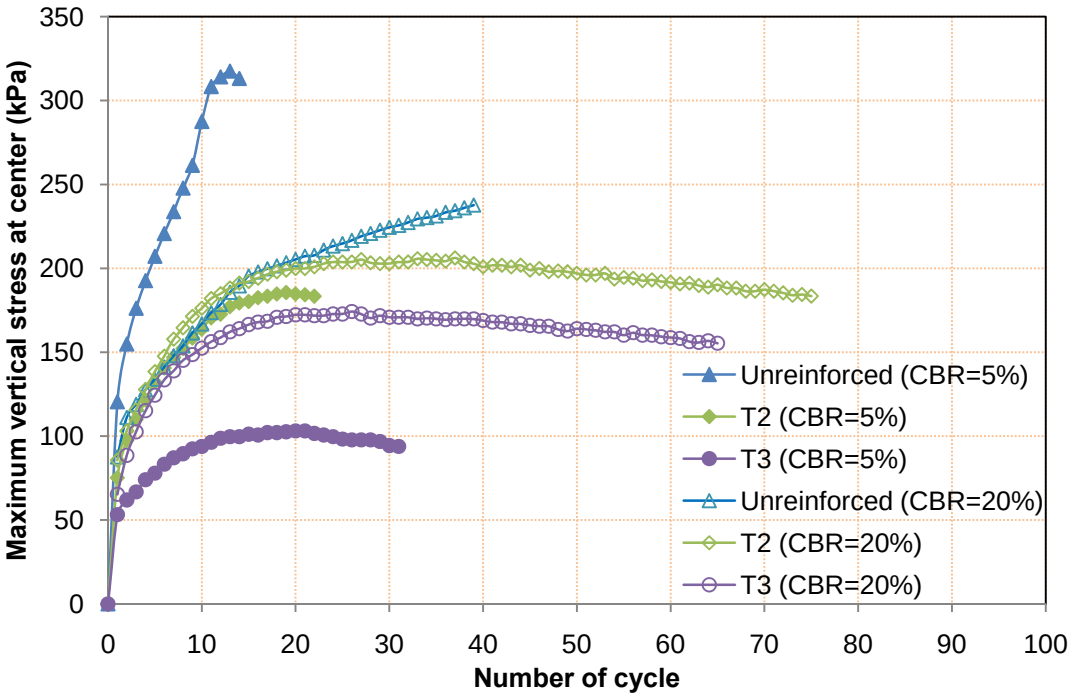

Figure 4.40 Maximum vertical stress at the interface between the base and the subgrade for 15cm thick base course with CBR=5% or 20%

With an increase in the number of loading cycles, the benefit of geogrids became more obvious. The tests with 20% CBR base courses resulted in less permanent displacement, and higher percent of resilient displacement than those with 5% CBR base courses. The dramatic difference in vertical stress between the 20% and 5% CBR is due in part to the fact that the 20% CBR base course can better support the applied loads and are subject to less degradation. However, unlike the control case, the vertical stress decreases with increasing load cycles for the 20% CBR subgrade soil. As such, Figure 4.40 demonstrates the potential short and long term benefits associated with the inclusion of triangular aperture geogrid with aggregate base courses and soft subgrade soils.

The numbers of cycles for the unreinforced, T2 and T3 geogrid-reinforced bases with 5% CBR at the permanent displacement of 75 mm were 14, 22, and 32, respectively. Therefore, the improvement factors for T2 and T3 geogrids, defined as the ratio of the number of cycles for the reinforced base to that for the unreinforced base at the permanent displacement of 75 mm, were 1.57 and 2.29, respectively. As discussed in Section 4.4.1, the 15cm thick T2 and T3 geogrid-reinforced base courses with 20% CBR had the improvement factors of 1.88 and 2.23, respectively. This comparison indicates that low stiffness or poorly compacted base course did not significantly reduce the benefit of the triangular aperture geogrids. This result needs to be further verified in the future study.

4.7 Influence of stiffness of subgrade on performance

In addition to the effect of the base course, the influence of the subgrade stiffness was investigated in this study as well. Approximately 3% CBR subgrade was prepared for one unreinforced base and one T1 geogrid-reinforced base test. The comparisons of the test results based on 2% and 3% CBR subgrades are presented in Figures 4.41 to 4.44.

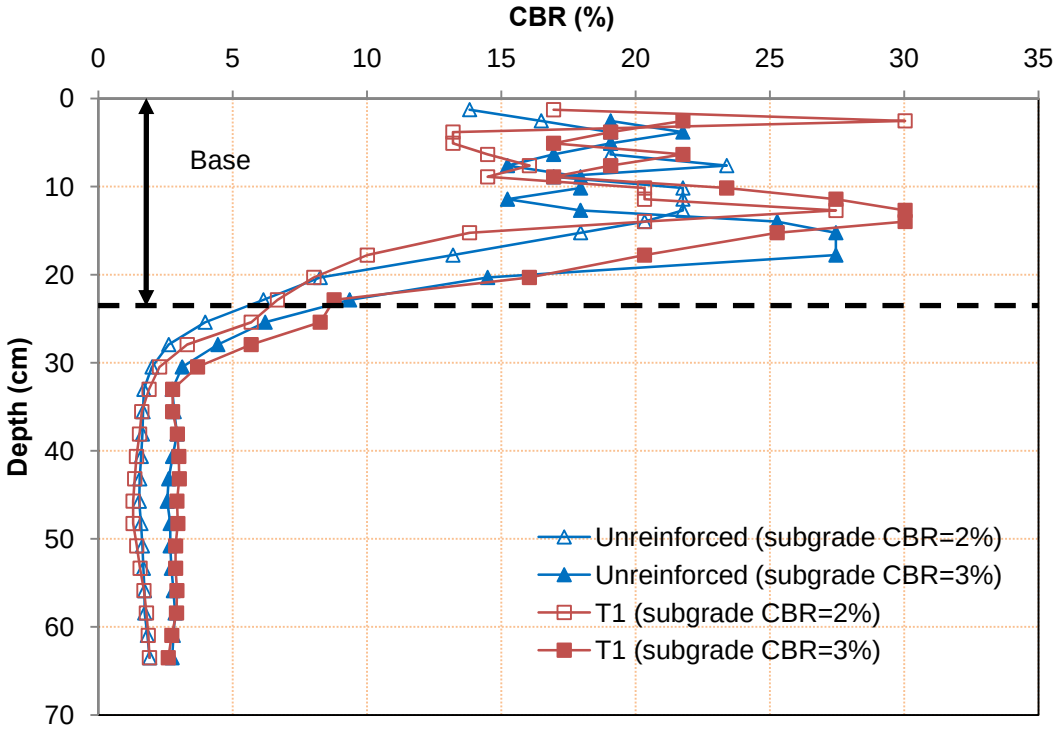

Figure 4.41 CBR profiles for the 23cm thick unreinforced and T1-reinforced base courses over the subgrade of CBR = 2% or 3%

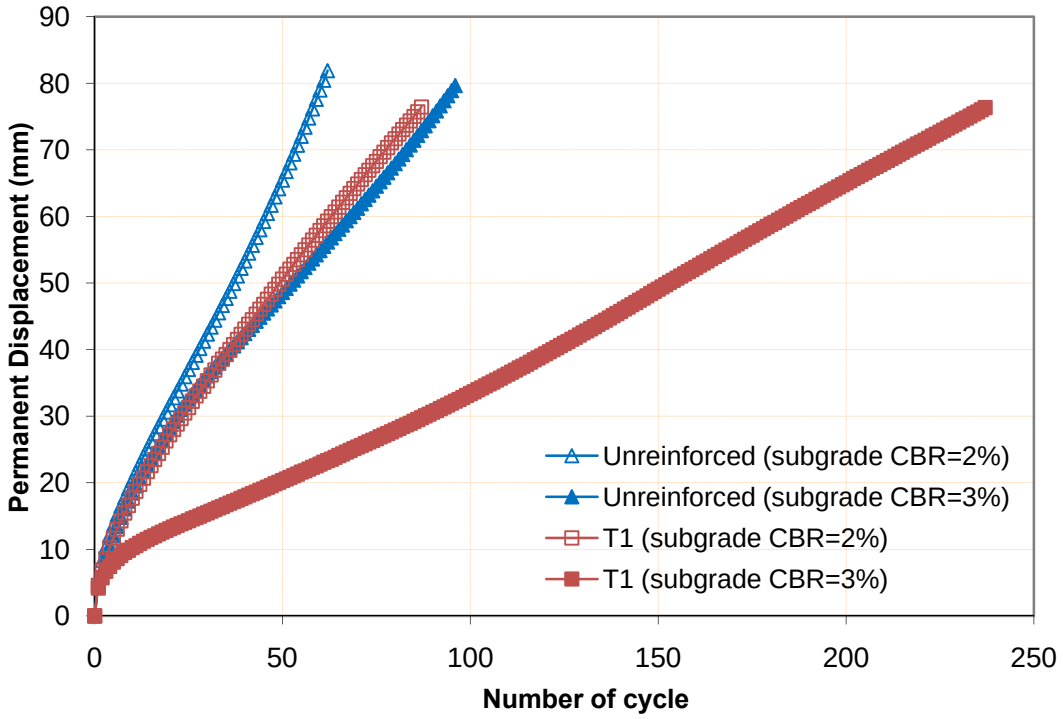

Figure 4.42 Permanent displacement of the loading plate versus the number of cycles for the 23cm thick base courses over the subgrade of CBR=2% or 3%

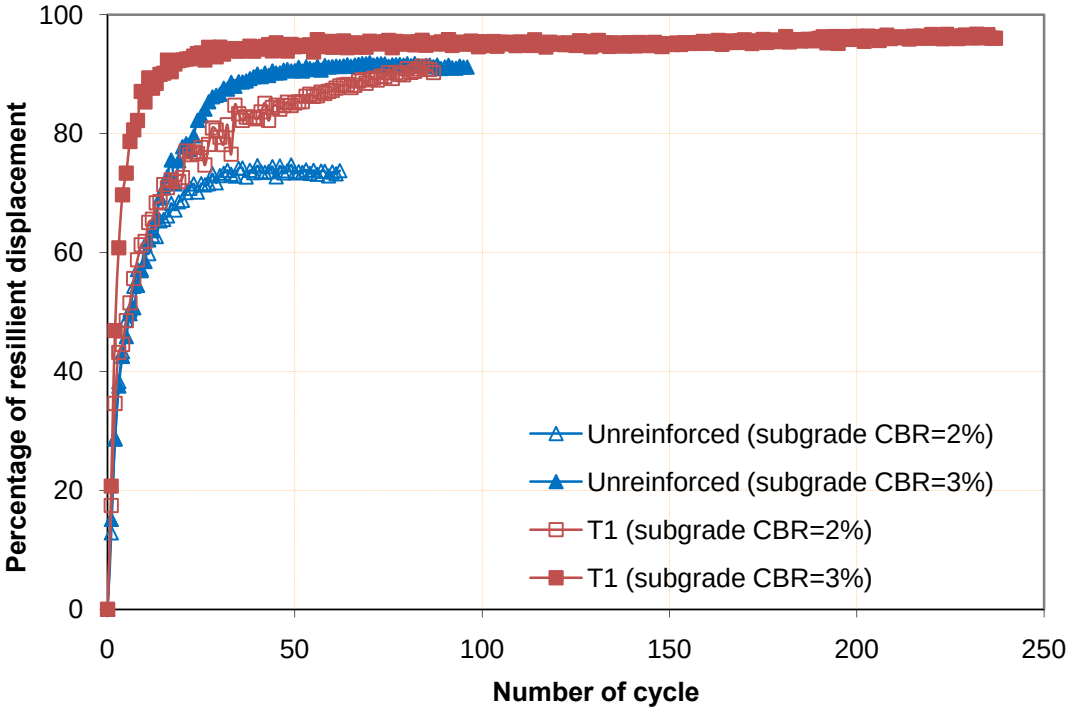

Figure 4.43 Percentage of resilient displacement of the loading plate versus the number of cycles for 23cm thick base courses over the subgrade of CBR=2% or 3%

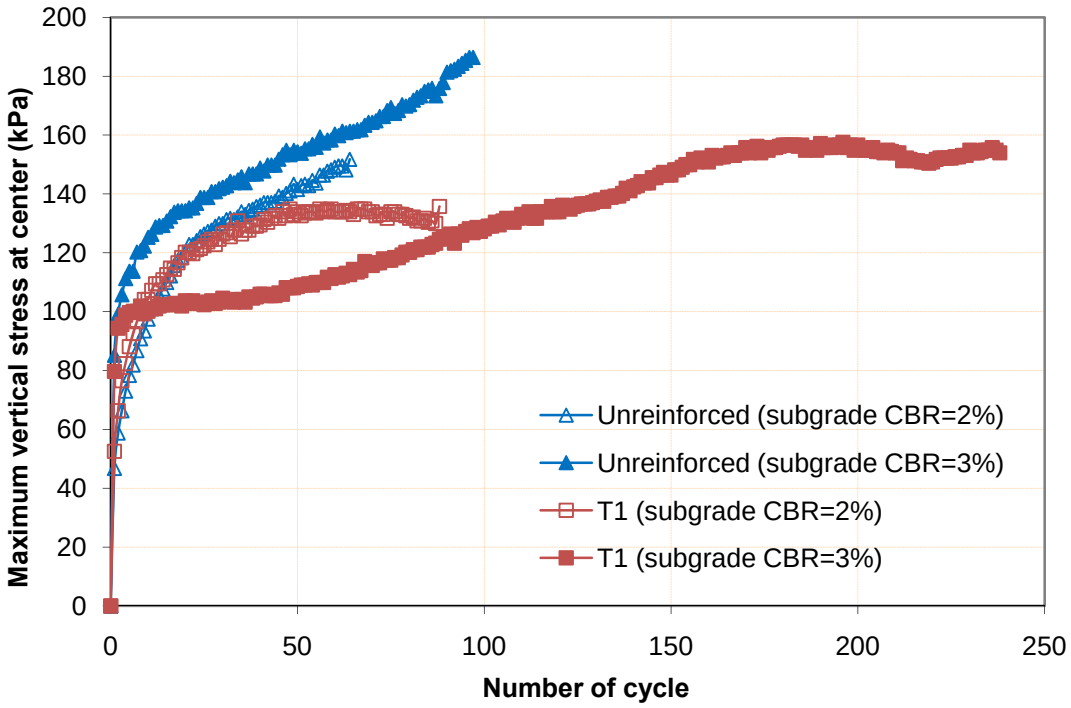

Figure 4.44 Maximum vertical stresses at the interface between the base and the subgrade for the 23cm thick base courses over the subgrade of CBR=2% or 3%

With an increase in the number of the loading cycles, the test sections with stiffer subgrade had much lower permanent displacement, especially for the T1 geogrid-reinforced base course, than those with softer subgrade. The numbers of cycles for the unreinforced and T1 geogrid-reinforced bases over 2% CBR subgrade at the permanent displacement of 75 mm were 57 and 85, respectively. Therefore, the improvement factor for the T1 geogrid-reinforced base was 1.49. The numbers of cycles for the unreinforced and T1 geogrid-reinforced bases over 3% subgrade at the permanent displacement of 75 mm were 90 and 223, respectively. Therefore, the improvement factor for the T1 geogrid-reinforced base was 2.48. The 1% increase in the CBR value of the subgrade resulted in 66% increase in the improvement factor

for the T1 geogrid-reinforced bases. The comparison also shows that the stiffer subgrade (CBR=3%) resulted in larger percentage of resilient displacement as compared with the softer subgrade (CBR=2%). In other words, the stiffer subgrade made the unpaved road section more resilient.

Chapter 5 CONCLUSION AND RECOMMENDATION

5.1 Summary

Past studies have shown that geogrids are an efficient and economical reinforcement material for unpaved roads under static or cyclic loading. The main benefits of the geogrid include base course reinforcement and subgrade stabilization. The reinforcement effects include: interlock with aggregates, lateral confinement, reduction of shear stress, tensioned membrane effect, and widened stress distribution. However, the past studies on the reinforcement of the geogrid have been focused on uniaxial or biaxial geogrids on weak subgrades. Research is needed on the performance of triangular aperture geogrids under static and cyclic loadings over weak subgrade.

This study was concentrated on the triangular aperture geogrid-reinforced unpaved bases over weak subgrade under cyclic loading through laboratory plate loading testing. Nineteen large-scale cyclic plate loading tests were conducted on granular bases over weak subgrade in a large test box. Three types of triangular aperture geogrids were used in this study for base courses of three different thicknesses. One layer of geogrid was placed at the interface between the base and the subgrade in each reinforced test section. Base courses of 5% or 20% CBR and subgrades of 2% or 3% CBR were investigated. Main test results include the profiles of DCP penetration index, the permanent displacement versus the number of cycle, the maximum vertical

stresses versus the number of cycles, and the surface profiles before and after each test. Based on the test data, displacement, stress, and modulus analyses were conducted. The relationship between the stress distribution angle and the ratio of modulus was established.

5.2 Conclusions

Based on the test results and analyses, the following conclusions can be drawn from this study:

1. Triangular aperture geogrids improved the performance of the reinforced base course over the weak subgrade as compared with the unreinforced base.
2. Triangular aperture geogrids increased the percentage of the resilient displacement of the total displacement.
3. Generally, the measured maximum vertical stresses at the interface between the base and the subgrade increased with an increase in the number of load cycles.
4. Triangular aperture geogrids significantly reduced the maximum vertical stress at the center of the plate transferred to the subgrade as compared with the unreinforced base. This reinforced base resulted in a more uniform stress distribution.
5. Triangular aperture geogrids increased the ratio of modulus of the base course over the subgrade. At failure, the modulus ratio of the base course over the subgrade was approximately 5 for all the tests.The stress distribution angle

depended on the modulus ratio, the thickness of the base course, and the robustness, thickness and mechanical properties of the specific geogrids tested in this study.

6. Only when the permanent displacement became large as compared to the thickness of the base course, did the tensioned membrane effect seem to have benefit. In this study, the tensioned membrane effect was only observed for the thinnest section (15 cm base) when the permanent deformation was larger than 45mm.

7. The increase in the CBR value of the subgrade from 2% to 3% significantly enhanced the benefits of the triangular aperture geogrids.

5.3 Recommendations

This study has been focused on the experimental tests on triangular aperture geogrid-reinforced bases over weak subgrade including obtaining, reducing, and analyzing the test data. The test data provides the basis for development of a comprehensive design method for this family of triangular aperture geogrids, and also serves as data for calibration of the Giroud-Han method. Lastly, this information can also be used for theoretical analyses including numerical modeling in the future.

REFERENCES

Al-Qadi, I.L, Brandon, T.L., Valentine, R.J., Lacina, B.A., and Smith, T.E. (1994). "Laboratory evaluation of geosynthetic-reinforced pavement sections." *Transportation Research Record 1439*, Washington D.C.: 25-31.

Al-Qadi, Tutumluer, E., Kwon, J., and Dessouky, S.H. (2007). "Accelerated full-scale testing of geogrid-reinforced flexible pavements." TRB 2007 Annual Meeting (CDROM), Transportation Research Board, National Research Council, Washington D.C.

ASTM (1997). Annual Books of ASTM Standards, Construction: Soil and Rock (I), Volume 04.08, American Society for Testing and Materials, Philadelphia, PA.

Austin, D.N., Wu, K.J., and White, D.F. (1993). "The Influence of Test Parameters and Procedures on the Tensile Modulus of Stiff Geogrids." *Geosynthetic soil Reinforcement Testing Procedures,* ASTM STP 1190, S.C., Jonathan Cheng, Ed., American Society for Testing and Materials, Philadelphia, PA, 90-110

Barber, V.C., Odom, E.C., and Patrick, R.W. (1978). *The Deterioration and Reliability of Pavements*. Technical Report. S-78-8, U.S. Army Engineering Waterways Experiment Station, Vicksburg, Miss.

Barksdale RD, Brown SF, Chan F. (1989). *Potential Benefits of Geosynthetics in Flexible Pavement System*. National Cooperative Highway Research Program Report No 315, Transportation Research Board. Washington DC, USA: National Research Council; pp. 56

Barenberg, E.J., Dowland, J.H., and Hales, J. II (1975). "Evaluation of soil-aggregate systems with Mirafi fabric." Department of Civil Engineering, University of Illinois.

Das, B.M. and Shin, E.C. (1998). "Strip foundation on geogrid-reinforced clay: behavior under cyclic loading." *Geotextiles and Geomembranes*, 13(10), 657-666.

Dong, Y.-L., Han, J., and Bai, X.-H. (2010). "A numerical study on stress-strain responses of biaxial geogrids under tension at different directions." Accepted for publication at ASCE G-I GeoFlorida Conference.

Duncan-Williams, E and Attoh-Okine, N. O., "Effect of geogrid in granular base-strength-an experimental investigation." *Journal of Construction and Building Materials*, Vol 22, pp 2180-2184, 2008

Gabr, M. (2001). *Cyclic Plate Loading Tests on Geogrid Reinforced Roads*. Research Report to Tensar Earth Technologies, Inc., NC State Univ.

Giroud, J.P. and Noiray, L. (1981). ‘‘Geotextile-reinforced unpaved road design.’’ *J. Geotech. Eng.,* 107(9), 1233–1254.

Giroud, J.P. and Han, J. (2004a). ‘‘Design method for geogrid-reinforced unpaved roads. I: Development of design method.’’ *J. Geotech. Geoenviron. Eng.*, 130(8), 775–786.

Giroud, J.P. and Han, J. (2004b). ‘‘Design method for geogrid-reinforced unpaved roads. II: Calibration and applications.’’ *J. Geotech. Geoenviron. Eng.*, 130(8), 787–797.

Haas, R., Wall, J., and Carroll, R.G. (1988). “Geogrid reinforcement of granular bases in flexible pavements.” *Transportation Research Record 1188*, Washington D.C., 19-27.

Harr M.E. (1966). *Foundations of Theoretical Soil Mechanics*, New York: McGraw-Hill.

Henry, K.S. (1999). “Geotextiles to stabilize unsurfaced roads on thawing, low-bearing capacity soils: A comparison of two design methods for use by the U.S. Army U.S.” Army Cold Regions Research and Engineering Laboratory, Special Report 99−7.

Hufenus, R., Rueegger, R., Banjac, R., Major, P., Springman, S.M., and Bronnimann, R. (2006). "Full-scale field tests on geosynthetic reinforced unpaved roads on soft subgrade." *Geotextiles and Geomembranes*, Vol. 24, 21-37.

Kinney, T.C. and Xiaolin, Y., (1995). "Geogrid reinforcement of granular bases in flexible pavements." *Transportation Research Record* 1188, pp. 19-27.

Love, J.P. (1984). *Model Testing of Geogrids in Unpaved Roads*. Doctoral Dissertation, University of Oxford, Oxford, UK.

Maxwell, S., Kim, W., Edil, T. B., and Benson, C.H. (2005). *Effectiveness of Geosynthetics in Stabilizing Soft Subgrades*. Report to the Wisconsin Department of Transportation

Perkins, S.W. (1999). "Mechanical response of geosynthetic- reinforced flexible pavements." *Geosynthetics International*, Vol. 6, No. 5, 347-382.

Rodin, S. (1965). "Ability of a clay fill to support construction plant." *Journal of Terramchanics*, 2, 51-68.

Shukla, S.K. (2002). *Geosynthetics and Their Applications* (1977). *Guidelines for Use*

of Fabrics in Construction and Maintenance of Low-Volume Roads. USDA, Forest Service Report PB-276 972, Portland, OR.

Ullidtz P. (1987). *Pavement Analysis*. Elsevier Science Publisher, New York.

Webster, S.L. (1993). *Geogrid Reinforced Base Course for Flexible Pavements for Light Aircraft, Test Section Construction, Behavior under Traffic, Laboratory Test Design Criteria.* Technical Report GL-93-6, U.S. Army Corps of Engineers, Waterways Experiment Station, Vicksburg, MS, USA.

White, D.J., Jahren, C.T., and Suleiman, M.T. (2007). *Effective Shoulder Design and Maintenance*. Final report, Iowa State University, IA.

Yoder, E.J. and Wwitczak, M.W. (1975), *Principles of Pavement Design*, Second Edition, John Wwiley & Sons, Inc.